

MASTER'S THESIS



THEORETICAL AND MATHEMATICAL PHYSICS
LUDWIG-MAXIMILIANS-UNIVERSITÄT MÜNCHEN
FACULTY OF PHYSICS

Spectral Functions and Exact Solutions in a Quantum Dimer Model for Pseudogap Metals

Johannes Feldmeier

Supervisor: Prof. Dr. Matthias Punk

Munich, February 1, 2018

Abstract

We study a two-species quantum dimer model on the square lattice originally proposed by Punk, Allais and Sachdev in Ref.[1] that captures several key properties of the pseudogap phase in high- T_c cuprates. The model features ordinary bosonic spin-singlets as well as fermionic dimers that can be viewed as bound states of spinon and holon monomer excitations in a hole-doped resonating valence bond (RVB) liquid. We develop a functional approach that yields the electronic spectral function in a perturbative regime of small interactions between the fermions and the RVB background. The corresponding results for quasiparticle dispersion and residuum are found to be in good agreement with existing numerical data obtained from exact diagonalization. We further identify a line in parameter space where the exact ground state wave functions can be constructed at an arbitrary density of fermionic dimers, resulting in a flat band of fermionic excitations. Perturbing around the exactly solvable line, this huge ground state degeneracy is lifted and the system realizes a fractionalized Fermi liquid with a small hole pocket Fermi surface in the low doping limit. Finally, we discuss finite size effects that can be compared to exact diagonalization outcomes.

Acknowledgements

I would like to thank Prof. Matthias Punk for giving me the opportunity to write this thesis under his supervision, his open office doors and constant advice have been invaluable to the genesis of this work.

Special thanks belong to my office mate Sebastian Huber, with whom I shared a pronounced passion for dimer models throughout the last year and who provided me with great advice and input in numerous discussions and gave helpful comments on this manuscript. Thanks are due to both Prof. Punk and Sebastian for the numerical data that was used in this work.

I further would like to thank my office mates Dimitri Pimenov and Michael Lichtenegger for insightful discussions and good humour, creating an ever cheerful atmosphere in our office. My gratitude also belongs to the whole group at the chair of theoretical solid state physics for providing a great environment and an open place in their midst.

Last but not least, I thank my friends and family for help and support in all thinkable ways.

Contents

1	Introduction	8
2	Preliminaries	11
2.1	The Rokhsar-Kivelson model	11
2.2	Correlations in the classical dimer model	14
2.3	A quantum dimer model for the cuprate pseudogap phase	18
2.3.1	Model	18
2.3.2	Mean field theory	20
3	Diagrammatic approach for the spectral function	24
3.1	Functional approach	24
3.1.1	The action	24
3.1.2	Spectral function	27
3.2	The particle-hole ladder	32
3.3	Including the t_2 -term	35
3.4	The hard-core constraint	37
3.5	Results	41
3.5.1	Symmetries	41
3.5.2	Dispersion and residuum	45
3.5.3	Discussion	55
4	Exact solution of a two-species quantum dimer model for pseudogap metals	57
4.1	Extending the dimer model	57
4.2	Exact ground states	58
4.3	Ground state properties	64
4.3.1	Perturbations around RK-Line	64
4.3.2	Fractionalized Fermi liquid structure	66
4.4	Summary	69
5	Finite size effects in the quantum dimer model	72
5.1	The strong coupling limit	72
5.2	Variational ansatz	77
6	Outlook	82

1 Introduction

More than 30 years since the discovery of high temperature superconductivity in cuprates, extensive experimental and theoretical effort that investigates the underlying mechanism remains among the most active fields of research in condensed matter physics. Today, it is widely believed that a thorough understanding of the so-called pseudogap phase is crucial to understanding the physics of hole-doped cuprates. For small temperatures, the pseudogap phase occurs in the so-called underdoped region, with sufficient hole density to destroy antiferromagnetic Néel ordering, but before the onset of d-wave superconductivity at even higher values of hole-doping, see the schematic phase diagram in Fig.(1) for illustration. A collection of experimental investigations on high- T_c cuprates have led to a detailed exploration of the pseudogap over the years, yielding insight on many unusual properties of this remarkable phase of matter. The pseudogap is characterized by a suppression in the density of states at the Fermi energy, as shown by measurements on electronic specific heat [2, 3], c-axis optical conductivity [4, 5] and the tunneling density of states [6]. Data of Knight shift measurements also show a decrease of the magnetic susceptibility at temperatures lower than T^* , which marks the onset of the pseudogap phase, indicating the existence of a pseudogap in the spin degree of freedom as well [7, 8]. Angle resolved photoemission spectroscopy (ARPES) studies have directly demonstrated the opening of a gap near the antinodal points $(\pi, 0)$ of the Brillouin zone and revealed the existence of non-closed Fermi arcs in the spectrum [9, 10, 11, 12, 13, 14, 15, 16]. These results are in contrast to transport measurements on cuprates that find normal Fermi liquid like behaviour in the pseudogap for quantities like quasiparticle lifetime [17] and magnetoresistance [18]. Hall measurements indicate however, that the charge carrier density in the pseudogap is given by the doping p as opposed to the actual number $1 + p$ of holes present in the system [19], therefore apparently presenting a violation of Luttinger's theorem which states that the area enclosed by the Fermi surface should be proportional to the total number of carriers relative to a completely filled band. A theoretical framework intended to describe the pseudogap cuprates should then reconcile the above experimental findings, in particular the Fermi liquid behaviour with the non-closed Fermi arcs.

One of the early ideas for such a theory is Anderson's resonating valence bond (RVB) model, which approaches the pseudogap from the Mott insulating phase of the Hubbard model and assumes that the insertion of holes effectively destroys the Néel ordering and induces singlet formation on the bonds of a lattice [20]. Hole doping into the RVB state leads to deconfined monomer excitations dubbed spinons and holons, where the former are uncharged $S = 1/2$ quasiparticles while the latter are charge $+e$ spinless quasiparticles corresponding to non-occupied sites. Although this model successfully describes the behaviour of the specific heat, the magnetic susceptibility and the c-axis conductivity in the pseudogap phase [21], it could not provide an explanation for the Fermi arcs observed in ARPES measurements, as the model does not feature single excitations with the hole quantum numbers $S = 1/2$, charge $+e$. Naturally, the next step is to stay in the RVB picture which already describes a number of experimental findings, but to construct a model which features hole-like quasiparticles with density p , thus being potentially able to additionally account for the results of ARPES measurements. Such a model can be realized by a fractionalized Fermi liquid (FL*), originally proposed by Senthil, Sachdev and Vojta

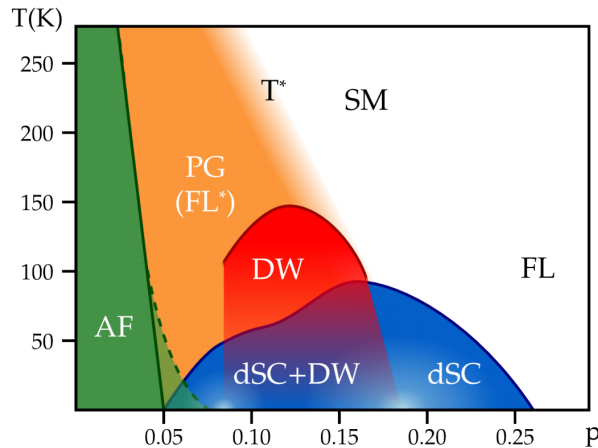


Figure 1: Schematic phase diagram of hole-doped cuprates as function of doping p and temperature T . Close to the Mott phase at $p = 0$, the ground state features antiferromagnetic order (AF). Upon doping away from the insulating phase, the system enters the pseudogap phase (PG) for $T < T^*$, with density wave order (DW) for small temperatures. For $T < T_c$ we enter the d-wave superconducting phase (dSC), while even higher values of doping leads the system into a normal Fermi liquid (FL), respectively a strange metal (SM) phase. Figure adapted from [1].

in the context of heavy fermion compounds, linking the apparent violation of Luttinger’s theorem to the appearance of topological order in systems with fractionalized excitations [22]. The concept of the FL* has been applied recently to the RVB picture of the pseudogap phase by Punk, Allais and Sachdev in [1] by assuming the formation of bound states between spinons and holons, thus effectively introducing a second species of bond variables besides the ordinary singlets. We are therefore guided to consider two-species quantum dimer models as a candidate theory for an effective low energy description of the pseudogap phase.

On a general note, see [23], quantum dimer models have been shown to be useful tools to study paramagnetic ground states of quantum antiferromagnets as they provide an effective description of low energy singlet excitations and feature rich phase diagrams, including a variety of different valence bond solids with broken lattice symmetries, as well as symmetric spin-liquid phases [24, 25, 26, 27, 28]. Subsequently, interesting connections to lattice gauge theories and loop gas models have been found, raising interest in quantum dimer models from various perspectives [29, 30, 31, 32, 33].

In this thesis, we focus on the dimer model introduced in [1] which provides a possible explanation for the observed Fermi arcs and features a sizeable gap around the antinodal points of the Brillouin zone as demonstrated in [34]. After a revision of some basic properties of dimer models and a discussion of the theoretical framework from [1] in the following section, we focus on a diagrammatic approach to the model in Sec.(3). We will use standard coherent states path integrals to examine the system at hand, which provides a so far unconventional way of tackling quantum dimer systems. We find that the approach successfully describes quasiparticle dispersion and residuum in a certain perturbative regime only due to the fact that the model realizes a FL*. The results are compared to data sets

obtained from exact diagonalization on a 6×6 square lattice that were kindly provided by M. Punk and S. Huber. In Sec.(4) we consider an extended version of the original model in order to gain insight on the ground state structure. We generalize an idea originally employed in the context of quantum dimer models by Rokhsar and Kivelson in [35] to write the dimer Hamiltonian as a sum of local projectors in order to determine exact ground state wave functions for an arbitrary ratio of the two dimer species present. This provides a rare example of an exactly solvable, strongly correlated fermionic lattice model in 2d. Perturbative computations around the resulting line of exactly solvable points in parameter space demonstrate the formation of hole pockets and can be compared to numerical results. We further discuss how properties of an FL* can be associated with the ground state structure. Finally, Sec.(5) considers finite size effects that become significant for large interactions between the RVB background and the fermionic dimers. We show how ground state wave functions can be approximated in this parameter regime using simple variational methods.

2 Preliminaries

The starting point of our work is a review of some of the central aspects of (quantum) dimer models that are relevant for this thesis. We introduce the underlying RK Hamiltonian and some properties of classical dimer models that are necessary to set up the model of [1].

2.1 The Rokhsar-Kivelson model

In this section we present a brief review of the ideas initially worked out by Rokhsar and Kivelson in [35]. We discuss the motivation behind the so-called RK model and determine its key properties.

Following the idea of Anderson [36], the pseudogap phase in hole-doped cuprates is approached from the Mott-insulating phase of the Hubbard model at large U . Interactions between spins on nearest neighbour sites of the square lattice lead to an antiferromagnetic ground state of this model for half-filling. Doping away from half filling leaves unoccupied sites which effectively destroy the antiferromagnetic ordering on the lattice when moving through the sample, see Fig.(2). The system thus becomes frustrated and needs to find a new way to satisfy the antiferromagnetic interaction between neighbouring spins. One way to do so is to assume the spins form singlet states on bonds connecting nearest neighbour sites. Such a resonating valence bond (RVB) state represents an alternative ground state to the antiferromagnetic Néel state. On a given link connecting the sites i and $i + \hat{\eta}$ with $\eta \in \{x, y\}$, the corresponding singlet residing on that link is defined as

$$\mathcal{Y}_{i,\eta} \frac{1}{\sqrt{2}} (c_{i,\uparrow}^\dagger c_{i+\hat{\eta},\downarrow}^\dagger - c_{i,\downarrow}^\dagger c_{i+\hat{\eta},\uparrow}^\dagger) |0\rangle \rightarrow D_{i,\eta}^\dagger |0\rangle, \quad (2.1)$$

where we introduced the creation operator D^\dagger of a bosonic dimer made up of a singlet state. The factors $\mathcal{Y}_{i,\eta}$ correspond to a gauge choice and we adopt the one by RK, $\mathcal{Y}_{i,y} = 1$, $\mathcal{Y}_{i,x} = (-1)^{i_y}$. As we restrict ourselves to the Hilbert space of the t - J -model, there can at maximum be one electron per site which in turn can only be part of at most one singlet state. Assuming that singlet formation is indeed dominant in the regime of low doping, all electrons will be part of exactly one singlet. Every site can then only be part of at most one dimer, yielding a hard-core constraint for the possible distributions of dimers on the lattice. Note that singlet states are invariant under $SU(2)$ transformations, thus no spin label is required to specify the operators D^\dagger .

We can now fully restrict ourselves to a Hilbert space of dimer coverings on the square lattice. The natural starting point for a RVB model of the pseudogap phase is thus a Hilbert space spanned by the close-packed hard-core dimer coverings, corresponding to vanishing doping in the language employed before. Illustrative examples for such coverings on a square lattice with periodic boundary conditions are shown in Fig.(3). Rokhsar and Kivelson then proposed a quantum model governing the interactions between said hard-core coverings. Expressed in terms of the newly introduced dimer operators D , their model Hamiltonian reads (with $\bar{\eta} = x$ if $\eta = y$ and vice versa)

$$H_{RK} = \sum_{i,\eta} V \cdot D_{i,\eta}^\dagger D_{i+\hat{\eta},\eta}^\dagger D_{i,\eta} D_{i+\hat{\eta},\eta} - J \cdot D_{i,\eta}^\dagger D_{i+\hat{\eta},\bar{\eta}}^\dagger D_{i+\hat{\eta},\bar{\eta}} D_{i,\eta}. \quad (2.2)$$

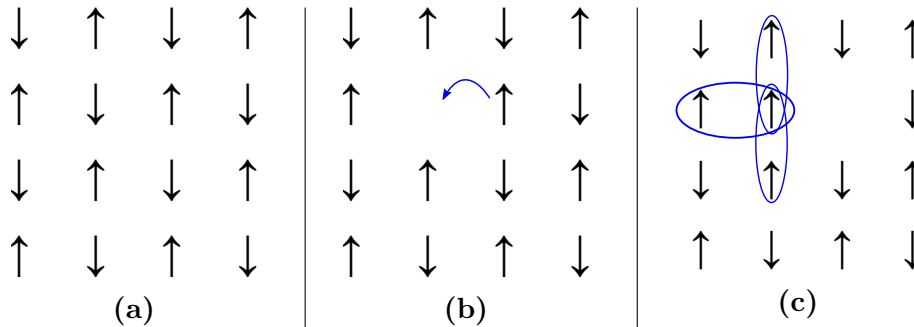


Figure 2: (a) shows antiferromagnetic ordering of spins on the sites of a square lattice. In (b) a hole is doped into the system and moves (c) to a neighbouring site, causing defects of the antiferromagnetic exchange on its starting site, marked in blue.

The first term proportional to V describes an energy offset for parallel dimer within a plaquette. The J -term then corresponds to a plaquette move that flips two such parallel dimers within a plaquette. Both V and J are taken to be positive in this work. We can also express Eq.(2.2) graphically via

$$H_{RK} = \sum_{\text{plaq}} V |00\rangle \langle 00| - J |00\rangle \langle \overline{00}| + (x \leftrightarrow y) \quad (2.3)$$

We remark at this point that two different dimer coverings on the square lattice are not in general orthogonal. If $|c\rangle, |c'\rangle \in \mathcal{H}$, where \mathcal{H} denotes the Hilbert space spanned by all hard-core coverings, then

$$\langle c | c' \rangle \neq 0 \quad (2.4)$$

in general, where the inner product is taken in the usual electron Hilbert space. Orthogonal basis states can then be constructed by Gram-Schmidt orthogonalization. The overlap between two configurations c and c' , see e.g. [37], can be computed by drawing their transition graph, see Fig.(3). A transition graph of two non-equivalent dimer configuration will feature closed loops. To compute the overlap of the two configurations, we start at an arbitrary site i which is part of a loop and set the spin on that site either to $\sigma_i = \uparrow$ or $\sigma_i = \downarrow$. We then start going along the loop in (w.l.o.g.) clockwise direction. Since for either c or c' there is a dimer connecting site i and the next site of the loop, the spin at this next site j must be fixed to the opposite of the spin at i , i.e. $\sigma_j = -\sigma_i$. We then apply the same reasoning to the next site of the loop and iterate this procedure over the whole loop. Thus, in order to have non-vanishing overlap, fixing one spin in a given loop fixes all the spins within this loop to a Néel configuration. For every loop there are thus 2 possibilities to fix the first spin and with it the rest of the spins along the loop. As every singlet state comes with a factor of $\frac{1}{\sqrt{2}}$, the total overlap of c and c' is

$$\langle c | c' \rangle = 2^{n_l} \cdot 2^{-L/2}, \quad (2.5)$$

where n_l is then number of loops in the transition graph of c and c' while L corresponds to the added lengths of all loops in the graph. The overlap of two configurations thus decreases exponentially with the length of their loop graphs, and for sufficiently large systems we

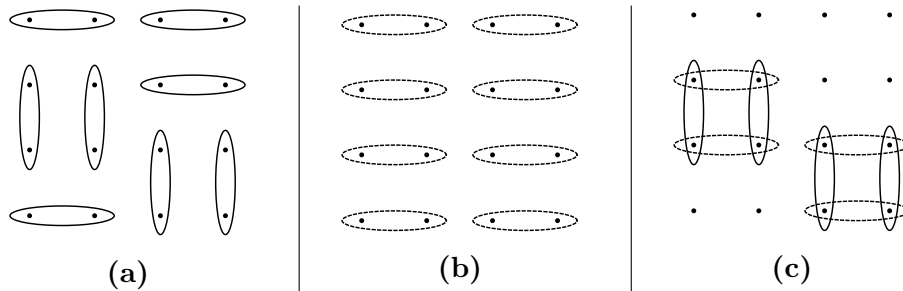


Figure 3: (a) and (b) show typical dimer configurations on a 4×4 square lattice. (c) shows their transition graph with two closed loops of length 4.

may assume the set of all hard core coverings to form an orthonormal basis set in the following.

Note also that we can classify the possible configurations according to their topological winding numbers \mathcal{W}_x and \mathcal{W}_y , defined as follows: Choose a straight line through the lattice, either horizontal or vertical. Then count the number of dimers in a given configuration that cross this line, with a positive sign for dimers emanating from the first sublattice and a negative sign for those emanating from the second sublattice. Using the operators from above we can write

$$\mathcal{W}_\eta = \sum_{i_\eta} (-1)^{i_\eta} D_{(i_\eta, i_{\bar{\eta}}), \bar{\eta}}^\dagger D_{(i_\eta, i_{\bar{\eta}}), \bar{\eta}} \quad (2.6)$$

for the winding numbers \mathcal{W}_η , $\eta = x, y$. These numbers are invariant under the local plaquette flips from above and are therefore topologically protected. Starting from a given configuration $|c\rangle$, the dynamics induced by the Hamiltonian Eq.(2.2) is ergodic only in the winding number sector of the starting configuration. Notice that the topological ground state degeneracy is what allows for the abovementioned apparent violation of the Luttinger theorem [1]. In all considerations of Sec.(3), (4) and (5) we will assume the system to be in the sector of vanishing winding number.

The ground states of the RK model can then be determined for the three parameter regions $V > J$, $V < J$ and $V = J$. For $V > J$, the energy offset of flippable plaquettes dominates and at $T = 0$ the ground state will be a staggered state, see. Fig.(4). On the other side, for $V < J$, the flip term dominates and favours an increased number of flippable plaquettes, therefore leading to a so-called plaquette phase for $V_c < V < J$. Upon decreasing $V < V_c$ further, the ground state maximizes the number of flippable plaquettes and shows columnar order, see also Fig.(4). In the above cases, the ground state is a so-called Valence Bond Solid (VBS) state. At the special point $J = V$, the Hamiltonian from Eq.(2.2) can be written as a sum of projectors,

$$H_{RK} = \sum_{\text{plaq}} V \left(|00\rangle - |\equiv\rangle \right) \left(\langle 00| - \langle \equiv| \right), \quad (2.7)$$

The unique ground state within each topological sector can then be shown to be the equal weight superposition of all states within that sector,

$$|RK\rangle = \frac{1}{\sqrt{\mathcal{N}}} \sum_c |c\rangle, \quad (2.8)$$

where the normalization \mathcal{N} is given by number of configurations. The exactly solvable RK point $V = J$ thus constitutes a critical point with a $U(1)$ spin liquid ground state which is unstable towards ordered VBS states for perturbations in the parameters V and J away from $V = J$. At the RK point, the expectation value of a given observable O can be computed as

$$\langle O \rangle = \langle RK | O | RK \rangle = \frac{\sum_{c,c'} \langle c | O | c' \rangle}{\sum_{c,c'} \langle c | c' \rangle}, \quad (2.9)$$

i.e. by the expectation value of the classical model at $T \rightarrow \infty$. We will make use of this correspondence throughout this work, as it will allow to employ the exact solution of the classical dimer problem, found in [38]. For a more complete introduction to dimer models, see e.g. [39].

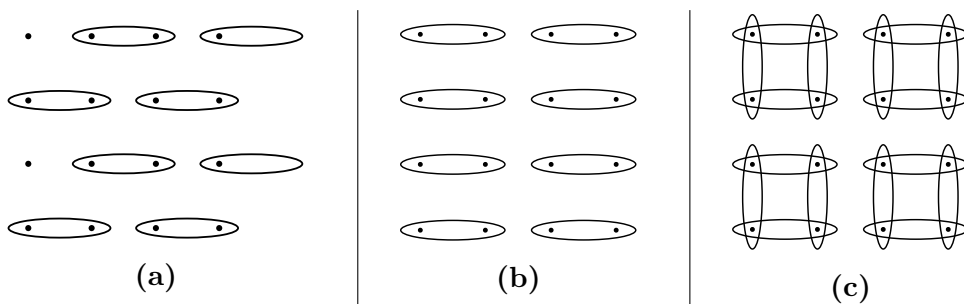


Figure 4: VBS ground states of the RK model, (a) staggered state for $V > J$, (b) columnar state for $V < V_c < J$, (c) plaquette phase for $V_c < V < J$. The state shown in (c) has to be interpreted as a probability distribution for the dimer density.

2.2 Correlations in the classical dimer model

As pointed out in the previous section, the RK-point allows to compute properties of the quantum model at $T = 0$ via the classical dimer problem at $T \rightarrow \infty$. An object of repeated interest in this work is the classical dimer correlation function

$$Q_c[(i, \eta), (j, \tau)] = \left\langle \hat{N}_{i, \eta} \hat{N}_{j, \tau} \right\rangle, \quad (2.10)$$

which counts the number of configurations with two dimers fixed at (i, η) and (j, τ) with respect to the total number of configurations. In this notation, (i, η) describes the link connecting the sites at i and $i + \hat{\eta}$. These correlations have first been solved by Fisher and Stephenson in [38]. Here, we will review how to calculate such correlations using a Grassmanian field theory, see [40] and the appendix of [1]. The idea is to implement the hard-core constraint that the dimers are subject to by setting up a quadratic action using Grassman variables and subsequently using Wick's theorem to compute the correlations of interest.

For the square lattice, we associate with every site i a pair $\eta_i, \bar{\eta}_i$ of Grassman variables. A dimer residing on the link between sites i and $i + \hat{\tau}$ has four possible representations:

1. $d_{i, \tau}^1 = \bar{\eta}_i \eta_{i + \hat{\tau}}$, graphically: $\begin{array}{c} \times \\ \leftarrow \\ i \end{array} \longrightarrow \begin{array}{c} \ominus \\ i + \tau \end{array}$

2. $d_{i,\tau}^2 = \bar{\eta}_{i+\hat{\tau}}\eta_i$, graphically: $\bigcirc_i \longleftarrow \times_{i+\tau}$
3. $d_{i,\tau}^3 = \eta_{i+\hat{\tau}}\bar{\eta}_i$, graphically: $\times_i \longleftarrow \bigcirc_{i+\tau}$
4. $d_{i,\tau}^4 = \eta_i\bar{\eta}_{i+\hat{\tau}}$, graphically: $\bigcirc_i \longrightarrow \times_{i+\tau}$

Here, \times labels the conjugate variables $\bar{\eta}$, \circ the η . The arrow on the bond then points into the direction of the variable to the right. The classical partition function is given by

$$Z_{class} = \int D[\eta, \bar{\eta}] \exp\{S[\eta, \bar{\eta}]\} \quad (2.11)$$

with an action $S[\eta, \bar{\eta}]$ which is quadratic in the Grassman fields. This partition function is supposed to simply count all allowed closed-packed dimer coverings on the square lattice. We thus need to set up $S[\eta, \bar{\eta}]$ such that expanding the exponential and integrating over $d\eta d\bar{\eta}$, only the close-packed coverings survive and yield a positive contribution. The natural Ansatz for S is thus

$$S[\eta, \bar{\eta}] = \sum_{i,\tau} d_{i,\tau}^{k_{i,\tau}}, \quad (2.12)$$

where the indices $k_{i,\tau} \in \{1, 2, 3, 4\}$ need to be fixed suitably for every link such that the hard-core constraint is implemented. Graphically, we need to cover the links of the square lattice with the graphical representations of d^k .

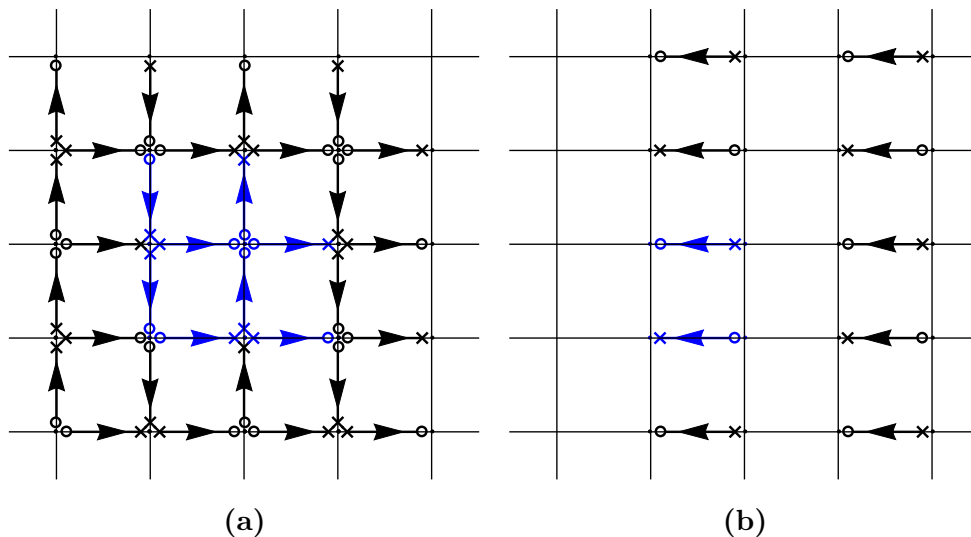


Figure 5: (a) shows a covering of the square lattice with Grassman variables, where \circ corresponds to η and \times to $\bar{\eta}$. The blue colored dimers represent the unit cell which fills the lattice upon repeated translations of twice the lattice constant. (b) shows a reference close packed dimer covering of the lattice, with ordering of \circ , \times and the arrows such that only allowed close-packed coverings yield positive contributions to the partition function of Eq.(2.11) with the action of Eq.(2.14). Again, the blue colored dimers mark the unit cell.

We show in Fig.(5a) such a covering that realizes the constraint. This is because at a given site i on the lattice, any dimer connected to this site must contribute a Grassman variable η_i if i is on the say A sublattice, and $\bar{\eta}_i$ if i is on the B sublattice. Thus, if in an expansion of the exponential with the action from Eq.(2.12) there were two dimers connected to site i , they would contribute either a factor $\eta_i^2 = 0$ or $\bar{\eta}_i^2 = 0$. Hence, such constraint-violating terms are automatically ruled out (i.e. they yield a vanishing contribution) by the covering of Fig.(5a). Note that a given term in the expansion of $\exp\{S\}$ only gives a non-vanishing contribution to Z_{class} if for every site i the two Grassman variables η_i and $\bar{\eta}_i$ appear in the term. This is due to the property $\int d\eta = 0$ of Grassman integrals. The covering of Fig.(5a) (which translates into an action S from Eq.(2.12)) yields terms that do not violate the constraint upon expanding the exponential, but only contributes at most either η_i or $\bar{\eta}_i$ at every link. In order to obtain non-vanishing contributions of the close-packed coverings we thus need to add a "reference covering" to the action Eq.(2.12). Such a reference covering is shown in Fig.(5b) and leads to a new action

$$S[\eta, \bar{\eta}] = \sum_{i,\tau} d_{i,\tau}^{k_{i,\tau}} + \sum_{i,\tau} c_{i,\tau} d_{i,\tau}^{q_{i,\tau}}, \quad (2.13)$$

where the indices $k_{i,\tau}$ are fixed by the covering shown in Fig.(5a) while the coefficients $c_{i,\tau} \in \{0, 1\}$ as well as the indices $q_{i,\tau}$ are fixed by the reference covering of Fig.(5b). Note that on sites where Fig.(5a) features only \circ (\times), Fig.(5b) features only \times (\circ), i.e. a reversed structure. This way, when expanding the exponential with the action of Eq.(2.13), only those terms survive the integral $\int d\eta d\bar{\eta}$ that correspond to close-packed coverings of the lattice, obtained by expanding in $\sum_{i,\tau} d_{i,\tau}^{k_{i,\tau}}$ and yielding either η_i or $\bar{\eta}_i$ at every site. The missing conjugate variables $\bar{\eta}_i$ and η_i then stem from expanding as well in the second term $\sum_{i,\tau} c_{i,\tau} d_{i,\tau}^{q_{i,\tau}}$.

We have thus shown that the structure of Fig.(5) implies that only close-packed coverings have non-vanishing contributions to the partition function. A non-trivial task is to show that indeed they all have a positive contribution $+1$. This is achieved by the ordering of the arrows in the coverings of Fig.(5). A detailed analysis of this problem and the proof that the arrows of Fig.(5) indeed yield positive contributions is given in [40]. As a short summary, the ordering of the arrows in Fig.(5a) has to be such that going clockwise around an elementary polygon, i.e. a plaquette, the number of arrows pointing in the anti-clockwise direction is odd. The ordering of the arrows in Fig.(5b) then needs to be exactly opposite to the corresponding arrows in Fig.(5a). Hence, other choices than those of Fig.(5) are possible as well, compare e.g. the Appendix of [1].

We are now able to write down the action of Eq.(2.13) explicitly by taking the graph-

ical representation of Fig.(5) and mapping back to the algebraic formulation:

$$\begin{aligned}
 S[\eta, \bar{\eta}] &= \sum_{i,\tau} d_{i,\tau}^{k_{i,\tau}} + \sum_{i,\tau} c_{i,\tau} d_{i,\tau}^{q_{i,\tau}} = \\
 &= \sum_{m,n} \left\{ \eta_{2m,2n} \bar{\eta}_{2m+1,2n} + \bar{\eta}_{2m,2n+1} \eta_{2m,2n} + \right. \\
 &\quad + \bar{\eta}_{2m+1,2n} \eta_{2m+1,2n+1} + \bar{\eta}_{2m,2n+1} \eta_{2m+1,2n+1} + \\
 &\quad + \eta_{2m,2n+2} \bar{\eta}_{2m,2n+1} + \eta_{2m+1,2n+1} \bar{\eta}_{2m+1,2n+2} + \\
 &\quad \left. + \bar{\eta}_{2m+1,2n} \eta_{2m+2,2n} + \eta_{2m+1,2n+1} \bar{\eta}_{2m+2,2n+1} \right\} + \\
 &\quad + \sum_{m,n} \left\{ \eta_{2m+1,2n} \bar{\eta}_{2m,2n} + \bar{\eta}_{2m+1,2n+1} \eta_{2m,2n+1} \right\}.
 \end{aligned} \tag{2.14}$$

To solve for the partition function we can rewrite the action of Eq.(2.14) in momentum space via the definition

$$\begin{aligned}
 \eta_{2m,2n} &= \int \frac{dp dq}{(2\pi)^2} e^{i(pm+qn)} \chi_{p,q}^1 \\
 \eta_{2m+1,2n} &= \int \frac{dp dq}{(2\pi)^2} e^{i(pm+qn)} \chi_{p,q}^2 \\
 \eta_{2m,2n+1} &= \int \frac{dp dq}{(2\pi)^2} e^{i(pm+qn)} \chi_{p,q}^3 \\
 \eta_{2m+1,2n+1} &= \int \frac{dp dq}{(2\pi)^2} e^{i(pm+qn)} \chi_{p,q}^4,
 \end{aligned} \tag{2.15}$$

which leads to

$$S[\chi, \bar{\chi}] = \int \frac{dp dq}{(2\pi)^2} (\bar{\chi})^T \begin{pmatrix} 0 & 1 - e^{ip} & -1 + e^{iq} & 0 \\ 1 & 0 & 0 & 0 \\ 0 & 0 & 0 & -1 \\ 0 & -1 + e^{-iq} & -1 + e^{-ip} & 0 \end{pmatrix} \bar{\chi} = \int \frac{dp dq}{(2\pi)^2} (\bar{\chi})^T \cdot \underline{K} \cdot \bar{\chi}. \tag{2.16}$$

Since Eq.(2.16) represents a quadratic theory, we can compute all correlations of interest by Gaussian integrals using Wick's theorem. As an example, we derive the probability of finding a dimer at an arbitrary link on the lattice, say e.g. the link $((2m, 2n), x)$. We find

$$\begin{aligned}
 Q_c[((2m, 2n), x)] &= \langle \eta_{2m,2n} \bar{\eta}_{2m+1,2n} \rangle = \int \frac{dp dq}{(2\pi)^2} \langle \chi_{p,q}^1 \bar{\chi}_{p,q}^2 \rangle = \int \frac{dp dq}{(2\pi)^2} [\underline{K}^{-1}]_{2,1}(p, q) = \\
 &= \int \frac{dp dq}{(2\pi)^2} \frac{1 - e^{-ip}}{4 - 2 \cos(p) - 2 \cos(q)} = \frac{1}{4},
 \end{aligned} \tag{2.17}$$

which corresponds to the expected outcome. Using Wick's theorem, we can compute higher correlation functions, e.g. the probability of having two dimers in a flippable plaquette position as defined in the previous section. The result is

$$\begin{aligned}
 Q_c[((2m, 2n), x), ((2m, 2n+1), x)] &= \langle \eta_{2m,2n} \bar{\eta}_{2m+1,2n} \bar{\eta}_{2m,2n+1} \eta_{2m+1,2n+1} \rangle = \\
 &= \langle \eta_{2m,2n} \bar{\eta}_{2m+1,2n} \rangle \langle \bar{\eta}_{2m,2n+1} \eta_{2m+1,2n+1} \rangle + \langle \eta_{2m,2n} \bar{\eta}_{2m,2n+1} \rangle \langle \eta_{2m+1,2n+1} \bar{\eta}_{2m+1,2n} \rangle
 \end{aligned} \tag{2.18}$$

The first term of Eq.(2.18) simply multiplies two probabilities of having a dimer at a given site. The same holds true for the two averages in the second term. We can thus compute

$$Q_c[((2m, 2n), x), ((2m, 2n + 1), x)] = \left(\frac{1}{4}\right)^2 + \left(\frac{1}{4}\right)^2 = \frac{1}{8}, \quad (2.19)$$

and the conditional probability for finding a second dimer in certain flippable plaquette position relative to a fixed first dimer is then given by $Q_c[((2m, 2n), x)|((2m, 2n + 1), x)] = 1/2$.

As a final example, we compute the probability of finding two dimers in a fixed relative position to each other described by

$$\begin{aligned} Q_c \left[\begin{array}{c} \text{---} \\ \text{---} \end{array} \right] &= \langle \eta_{2m, 2n} \bar{\eta}_{2m+1, 2n} \bar{\eta}_{2m+2, 2n+1} \eta_{2m+2, 2n} \rangle = \\ &= \langle \eta_{2m, 2n} \bar{\eta}_{2m+1, 2n} \rangle \langle \bar{\eta}_{2m+2, 2n+1} \eta_{2m+2, 2n} \rangle + \\ &\quad + \langle \eta_{2m, 2n} \bar{\eta}_{2m+2, 2n+1} \rangle \langle \eta_{2m+2, 2n} \bar{\eta}_{2m+1, 2n} \rangle = \\ &= \left(\frac{1}{4}\right)^2 + \int \frac{dp dq}{(2\pi)^2} e^{-ip} [\underline{K}^{-1}]_{3,1}(p, q) \times \left(-\frac{1}{4}\right) = \\ &= \frac{1}{16} + \frac{1}{4} \int \frac{dp dq}{(2\pi)^2} e^{-ip} \frac{1 - e^{-iq}}{4 - 2 \cos(p) - 2 \cos(q)} = \frac{1}{4\pi}. \end{aligned} \quad (2.20)$$

Note also that within this framework the long-range correlations of the classical dimer model can be determined as well, see e.g. [38, 41]. These correlations take the form

$$Q_c[(0, x), ((X, Y), x)] = \frac{1}{16} + \frac{1}{2\pi^2} \left[(-1)^{X+Y} \frac{Y^2 - X^2}{R^4} + (-1)^X \frac{1}{R^2} \right], \quad (2.21)$$

as an example for two x -oriented dimers, with $R^2 = X^2 + Y^2$. We note that the classical correlations on the square lattice generally decay algebraically with exponent ≥ 2 .

2.3 A quantum dimer model for the cuprate pseudogap phase

We review the construction of the dimer model from [1] and consider a mean field approach that has been carried out in [42] and the Appendix of [1] in order to compute the fermionic quasiparticle dispersion.

2.3.1 Model

The basic ingredient of this model is the presence of a new species of dimers that is expected to arise upon doping the system away from half-filling. Doping holes into the system breaks up bosonic singlet dimers and leaves unoccupied sites as well as spin $S = 1/2$ particles. These can be regarded as two separate quasiparticles into which the inserted hole fractionalizes. The first is the so-called holon, which corresponds to a charge $+e$, spinless particle. The second is the spinon, which carries spin $1/2$ but no charge. In the 2D square lattice RK model at the RK-point, these fractionalized excitations are in a deconfined phase and can in principle move freely on the lattice. The central idea of [1] is to assume that in a hole-doped antiferromagnet, spinon and holon form a bound state across two neighbouring

lattice sites, thus forming a fermionic dimer with charge $+e$ and spin $S = 1/2$, the quantum numbers of the inserted holes. This fermionic dimer can then be described by the expression

$$F_{i,\eta,\alpha}^\dagger |0\rangle \rightarrow \mathcal{Y}_{i,\eta} \frac{1}{\sqrt{2}} \left(c_{i,\alpha}^\dagger + c_{i+\hat{\eta},\alpha}^\dagger \right) |0\rangle \quad (2.22)$$

and the low energy Hilbert space is considered to be the space of hard-core coverings on the lattice with a certain number of fermionic dimers, corresponding to a fixed doping $p = N_f/N$. Note that since spinon and holon are deconfined at the RK-point, the formation of bound states is solely due to energetic favourability. A 2-site DMFT analysis conducted in [43] on the Hubbard model confirms that such bound states indeed occur in the low energy regime of the respective models away from half-filling. In all following considerations, the system is assumed to be at the RK-point, or close enough to have a large confinement scale compared to the separation between fermionic dimers such that the above mentioned Hilbert space can capture the low energy behaviour of the model. With this setup, there are electron-like fermions with density p in the system, as required to explain the Fermi liquid behaviour proportional to a carrier density p that was experimentally found in transport measurements.

The Hamiltonian introduced in [1] for the newly introduced Hilbert space reads

$$\begin{aligned} H &= H_{RK} + H_1 \\ H_1 &= -t_1 \sum_i F_{i,x,\alpha}^\dagger D_{i+\hat{y},x}^\dagger D_{i,x} F_{i+\hat{y},x,\alpha} + 3 \text{ terms} \\ &\quad - t_2 \sum_i F_{i,x,\alpha}^\dagger D_{i+\hat{y},x}^\dagger D_{i+\hat{x},y} F_{i,y,\alpha} + 7 \text{ terms} \\ &\quad - t_3 \sum_i F_{i,x,\alpha}^\dagger D_{i+2\hat{x},y}^\dagger D_{i,x} F_{i+2\hat{x},y,\alpha} + 7 \text{ terms} \\ &\quad - t_3 \sum_i F_{i,x,\alpha}^\dagger D_{i+\hat{x}+\hat{y},y}^\dagger D_{i,x} F_{i+\hat{x}+\hat{y},y,\alpha} + 7 \text{ terms,} \end{aligned} \quad (2.23)$$

where the terms not explicitly written out are obtained by lattice symmetry group operations on the displayed terms. The parameters t_i of Eq.(2.23) can be related directly to the parameters of the t - J -model via a perturbative mapping described in the Appendix of [1]. The terms of H_1 are displayed graphically in Fig.(6).

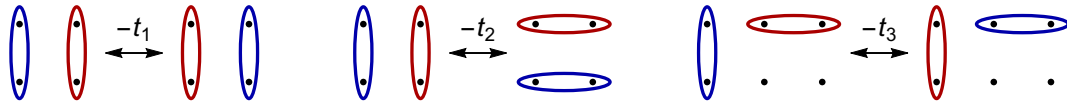


Figure 6: Resonance processes between fermionic (red) and bosonic (blue) dimers from the Hamiltonian of Eq.(2.23)

The authors of [1] carried out exact diagonalization studies in systems with one fermionic dimer on lattice sizes up to 8×8 to find the dispersion of the fermionic quasiparticles, as well as the corresponding quasiparticle residuum, defined by

$$\mathcal{Z}(\mathbf{p}) = |\langle \psi_0(\mathbf{p}) | c_{-\mathbf{p}} | RK \rangle|^2, \quad (2.24)$$

with the ground state $\psi_0(\mathbf{p})$ of momentum \mathbf{p} that includes one fermionic dimer. In order to evaluate this expression within the dimer Hilber space, a representation of the electron operator on a given site i of the lattice in the dimer basis can be found as shown in [1],

$$c_{i,\alpha} = \frac{\epsilon_{\alpha\gamma}}{2} \left(F_{i,x,\gamma}^\dagger D_{i,x} + F_{i-\hat{x},x,\gamma}^\dagger D_{i-\hat{x},x} + F_{i,y,\gamma}^\dagger D_{i,y} + F_{i-\hat{y},y,\gamma}^\dagger D_{i-\hat{y},y} \right), \quad (2.25)$$

where $\epsilon_{\alpha\gamma}$ is the unit antisymmetric tensor.

2.3.2 Mean field theory

We review the construction of a mean field theory from [1] and [42] that maps the system specified by the Hamiltonian of Eq.(2.23) to a theory of non-interacting fermions, which allows to approximate the fermion dispersion in the regime $t_i \ll J = 1$ of small interactions between fermions and bosons. Energies are given in units of J .

To gain information about the behaviour of the fermionic quasiparticles in the system we can decouple the mixed dimer species interaction terms of H_1 in the bosonic channel to produce a mean field model for the fermions. The mean field Hamiltonian obtained by this procedure reads

$$\begin{aligned} H_1^{MF} = & -t_1 \sum_i F_{i,x,\alpha}^\dagger \left\langle D_{i+\hat{y},x}^\dagger D_{i,x} \right\rangle F_{i+\hat{y},x,\alpha} + 3 \text{ terms} \\ & -t_2 \sum_i F_{i,x,\alpha}^\dagger \left\langle D_{i+\hat{y},x}^\dagger D_{i+\hat{x},y} \right\rangle F_{i,y,\alpha} + 7 \text{ terms} \\ & -t_3 \sum_i F_{i,x,\alpha}^\dagger \left\langle D_{i+2\hat{x},y}^\dagger D_{i,x} \right\rangle F_{i+2\hat{x},y,\alpha} + 7 \text{ terms} \\ & -t_3 \sum_i F_{i,x,\alpha}^\dagger \left\langle D_{i+\hat{x}+\hat{y},y}^\dagger D_{i,x} \right\rangle F_{i+\hat{x}+\hat{y},y,\alpha} + 7 \text{ terms,} \end{aligned} \quad (2.26)$$

which is described by the mean fields $\chi_{(i,\eta),(j,\tau)} := \left\langle D_{i,\eta}^\dagger D_{j,\tau} \right\rangle$. To ensure invariance of the mean field Hamiltonian H_1^{MF} with respect to the underlying symmetries of the model, the mean fields χ must be invariant under transformations of the symmetry group of the square lattice. In result, we are left with merely three distinct mean fields in Eq.(2.26),

$$\chi_1 = \left\langle D_{i+\hat{y},x}^\dagger D_{i,x} \right\rangle, \quad \chi_2 = \left\langle D_{i,x}^\dagger D_{i,y} \right\rangle, \quad \chi_3 = \left\langle D_{i+2\hat{x},y}^\dagger D_{i,x} \right\rangle \quad (2.27)$$

which can be absorbed into a redefinition $t_i \rightarrow \chi_i t_i =: \tilde{t}_i$ of the interaction parameters t_i . The resulting quadratic, noninteracting model can be expressed in momentum space in 2×2 matrix structure

$$H_1^{MF} = \begin{pmatrix} F_{\mathbf{p},x,\alpha}^\dagger \\ F_{\mathbf{p},y,\alpha}^\dagger \end{pmatrix} \cdot \begin{pmatrix} -2\tilde{t}_1 \cos(p_y) & C(\mathbf{p}) \\ C^*(\mathbf{p}) & -2\tilde{t}_1 \cos(p_x) \end{pmatrix} \cdot \begin{pmatrix} F_{\mathbf{p},x,\alpha} \\ F_{\mathbf{p},y,\alpha} \end{pmatrix}, \quad (2.28)$$

where the two components of $(F_{\mathbf{p},x,\alpha}^\dagger, F_{\mathbf{p},y,\alpha}^\dagger)$ correspond to the orientation flavor of the fermions. The term $C(\mathbf{p})$ is given by

$$C(\mathbf{p}) = -\tilde{t}_2(1 + e^{ip_x})(1 + e^{-ip_y}) - \tilde{t}_3 \left[(1 + e^{ip_x})(e^{ip_y} + e^{-2ip_y}) + (1 + e^{-ip_y})(e^{2ip_x} + e^{-ip_x}) \right]. \quad (2.29)$$

Eq.(2.28) describes a tight-binding model of fermions hopping on the links of a square lattice. The corresponding fermionic dispersion is given by the eigenvalues of the 2×2 matrix in H_1^{MF} , i.e.

$$\varepsilon(\mathbf{p}) = -\tilde{t}_1(\cos(p_x) + \cos(p_y)) \pm \sqrt{\tilde{t}_1^2(\cos(p_x) - \cos(p_y))^2 + |C(\mathbf{p})|^2}. \quad (2.30)$$

In order to compare this dispersion to numerical results, an estimate for χ_1 , χ_2 and χ_3 is required. Usually, the parameters of a given mean field model are determined by imposing a self-consistent equation for the mean-fields. Equivalently, the resulting free energy has to be minimized with respect to the mean-fields χ_i . Note that decoupling the bosons from the fermions in the Hamiltonian of Eq.(2.26) leaves us merely with a non-interacting fermionic system. In particular, the mean-field decoupled H_1^{MF} does not feature a penalty term for values of the mean fields differing from some favoured value in the limit $t_i = 0$ of vanishing inter-dimer species interactions. Such a penalty term is expected to arise from the usual bosonic RK Hamiltonian, which we could in principle decouple in the same channel as performed for the part H_1 of the full Hamiltonian. However, a mean field decoupled version of H_{RK} will not be able to provide a reliable description of the RK model. Instead, in the range of small interaction parameters $t_i/J \ll 1$ we can do much better since an exact solution of the RK model is available and can be traced back to the classical case explored in the previous sections. Here, a suitable approximation in the regime of small $t_i \ll J$ is to fix the χ_i via the classical correlations introduced in the previous section. This idea corresponds to multiplying the original interaction parameter t_i with the classical conditional probability of finding a bosonic dimer in a suitable position relative to the fermion such that a t_i process can occur, yielding the hopping parameters

$$\tilde{t}_i = t_i \cdot \frac{Q_c[(0, x), (\mathbf{r}_{t_i}, x + \eta_{t_i})]}{Q_c[(0, x)]} \equiv t_i \cdot Q_c[(\mathbf{r}_{t_i}, x + \eta_{t_i})|(0, x)] \quad (2.31)$$

where \mathbf{r}_{t_i} and η_{t_i} are displacement vector and change in orientation of the bosonic dimer relative to the fermion in a given t_i process. As laid out in [1], this approach assumes an equal weight bosonic background configuration, which can be assumed true for the considered limit $t_i \ll J$. Using the relations found in Eq.(2.19) and (2.20) we find $\tilde{t}_1 = \frac{1}{2}t_1$, $\tilde{t}_2 = \frac{1}{2}t_2$ and $\tilde{t}_3 = \frac{1}{\pi}t_3$. Examples for the resulting fermion dispersion from Eq.(2.30) and comparison with results obtained from exact diagonalization studies on a 6×6 lattice are given in Fig.(15) and (16).

Note that for parameters outside the regime of small boson-fermion interactions, we can interpret the mean-fields as effective classical dimer correlations which differ from the just introduced $t_i = 0$ correlations due to the presence of fermionic interactions with the bosonic background. Close to such an inserted fermion, the t_i interactions will cause modified correlations with respect to the classical dimer model that resume their classical values upon moving away from the fermion and into the bosonic bulk. The H_{RK} Hamiltonian then penalizes the modifications of the correlations close to the fermion and thus limits the region in which such modifications take place. The crucial ingredient in modelling such an approach is to find a suitable expression for the energy penalty associated to altered correlations. We will come back to this question in the context of a maximally simplified fermion-boson model (featuring only t_1 -processes) later in Sec.(5). For now, we intend to

find a suitable description not only of the dispersion but also the quasiparticle residue and thus of the coherent part of the spectral function in the regime of small t_i . As opposed to the mean-field approximation just reviewed, we will explore the use of diagrammatic techniques within this model, which we will find are made possible only because our dimer Hamiltonian effectively realizes a fractionalized Fermi liquid.

3 Diagrammatic approach for the spectral function

We present a diagrammatic approach to the dimer model at hand and compute the electron spectral function, from which dispersion and quasiparticle residuum can be inferred via a Bethe-Salpeter equation for the effective four-point vertex. Although our model Hamiltonian does not contain a quadratic part and therefore neither a small parameter that would rigorously justify the use of such a diagrammatic approach, we nevertheless find the results to give a good match to the numerical outcomes in a certain region of parameter space. We comment on the validity of this approach and note that diagrammatic approaches to systems without small parameters have successfully been applied before, see e.g. [44] for an fRG approach to a slave-fermion description of the frustrated Heisenberg model on a square lattice. Our model yet differs from such slave fermion descriptions of spin systems, as we also encounter bosons on the links of the lattice, which leads to complications in the diagrammatic implementation of the hard-core constraint. Furthermore, the RK model can be rephrased as a U(1) gauge theory with instabilities towards confining VBS states for any set of parameters differing from $J = V$. A perturbative expansion in J or V can thus not be realized within a diagrammatic approach and we need to implement to properties of the bosonic background system at $J = V$ into the following diagrammatics via a different method, laid out in Sec.(3.4). A condensed version of the following results can be found as a section in [34].

3.1 Functional approach

This section is devoted to establishing the basis of our approach and to developing functional expressions for the quantities we aim to investigate. We set up the path integral action of our dimer model and express the electronic spectral function in a way suitable to be tackled within this framework. We go through this calculation step by step to keep track of the correct signs and prefactors.

3.1.1 The action

We introduce imaginary time-dependent complex-valued fields $\bar{D}_{i,\eta}(\tau), D_{i,\eta}(\tau)$ for the bosonic, as well as Grassmann-valued fields $\bar{F}_{i,\eta,\alpha}(\tau), F_{i,\eta,\alpha}(\tau)$ for the fermionic degrees of freedom and start out with the functional integral expression for the partition function,

$$Z = \int \mathcal{D}[\bar{D}, \bar{F}, D, F] \exp\left\{-S[\bar{D}, \bar{F}, D, F]\right\}, \quad (3.1)$$

and the associated expectation values, respective correlation functions,

$$\langle A[\bar{D}, \bar{F}, D, F] \rangle = \frac{1}{Z} \int \mathcal{D}[\bar{D}, \bar{F}, D, F] A[\bar{D}, \bar{F}, D, F] \exp\left\{-S[\bar{D}, \bar{F}, D, F]\right\}, \quad (3.2)$$

where the quantity $A[\bar{D}, \bar{F}, D, F]$ depends on the fields \bar{D}, \bar{F}, D, F . The above expressions are determined by the imaginary time action

$$\begin{aligned}
 S[\bar{F}, \bar{D}, F, D] = \int_0^\beta d\tau \left\{ H[\bar{F}(\tau), \bar{D}(\tau), F(\tau), D(\tau)] + \sum_{i,\eta,\alpha} \bar{F}_{i,\eta,\alpha}(\tau) (\partial_\tau - \mu_f) F_{i,\eta,\alpha}(\tau) \right. \\
 \left. + \sum_{i,\eta} \bar{D}_{i,\eta}(\tau) (\partial_\tau - \mu_b) D_{i,\eta}(\tau) \right\},
 \end{aligned} \tag{3.3}$$

with the full, normal ordered model Hamiltonian and with additional chemical potentials μ_f and μ_b fixing the densities of fermionic and bosonic dimers on a mean field level. The imaginary time label assumes values in $[0, \beta]$, where β denotes inverse temperature.

Note that assuming constant chemical potentials for the two dimer species (i.e. translational invariant, $\mu_{b/f,i,\eta_1} = \mu_{b/f,j,\eta_2}$ and independent of each other) corresponds to a parameter regime in which the ground state is translational invariant, consistent with the RVB state which the bosonic background is assumed to adopt. In other words, we expect our approach to be valid in a regime of small t_i -parameters, as for $t_i = 0$, the translational invariant RVB state is the exact ground state of the model. More precisely, $t_i/J \ll 1$ and small doping $p \ll 1$ are two requirements for the validity of this functional approach. In the following we will work with the chemical potentials that arise from the conditions

$$n_F(-\mu_f) = \frac{1}{e^{-\beta\mu_f} + 1} = \frac{p}{4} \tag{3.4}$$

and

$$n_B(-\mu_b) = \frac{1}{e^{-\beta\mu_b} - 1} = \frac{1-p}{4} \tag{3.5}$$

for the average fermionic/bosonic dimer density on a given link of the lattice. Here, n_F and n_B denote the Fermi-Dirac- and the Bose-Einstein-distribution, respectively. They obey the relation

$$n_F(-\mu_f) + n_B(-\mu_b) = \frac{1}{4} \tag{3.6}$$

for all values p of the doping (as well as for all temperatures, where we will always take the limit $T \rightarrow 0$ to compare the results to exact diagonalization outcomes), in concordance with the hard-core requirement on a mean field level.

As mentioned in the prelude to Sec.(3), we can not expect a perturbative expansion of the action in H_{RK} to yield realistic results. Thus, for all practical purposes, we neglect H_{RK} in the action of Eq.(3.3) and only use the boson-fermion interactions of H_1 for expansions in the parameters t_i . This leaves us with an action that assumes a translational invariant and static bosonic background, with the hard-core constraint implemented on a mean field level via the chemical potential.

Changing into momentum and frequency basis results in the following action,

$$\begin{aligned}
 S[\bar{F}, \bar{D}, F, D] = \sum_{q_1, q_2, q_3, q_4} \left\{ H[\bar{F}_{q_1}, \bar{D}_{q_2}, D_{q_3}, F_{q_4}] \right\} \times \delta(q_1 + q_2 - q_3 - q_4) + \\
 + \sum_{q,\eta,\alpha} \bar{F}_{q,\eta,\alpha}(i\omega) (-i\omega - \mu_f) F_{q,\eta,\alpha}(i\omega) + \sum_{q,\eta} \bar{D}_{q,\eta}(i\omega) (-i\omega - \mu_b) D_{q,\eta}(i\omega).
 \end{aligned} \tag{3.7}$$

Here, $q = (\mathbf{q}, i\omega)$ with $\mathbf{q} = (q_x, q_y)$ and $\sum_q = \sum_{\mathbf{q}, i\omega}$ denotes the sum over momenta \mathbf{q} as well as Matsubara frequencies $i\omega$, which take the values $i\omega = 2\pi in/\beta$ for bosonic and $\pi i(2n+1)/\beta$ for fermionic degrees of freedom ($n \in \mathbb{N}$). The momentum space form of the part of the Hamiltonian which contains interactions between fermionic and bosonic dimers is in turn given by

$$H_1 = H_{t_1} + H_{t_2} + H_{t_3}, \quad (3.8)$$

where the three terms corresponding to the three fundamental interaction processes are

$$H_{t_1} = -\frac{t_1}{\beta N} \sum_{q_1, \dots, q_4} \left\{ (e^{i(q_{4,y}-q_{2,y})} + e^{i(q_{3,y}-q_{1,y})}) \bar{F}_{q_1,x} \bar{D}_{q_2,x} D_{q_3,x} F_{q_4,x} + \right. \\ \left. + (e^{i(q_{4,x}-q_{2,x})} + e^{i(q_{3,x}-q_{1,x})}) \bar{F}_{q_1,y} \bar{D}_{q_2,y} D_{q_3,y} F_{q_4,y} \right\} \delta(q_1 + q_2 - q_3 - q_4), \quad (3.9)$$

$$H_{t_2} = -\frac{t_2}{\beta N} \sum_{q_1, \dots, q_4} \left\{ (e^{i(q_{3,x}-q_{2,y})} + e^{i(q_{3,x}-q_{1,y})} + e^{i(q_{4,x}-q_{2,y})} + e^{i(q_{4,x}-q_{1,y})}) \bar{F}_{q_1,x} \bar{D}_{q_2,x} D_{q_3,y} F_{q_4,y} \right. \\ \left. + (x \leftrightarrow y) \bar{F}_{q_1,y} \bar{D}_{q_2,y} D_{q_3,x} F_{q_4,x} \right\} \delta(q_1 + q_2 - q_3 - q_4) \quad (3.10)$$

and

$$H_{t_3} = -\frac{t_3}{\beta N} \sum_{q_1, \dots, q_4} \left\{ (e^{i(q_{4,x}+q_{4,y}-q_{2,x}-q_{2,y})} + e^{i(q_{4,x}-q_{2,x})} + e^{i(q_{4,y}-2q_{4,x}-q_{2,y}+2q_{2,x})} + \right. \\ \left. + e^{i(-2q_{4,x}+2q_{2,x})} + e^{i(2q_{4,y}-2q_{2,y})} + e^{i(2q_{4,y}-q_{4,x}-2q_{2,y}+q_{2,x})} + e^{i(-q_{4,y}+q_{2,y})} + \right. \\ \left. + e^{i(-q_{4,x}-q_{4,y}+q_{2,x}+q_{2,y})}) \bar{F}_{q_1,y} \bar{D}_{q_2,x} D_{q_3,y} F_{q_4,x} + \right. \\ \left. + [\mathbf{q}_4 \leftrightarrow \mathbf{q}_3, \mathbf{q}_2 \leftrightarrow \mathbf{q}_1] \bar{F}_{q_1,x} \bar{D}_{q_2,y} D_{q_3,x} F_{q_4,y} \right\} \delta(q_1 + q_2 - q_3 - q_4), \quad (3.11)$$

with the total number N of lattice sites. As there are no quadratic terms in the Hamiltonian H , the bare Green's functions for the two dimer species are, respectively,

$$G_f^0(i\omega) = \frac{1}{i\omega + \mu_f} \quad (3.12)$$

for fermionic dimers and

$$G_b^0(i\omega) = \frac{1}{i\omega + \mu_b} \quad (3.13)$$

for bosonic dimers, where the Matsubara frequency involved is either fermionic or bosonic. Note that these bare propagators are diagonal in frequency, momentum and dimer orientation index, as well as independent of the latter two. Furthermore, changing into real space, the $G_{f/b}^0(i\omega)$ take the same form as in Eq.(3.12) and (3.13) and are thus diagonal in site index i as well. From here one can readily see that the absence of a dispersion in the propagators persists for the full propagators $G_{f/b}$, as hopping terms would violate the

hard-core constraint. We hence obtain the conditions for the real space dimer density on a given link, Eq.(3.4) and Eq.(3.5), from this functional approach via

$$\frac{1-p}{4} = \lim_{\tau \rightarrow 0^-} -G_b^0(\tau) = -\frac{1}{\beta} \sum_{i\omega} G_b^0(i\omega) e^{i\omega 0^+} = -\frac{1}{\beta} \sum_{i\omega} \frac{1}{i\omega + \mu_b} e^{i\omega 0^+} = n_b(-\mu_b), \quad (3.14)$$

where a convergence generating factor $e^{i\omega 0^+}$ is included in order for the sum over the bosonic Matsubara frequencies to converge. This important factor arises when going back to the derivation of the path integral expression for the propagator $G_b^0(i\omega) = -\langle D(i\omega) \bar{D}(i\omega) \rangle_0$ by splitting the imaginary time integral into small time steps and inserting complete sets of coherent eigenstates. The same argument of course holds true likewise for the fermionic dimer Green's function.

3.1.2 Spectral function

The quantity of interest in this section is the electronic spectral function which is defined as

$$\mathcal{A}(\mathbf{p}, \omega_p) = \frac{1}{\pi} \text{Im} \left[\frac{1}{\beta} \int d\tau e^{i\omega_p \tau} \left\langle \hat{\mathcal{T}}_\tau c_{\mathbf{p},\alpha}(\tau) c_{\mathbf{p},\alpha}^\dagger(0) \right\rangle \right]_{i\omega_p \rightarrow \omega_p + i0^+}, \quad (3.15)$$

where $c_{\mathbf{p},\alpha}(\tau)/c_{\mathbf{p},\alpha}^\dagger(\tau)$ denotes an electron annihilation/creation operator of momentum \mathbf{p} , spin α at imaginary time τ , the $i\omega_p$ are fermionic Matsubara frequencies. We hence need to calculate the imaginary time ordered electronic propagator expressed in momentum coordinates

$$\mathcal{G}_c(\mathbf{p}, \tau) = -\left\langle \hat{\mathcal{T}}_\tau c_{\mathbf{p},\alpha}(\tau) c_{\mathbf{p},\alpha}^\dagger(0) \right\rangle, \quad (3.16)$$

where $\hat{\mathcal{T}}_\tau$ represents the ordering operator for the imaginary time index τ . In order to switch to dimer representation, we employ the expression from Eq.(2.25) for the $c_{i,\alpha}$ in terms of dimer operators. After inserting the Fourier transform

$$F_{i-\hat{a},\eta,\gamma}^\dagger D_{i-\hat{a},\eta} = \frac{1}{N} \sum_{\mathbf{q}_1, \mathbf{q}_2} e^{-i(\mathbf{q}_1 - \mathbf{q}_2) \cdot \mathbf{i}} e^{i(\mathbf{q}_1 - \mathbf{q}_2) \cdot \hat{a}} F_{\mathbf{q}_1, \eta, \gamma}^\dagger D_{\mathbf{q}_2, \eta} \quad (3.17)$$

into Eq.(2.25) while staying in imaginary time formalism, we obtain the expression

$$c_{\mathbf{p},\alpha}(\tau) = \frac{\epsilon_{\alpha\gamma}}{2\sqrt{N}} \sum_{\eta \in \{x,y\}} (1 + e^{ip\eta}) \sum_q F_{\mathbf{q}, \eta, \gamma}^\dagger(\tau) D_{\mathbf{q}+\mathbf{p}, \eta}(\tau). \quad (3.18)$$

This leads to the relation

$$\begin{aligned} c_{\mathbf{p},\alpha}(\tau) c_{\mathbf{p},\alpha}^\dagger(0) &= \\ &= \frac{1}{4N} \sum_{\eta_1, \eta_2 \in \{x,y\}} (1 + e^{-ip\eta_1}) (1 + e^{ip\eta_2}) \sum_{\mathbf{q}_1, \mathbf{q}_2} F_{\mathbf{q}_1, \eta_1, \gamma}^\dagger(\tau) D_{\mathbf{q}_1+\mathbf{p}, \eta_1}(\tau) D_{\mathbf{q}_2+\mathbf{p}, \eta_2}^\dagger(0) F_{\mathbf{q}_2, \eta_2, \gamma}(0), \end{aligned} \quad (3.19)$$

where the fermionic dimer spin index is now implicitly fixed to $\gamma = -\alpha$, implying that the removal of an electron of spin α can only leave behind a fermion of spin $-\alpha$.

In order to find the spectral function, Eq.(3.19) shows that one needs to compute the imaginary time-ordered 4-point dimer correlation function

$$\left\langle \hat{\mathcal{T}}_\tau F_{\mathbf{q}_1, \eta_1, \gamma}^\dagger(\tau) D_{\mathbf{q}_1 + \mathbf{p}, \eta_1}(\tau) D_{\mathbf{q}_2 + \mathbf{p}, \eta_2}^\dagger(0) F_{\mathbf{q}_2, \eta_2, \gamma}(0) \right\rangle \quad (3.20)$$

which, within the functional framework, can be rewritten as

$$\left\langle \bar{F}_{\mathbf{q}_1, \eta_1, \gamma}(\tau) D_{\mathbf{q}_1 + \mathbf{p}, \eta_1}(\tau) \bar{D}_{\mathbf{q}_2 + \mathbf{p}, \eta_2}(0) F_{\mathbf{q}_2, \eta_2, \gamma}(0) \right\rangle, \quad (3.21)$$

where the average $\langle \dots \rangle$ is now taken in the functional sense of Eq.(3.2) with respect to the action given in Eq.(3.3). The time ordering from Eq.(3.20) is automatically accounted for in the functional approach. From here we change to Matsubara formalism by inserting a Fourier transform with respect to imaginary time:

$$\psi(i\omega) = \frac{1}{\sqrt{\beta}} \int_0^\beta d\tau e^{i\omega\tau} \psi(\tau) \longrightarrow \psi(\tau) = \frac{1}{\sqrt{\beta}} \sum_{i\omega} e^{-i\omega\tau} \psi(i\omega) \quad (3.22)$$

which leads to

$$\begin{aligned} \mathcal{G}_c(\mathbf{p}, \alpha, \tau) &= \\ &= -\frac{1}{4\beta N} \sum_{\eta_1, \eta_2 \in \{x, y\}} (1 + e^{-ip\eta_1}) (1 + e^{ip\eta_2}) \sum_{i\omega_1, \dots, i\omega_4} \sum_{\mathbf{q}_1, \mathbf{q}_2} \left\{ e^{(i\omega_1 - i\omega_4)\tau} \times \right. \\ &\quad \left. \left\langle \bar{F}_{\mathbf{q}_1, \eta_1, \gamma}(i\omega_1) D_{\mathbf{q}_1 + \mathbf{p}, \eta_1}(i\omega_4) \bar{D}_{\mathbf{q}_2 + \mathbf{p}, \eta_2}(i\omega_3) F_{\mathbf{q}_2, \eta_2, \gamma}(i\omega_2) \right\rangle \right\} \delta(i\omega_1 + i\omega_3 - i\omega_2 - i\omega_4). \end{aligned} \quad (3.23)$$

Applying another Fourier transform results in an expression for the electronic Green's function expressed in terms of Matsubara frequencies:

$$\begin{aligned} \mathcal{G}_c(\mathbf{p}, i\omega_p, \alpha) &= \frac{1}{\beta} \int d\tau e^{i\omega_p\tau} \mathcal{G}_c(\mathbf{p}, \tau, \alpha) = \\ &= -\frac{1}{4\beta^2 N} \int d\tau \sum_{\eta_1, \eta_2 \in \{x, y\}} (1 + e^{-ip\eta_1}) (1 + e^{ip\eta_2}) \sum_{i\omega_1, \dots, i\omega_4} \sum_{\mathbf{q}_1, \mathbf{q}_2} \left\{ e^{(i\omega_p + i\omega_1 - i\omega_4)\tau} \times \right. \\ &\quad \left. \left\langle \bar{F}_{\mathbf{q}_1, \eta_1, \gamma}(i\omega_1) D_{\mathbf{q}_1 + \mathbf{p}, \eta_1}(i\omega_4) \bar{D}_{\mathbf{q}_2 + \mathbf{p}, \eta_2}(i\omega_3) F_{\mathbf{q}_2, \eta_2, \gamma}(i\omega_2) \right\rangle \right\} \delta(i\omega_1 + i\omega_3 - i\omega_2 - i\omega_4) = \\ &= -\frac{1}{4\beta N} \sum_{\eta_1, \eta_2 \in \{x, y\}} (1 + e^{-ip\eta_1}) (1 + e^{ip\eta_2}) \times \\ &\quad \sum_{i\omega_1, i\omega_2} \sum_{\mathbf{q}_1, \mathbf{q}_2} \left\{ \left\langle \bar{F}_{\mathbf{q}_1, \eta_1, \gamma}(i\omega_1) D_{\mathbf{q}_1 + \mathbf{p}, \eta_1}(i\omega_1 + i\omega_p) \bar{D}_{\mathbf{q}_2 + \mathbf{p}, \eta_2}(i\omega_2 + i\omega_p) F_{\mathbf{q}_2, \eta_2, \gamma}(i\omega_2) \right\rangle \right\}, \end{aligned} \quad (3.24)$$

where we inserted the identity

$$\frac{1}{\beta} \int d\tau e^{(i\omega_p + i\omega_1 - i\omega_4)\tau} = \delta(i\omega_p + i\omega_1 - i\omega_4). \quad (3.25)$$

Using the compact notation $q \equiv (i\omega_q, \mathbf{q})$, we obtain in a more dense form the relation

$$\mathcal{G}_c(\mathbf{p}, i\omega_p, \alpha) = \frac{1}{4\beta N} \sum_{\eta_1, \eta_2 \in \{x, y\}} (1 + e^{-ip\eta_1}) (1 + e^{ip\eta_2}) \sum_{q_1, q_2} \left\langle F_{q_2, \eta_2} D_{q_1+p, \eta_1} \bar{D}_{q_2+p, \eta_2} \bar{F}_{q_1, \eta_1} \right\rangle, \quad (3.26)$$

in which the spin index $\gamma = -\alpha$ is implicitly implied for all fermionic Dimer operators and where the expression acquires an additional minus sign from exchanging the position of the two Grassmann variables F and \bar{F} . We are now in a position to calculate this Green's function using the action from Eq.(3.7) by means of ordinary functional methods from many body theory, starting from the bare propagators Eq.(3.12) and Eq.(3.13) and the interacting Hamiltonian from Eq.(3.8).

Subsequently, the electronic spectral function follows from

$$\mathcal{A}(\mathbf{p}, \omega_p) = -\frac{1}{\pi} \text{Im} [\mathcal{G}_c^R(\mathbf{p}, \omega_p)] \quad (3.27)$$

where the so-called retarded Green's function is obtained from the analytic continuation procedure

$$\mathcal{G}_c^R(\mathbf{p}, \omega_p) = \mathcal{G}_c(\mathbf{p}, i\omega_p \rightarrow \omega_p + i0^+). \quad (3.28)$$

The focus of our calculations will now be to evaluate the expression for the functional average in Eq.(3.26),

$$\begin{aligned} \left\langle F_{q_2, \eta_2} D_{q_1+p, \eta_1} \bar{D}_{q_2+p, \eta_2} \bar{F}_{q_1, \eta_1} \right\rangle &= \delta_{q_1, q_2} G_f(q_1) G_b(q_1 + p) + \\ &+ G_f(q_2) G_b(q_1 + p) \tilde{\Gamma}^{\eta_1, \eta_2, \eta_1, \eta_2}(q_1, q_2 + p, q_1 + p, q_2) G_b(q_2 + p) G_f(q_1). \end{aligned} \quad (3.29)$$

The first contribution is just the zeroth order and thus disconnected part of a diagrammatic treatment while the second term is expressed via the full 4-point interaction vertex

$$\tilde{\Gamma}^{\eta_1, \eta_2, \eta_1, \eta_2}(q_1, q_2 + p, q_1 + p, q_2) \quad (3.30)$$

which describes the effective interaction process between an ingoing fermionic dimer with a set of indices (q_2, η_2) and an ingoing bosonic dimer with $(q_1 + p, \eta_1)$ which leads to outgoing (q_1, η_1) (fermionic) and $(q_2 + p, \eta_2)$ (bosonic) dimers. Hence, in this particular choice of notation,

$$\tilde{\Gamma} = \tilde{\Gamma}^{\eta_{f, \text{out}}, \eta_{b, \text{out}}, \eta_{b, \text{in}}, \eta_{f, \text{in}}}(q_{f, \text{out}}, q_{b, \text{out}}, q_{b, \text{in}}, q_{f, \text{in}}). \quad (3.31)$$

Note that the bare interaction vertex, denoted by Γ , is fully determined by the Hamiltonian from Eq.(3.8).

To proceed with our calculation a choice needs to be made for the full fermionic and bosonic dimer propagators G_f and G_b which appear in Eq.(3.29) and are initially unknown. In our approach, we choose to make the approximation to replace these by their respective initial bare propagator, whose form we determined in Eq.(3.12) and Eq.(3.13), i.e.

$$G_f(q) \rightarrow G_f^0(q) \quad \text{and} \quad G_b(q) \rightarrow G_b^0(q). \quad (3.32)$$

The motivation for this approximation originates from the diagonality of the propagators, which, as mentioned above, holds true for bare as well as full propagators since the dimer-dimer interactions of our model locally conserve the hard-core constraint. Therefore, the

full propagator can not develop an effective dispersion for either of the two dimer species, which would result in a propagator of the form

$$G_f(q) = \frac{1}{i\omega_q - \varepsilon_q + \mu_f}. \quad (3.33)$$

Furthermore, the chemical potentials μ_f and μ_b are already fixed to the values in Eq.(3.4) and Eq.(3.5), again as a consequence of the hard-core constraint which fixes the average dimer densities associated to the chemical potentials. The self-energy of bosonic as well as fermionic dimers can hence only be purely imaginary, i.e.

$$\Sigma_{f/b}(\mathbf{q}, i\omega_q)^* = -\Sigma_{f/b}(\mathbf{q}, i\omega_q). \quad (3.34)$$

Typically, we expect this imaginary part to be of a form $\Sigma_{f/b}(\mathbf{q}, i\omega_q) = \frac{1}{\tau_{f/b}} \text{sgn}(\omega_q)$ that leads to finite particle lifetimes $\tau_{f/b}$ which merely result in a broadening of the associated spectral delta peaks into lorentzian shape. But such a broadening can also be done at a later point by hand via replacing $i\omega_p \rightarrow \omega_p + i\frac{1}{\tau}$ instead of $i\omega_p \rightarrow \omega_p + i0^+$ in Eq.(3.28). We therefore keep the propagators in their bare form to simplify calculations. Generically, the purely imaginary self-energy of Eq.(3.34) also allows for a momentum dependence and a more complicated dependence on the Matsubara frequency, yet here we assume these dependencies to be negligible.

With this approximation at hand we update our expression for the electronic Green's function to

$$\begin{aligned} \mathcal{G}_c(p) = \frac{1}{4\beta N} \sum_{\eta_1, \eta_2} (1 + e^{-ip\eta_1}) (1 + e^{ip\eta_2}) \sum_{q_1, q_2} \left[\delta_{q_1, q_2} \delta_{\eta_1, \eta_2} G_f^0(i\omega_1) G_b^0(i\omega_1 + i\omega_p) + \right. \\ \left. + G_f^0(i\omega_1) G_b^0(i\omega_1 + i\omega_p) \tilde{\Gamma}^{\eta_1, \eta_2, \eta_1, \eta_2}(q_1, q_2 + p, q_1 + p, q_2) G_f^0(i\omega_2) G_b^0(i\omega_2 + i\omega_p) \right]. \end{aligned} \quad (3.35)$$

Note that the first term in the square brackets, i.e. the zeroth order contribution to the Green's function, reduces to

$$\begin{aligned} \delta_{\eta_1, \eta_2} \sum_{q_1, q_2} \delta_{q_1, q_2} G_f^0(i\omega_1) G_b^0(i\omega_1 + i\omega_p) = \delta_{\eta_1, \eta_2} N \cdot \sum_{i\omega_1} \frac{1}{i\omega_1 + \mu_f} \cdot \frac{1}{i\omega_1 + i\omega_p + \mu_b} = \\ = \delta_{\eta_1, \eta_2} N \beta \psi(i\omega_p), \end{aligned} \quad (3.36)$$

where we defined the function

$$\psi(i\omega_p) = \frac{n_F(-\mu_f) + n_B(-\mu_b)}{i\omega_p + \mu_b - \mu_f} = \frac{1}{4} \frac{1}{i\omega_p + \mu_b - \mu_f} \quad (3.37)$$

which results from performing the (fermionic) Matsubara sum in Eq.(3.36) and which will appear again later in this calculation. Note here that $\psi(i\omega_p) \propto n_F(-\mu_f) + n_B(-\mu_b) = n_D$ is proportional to the total average dimer density n_D on a given link, i.e. formally $n_D = n_{D, i, \eta}$. We will use this property later in the context of implementing the hard-core constraint more rigorously into our approach. Note further that because the bare propagators do not depend on momentum, the momentum summations in the second term in the square brackets of Eq.(3.35) are attached to the interaction vertex only.

For $T \rightarrow 0$, both $\mu_f \rightarrow 0$ and $\mu_b \rightarrow 0$ and the zeroth order spectral function is just a delta peak at $\omega_p = 0$ with quasiparticle weight

$$\mathcal{Z}_0(\mathbf{p}) = \frac{1}{16} \sum_{\eta} (1 + e^{-ip_{\eta}}) (1 + e^{ip_{\eta}}) = \frac{1}{4} \left[\cos^2 \left(\frac{p_x}{2} \right) + \cos^2 \left(\frac{p_y}{2} \right) \right], \quad (3.38)$$

which can be deduced easily from the form of the zeroth order electronic Green's function

$$\mathcal{G}_c^0(p) = \frac{1}{4} \sum_{\eta_1, \eta_2} \delta_{\eta_1, \eta_2} (1 + e^{-ip_{\eta_1}}) (1 + e^{ip_{\eta_2}}) \psi(i\omega_p). \quad (3.39)$$

As will be proven later in this thesis, this result for the quasiparticle residuum is indeed exact at the non-interacting point where all $t_i = 0$. This is just what we expect for a zeroth order approximation in the noninteracting limit, giving us confidence that this diagrammatic approach can indeed capture the essential features of the dimer model at hand. Furthermore, the result of Eq.(3.39) can be shown to yield the correct normalization of the spectral function. That is, if we recall the definition of the spectral function for the system with one fermionic dimer considered in [1], the non-vanishing hole-part written in Lehmann representation and in the zero temperature limit is given by

$$\mathcal{A}_-(\mathbf{p}, \omega) = \sum_n |\langle n | c_{-\mathbf{p}} | RK \rangle|^2 \delta(\omega - (\epsilon_{RK} - \epsilon_n)), \quad (3.40)$$

where the sum \sum_n runs over all eigenstates of the full Hamiltonian H with one fermionic dimer and where we suppressed the electron spin index α . The particle-part of the spectral function would correspondingly be given by

$$\mathcal{A}_+(\mathbf{p}, \omega) = \sum_m \left| \langle m | c_{-\mathbf{p}}^\dagger | RK \rangle \right|^2 \delta(\omega + (\epsilon_{RK} - \epsilon_m)) = 0 \quad (3.41)$$

and has to vanish due to $\langle c_{-\mathbf{p}}^\dagger | RK \rangle = 0$ using the dimer representation of $c_{-\mathbf{p}}$ from Eq.(2.25), as no fermionic dimers can be removed from the already purely bosonic RK wave function. Normalization by integration over frequency thus yields

$$\int d\omega \mathcal{A}(\mathbf{p}, \omega) = \int d\omega \mathcal{A}_-(\mathbf{p}, \omega) = \langle RK | c_{-\mathbf{p}}^\dagger c_{-\mathbf{p}} | RK \rangle = \mathcal{Z}_0(\mathbf{p}), \quad (3.42)$$

where the last equality can be shown by expressing Eq.(3.42) again in terms of the real space form of the operators c_i in dimer representation. The normalization of the spectral function thus deviates from the usual normalization to unity for fermionic particles. This discrepancy is due to expressing the electron operator in the reduced Hilbert space of dimer coverings, an aspect which we will return to in Sec.(4).

Note also that if we wanted to attach a dispersion to the effective fermionic quasiparticles created by inserting holes into the system at $t_i = 0$, we would simply obtain a flat band in the BZ located at an energy $\epsilon_{\mathbf{p}} = 0$ in the zero temperature limit $T \rightarrow 0$.

3.2 The particle-hole ladder

We turn our attention to the second term in Eq.(3.35) and calculate the effective interaction vertex $\tilde{\Gamma}$ using a ladder approximation which can be carried out by solving a Bethe-Salpeter equation. We find that in the given model, the exchange channel particle-hole ladder can indeed be computed exactly and can be shown to yield a good approximation for the vertex. One can verify this by comparing the resulting dispersion and quasiparticle residuum to the outcomes of the mean field approach and exact diagonalization studies.

We start with the particle-hole ladder displayed diagrammatically in Fig.(7). The corresponding Bethe-Salpeter equation we have to solve reads

$$\begin{aligned} \tilde{\Gamma}^{\eta_f, \sigma \eta_b, \sigma \eta_b, i \eta_f, i}(q_1, q_2 + p, q_1 + p, q_2) &= \Gamma^{\eta_f, \sigma \eta_b, \sigma \eta_b, i \eta_f, i}(q_1, q_2 + p, q_1 + p, q_2) + \\ &+ \sum_{\tilde{\eta}_f, \tilde{\eta}_b, \tilde{q}} \left\{ \Gamma^{\eta_f, \sigma \tilde{\eta}_b \eta_b, i \tilde{\eta}_f}(q_1, \tilde{q} + p, q_1 + p, \tilde{q}) G_f^0(\tilde{q}) G_b^0(\tilde{q} + p) \tilde{\Gamma}^{\tilde{\eta}_f \eta_b, \sigma \tilde{\eta}_b \eta_f, i}(\tilde{q}, q_2 + p, \tilde{q} + p, q_2) \right\}, \end{aligned} \quad (3.43)$$

where our aim is to determine the effective vertex $\tilde{\Gamma}$ as a function of the known bare vertex Γ .

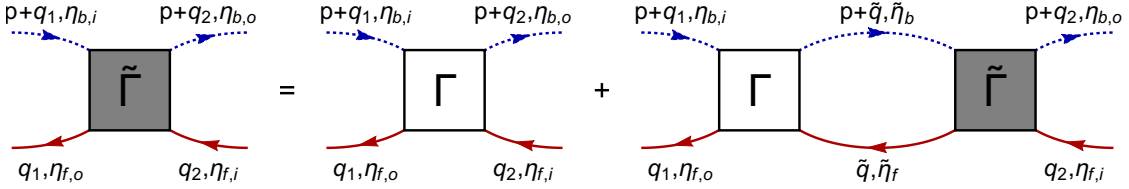


Figure 7: Bethe-Salpeter equation for the effective interaction vertex $\tilde{\Gamma}$. Dashed blue lines mark the bare propagators of bosonic dimers, solid red lines those of fermionic dimers. Blank boxes represent the bare vertex Γ while shaded boxes mark the effective 4-point interaction vertex. This diagrammatic approach sums over all m -rung (i.e. m loops) particle-hole ladder diagrams from $m = 0$ to $m \rightarrow \infty$.

Since the bare vertex Γ is obviously independent of frequency, i.e.

$$\Gamma^{\eta_f, \sigma \eta_b, \sigma \eta_b, i \eta_f, i}(q_1, q_2 + p, q_1 + p, q_2) = \Gamma^{\eta_f, \sigma \eta_b, \sigma \eta_b, i \eta_f, i}(\mathbf{q}_1, \mathbf{q}_2 + \mathbf{p}, \mathbf{q}_1 + \mathbf{p}, \mathbf{q}_2), \quad (3.44)$$

and we are evaluating only the contribution of the particle-hole ladder to the full vertex, $\tilde{\Gamma}$ can only depend on the difference of the frequencies of an ingoing fermionic (bosonic) dimer and an outgoing bosonic (fermionic) dimer. This is just given by the frequency $i\omega_p$, i.e. the electronic Matsubara frequency. Hence, we can insert

$$\tilde{\Gamma}^{\eta_f, \sigma \eta_b, \sigma \eta_b, i \eta_f, i}(q_1, q_2 + p, q_1 + p, q_2) = \tilde{\Gamma}^{\eta_f, \sigma \eta_b, \sigma \eta_b, i \eta_f, i}(\mathbf{q}_1, \mathbf{q}_2 + \mathbf{p}, \mathbf{q}_1 + \mathbf{p}, \mathbf{q}_2, i\omega_p) \quad (3.45)$$

into Eq.(3.43). The summation over the Matsubara frequencies $i\omega_{\tilde{q}}$ then only runs over the product of the two bare propagators $G_f^0(i\omega_{\tilde{q}}) G_b^0(i\omega_{\tilde{q}} + i\omega_p)$ and results in the function $\psi(i\omega_p)$ for the particle-hole bubble to yield

$$\begin{aligned} \Gamma^{\eta_1 \eta_2 \eta_1 \eta_2}(q_1, q_2 + p, q_1 + p, q_2) &= \tilde{\Gamma}^{\eta_1 \eta_2 \eta_1 \eta_2}(q_1, q_2 + p, q_1 + p, q_2) - \\ &- \sum_{\tilde{\eta}_f, \tilde{\eta}_b} \beta \psi(i\omega_p) \left\{ \sum_{\tilde{q}} \Gamma^{\eta_1 \tilde{\eta}_b \eta_1 \tilde{\eta}_f}(q_1, \tilde{q} + p, q_1 + p, \tilde{q}) \tilde{\Gamma}^{\tilde{\eta}_f \eta_2 \tilde{\eta}_b \eta_2}(\tilde{q}, q_2 + p, \tilde{q} + p, q_2) \right\}, \end{aligned} \quad (3.46)$$

where the equation was rearranged and the values for $\eta_{f,i}, \eta_{f,o}, \eta_{b,i}, \eta_{b,o}$ from Eq.(3.29) were plugged in. Such Bethe-Salpeter equations can typically not be solved in general, but we will now make contact with the explicit form of the bare vertex from Eq.(3.8) to see that in the particle-hole ladder, the usually complicated sum over $\tilde{\mathbf{q}}$ becomes trivial.

First, one can see from the diagram in Fig.(8) that for an ingoing fermionic and bosonic dimers with respective orientations η_2 and η_1 which exchange this orientation in the course of a particle-hole ladder like process, the virtual orientations $\tilde{\eta}_f$ and $\tilde{\eta}_b$ of the intermediate steps have to be equal. This becomes clear when looking at the general m-rung ladder diagram, starting from one of its end points. If one e.g. looks at the rightmost interaction line of the diagram in Fig.(8), the orientation of the ingoing fermionic dimer (η_2) equals the orientation of the outgoing bosonic dimer (also η_2). If this rightmost interaction line corresponded to a t_1 interaction (i.e. we take the Γ_{t_1} part of the bare vertex), then $\tilde{\eta}_{f,m} = \eta_2 = \tilde{\eta}_{b,m} = \eta_2$ would be implied immediately. Analogously, if we consider a t_3 interaction line, $\tilde{\eta}_{f,m} = \tilde{\eta}_{b,m} = \eta_2$ is automatically fixed. A t_2 interaction on the other hand is not possible in such a particle-hole like diagram, as for this interaction type, ingoing and outgoing dimers of a given interaction line must have differing orientation indices. Since at the rightmost interaction line $\eta_{f,i} = \eta_{b,o} = \eta_2$, this rightmost line can not be a t_2 line. On the other hand, we know that for t_1 and t_3 , $\tilde{\eta}_{f,m} = \tilde{\eta}_{b,m}$ is implied and hence also the second rightmost interaction line can not be a t_2 line. It follows that in the particle-hole ladder, only t_1 and t_3 do contribute, t_2 can not appear in this approximation.

So far, our particle-hole ladder approach can hence not capture the effects of the t_2 interaction and the model which we can hope to describe by this Ansatz is for now effectively reduced to the $t_2 = 0$ case. Nevertheless, the absence of t_2 in the particle-hole ladder is the crucial part which will allow to solve the corresponding Bethe-Salpeter equation exactly.

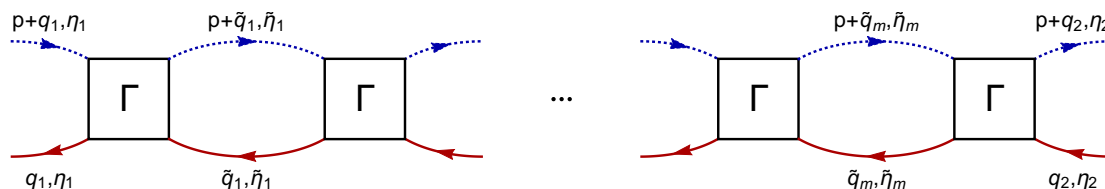


Figure 8: Diagram of the m -rung contribution to the sum over all particle-hole ladder diagrams. As explained in the main text, a diagram like this can never contain t_2 interactions, i.e. $\Gamma = \Gamma_{t_1}$ or $\Gamma = \Gamma_{t_3}$ holds true for every bare vertex in this diagram.

We insert $\tilde{\eta}_f = \tilde{\eta}_b = \tilde{\eta}$ into Eq.(3.46) and obtain

$$\Gamma^{\eta_1 \eta_2 \eta_1 \eta_2}(q_1, q_2 + p, q_1 + p, q_2) = \tilde{\Gamma}^{\eta_1 \eta_2 \eta_1 \eta_2}(q_1, q_2 + p, q_1 + p, q_2) - \sum_{\tilde{\eta}} \beta \psi(i\omega_p) \left\{ \sum_{\tilde{q}} \Gamma^{\eta_1 \tilde{\eta} \eta_1 \tilde{\eta}}(q_1, \tilde{q} + p, q_1 + p, \tilde{q}) \tilde{\Gamma}^{\tilde{\eta} \eta_2 \tilde{\eta} \eta_2}(\tilde{q}, q_2 + p, \tilde{q} + p, q_2) \right\}. \quad (3.47)$$

The relevant bare vertices that enter Eq.(3.47) are hence

$$\Gamma^{xxxx}(q_1, q_2 + p, q_1 + p, q_2) = \Gamma^{xxxx}(p) = \frac{2t_1}{\beta N} \cos(p_y) \quad (3.48)$$

$$\Gamma^{yyyy}(q_1, q_2 + p, q_1 + p, q_2) = \Gamma^{yyyy}(p) = \frac{2t_1}{\beta N} \cos(p_x) \quad (3.49)$$

$$\begin{aligned} \Gamma^{xyxy}(q_1, q_2 + p, q_1 + p, q_2) &= \Gamma^{xyxy}(p) \equiv \frac{t_3}{\beta N} C(\mathbf{p}) = \\ &= \frac{t_3}{\beta N} (e^{i(p_x+p_y)} + e^{ip_x} + e^{i(p_y-2p_x)} + e^{-2ip_x} + e^{2ip_y} + e^{i(2p_y-p_x)} + e^{-ip_y} + e^{-i(p_x+p_y)}) \end{aligned} \quad (3.50)$$

$$\Gamma^{yxyx}(q_1, q_2 + p, q_1 + p, q_2) = \Gamma^{yxyx}(p) = \frac{t_3}{\beta N} C^*(\mathbf{p}) = \frac{t_3}{\beta N} C(-\mathbf{p}) \quad (3.51)$$

which follow from the Hamiltonian and contain only t_1 and t_3 as parameters. These vertices further depend only on the electronic momentum \mathbf{p} and we can therefore assume the same property for the effective vertex, i.e.

$$\tilde{\Gamma}^{\eta_1\eta_2\eta_1\eta_2}(q_1, q_2 + p, q_1 + p, q_2) = \tilde{\Gamma}^{\eta_1\eta_2\eta_1\eta_2}(p). \quad (3.52)$$

The integral over the loop momentum $\tilde{\mathbf{q}}$ in Eq.(3.47) is now trivial and we arrive at the equation

$$\Gamma^{\eta_1\eta_2\eta_1\eta_2}(\mathbf{p}) = \tilde{\Gamma}^{\eta_1\eta_2\eta_1\eta_2}(p) - \beta N \psi(i\omega_p) \sum_{\tilde{\eta}} \left\{ \Gamma^{\eta_1\tilde{\eta}\eta_1\tilde{\eta}}(\mathbf{p}) \tilde{\Gamma}^{\tilde{\eta}\eta_2\tilde{\eta}\eta_2}(p) \right\}. \quad (3.53)$$

We can solve this equation for $\tilde{\Gamma}$ by bringing it into matrix form with respect to the dimer orientation indices. To this end, we rewrite Eq.(3.53) as

$$\Gamma^{\eta_1\eta_2\eta_1\eta_2}(\mathbf{p}) = \sum_{\tilde{\eta}_1, \tilde{\eta}_2} \left\{ \delta_{\eta_1, \tilde{\eta}_1} \delta_{\eta_2, \tilde{\eta}_2} - \beta N \psi(i\omega_p) \Gamma^{\eta_1\tilde{\eta}_1\eta_1\tilde{\eta}_1}(\mathbf{p}) \delta_{\eta_2, \tilde{\eta}_2} \right\} \tilde{\Gamma}^{\tilde{\eta}_1\tilde{\eta}_2\tilde{\eta}_1\tilde{\eta}_2}(p). \quad (3.54)$$

Upon defining the vectors

$$\vec{\Gamma}(\mathbf{p}) \equiv \begin{pmatrix} \Gamma^{xxxx}(\mathbf{p}) \\ \Gamma^{xyxy}(\mathbf{p}) \\ \Gamma^{yxyx}(\mathbf{p}) \\ \Gamma^{yyyy}(\mathbf{p}) \end{pmatrix} \quad \text{and} \quad \vec{\tilde{\Gamma}}(\mathbf{p}) \equiv \begin{pmatrix} \tilde{\Gamma}^{xxxx}(p) \\ \tilde{\Gamma}^{xyxy}(p) \\ \tilde{\Gamma}^{yxyx}(p) \\ \tilde{\Gamma}^{yyyy}(p) \end{pmatrix}, \quad (3.55)$$

we can express Eq.(3.54) as a matrix equation:

$$\begin{aligned} \vec{\Gamma}(\mathbf{p}) &= \begin{pmatrix} 1 - \beta N \psi \Gamma^{xxxx} & 0 & -\beta N \psi \Gamma^{xyxy} & 0 \\ 0 & 1 - \beta N \psi \Gamma^{xxxx} & 0 & -\beta N \psi \Gamma^{xyxy} \\ -\beta N \psi \Gamma^{yxyx} & 0 & 1 - \beta N \psi \Gamma^{yyyy} & 0 \\ 0 & -\beta N \psi \Gamma^{yxyx} & 0 & 1 - \beta N \psi \Gamma^{yyyy} \end{pmatrix} \cdot \vec{\tilde{\Gamma}}(p) = \\ &\mathcal{M}(p) \cdot \vec{\tilde{\Gamma}}(p) \end{aligned} \quad (3.56)$$

where the dependencies $\psi = \psi(i\omega_p)$ and $\Gamma = \Gamma(\mathbf{p})$ are assumed implicitly. Inserting the vertices from Eq.(3.48)-(3.51), the matrix \mathcal{M} becomes

$$\mathcal{M}(p) = \begin{pmatrix} 1 - 2t_1\psi \cos(p_y) & 0 & -t_3\psi C(\mathbf{p}) & 0 \\ 0 & 1 - 2t_1\psi \cos(p_y) & 0 & -t_3\psi C(\mathbf{p}) \\ -t_3\psi C^*(\mathbf{p}) & 0 & 1 - 2t_1\psi \cos(p_x) & 0 \\ 0 & -t_3\psi C^*(\mathbf{p}) & 0 & 1 - 2t_1\psi \cos(p_x) \end{pmatrix} \quad (3.57)$$

and

$$\vec{\Gamma}(\mathbf{p}) = \frac{1}{\beta V} \begin{pmatrix} 2t_1 \cos(p_y) \\ t_3 C(\mathbf{p}) \\ t_3 C^*(\mathbf{p}) \\ 2t_1 \cos(p_x) \end{pmatrix}. \quad (3.58)$$

The effective vertex may then be extracted by straightforward matrix inversion,

$$\vec{\Gamma}(p) = [\mathcal{M}(p)]^{-1} \cdot \vec{\Gamma}(\mathbf{p}). \quad (3.59)$$

Before examining the spectral function that results from Eq.(3.59), we comment on the ladder approach that was employed. Since we only included the t_1 - and t_3 -exchange interactions for now, the particle-hole bubble $\psi(i\omega_p)$ is trivial to compute and we expect the ladder approach in the exchange channel we employed above to yield realistic results for the system. An analysis of the vertex structure thus naturally leads to the above ladder approach which results in a simple geometric sum equation for the effective vertex, only with an additional matrix structure corresponding to the dimer orientation index. In order to proceed and also include the t_2 -terms within our approach, we can thus try to project the correlated hopping terms t_2 to effective exchange interactions, making them accessible within the above ladder approach. We will explore and implement this projection procedure in the following section.

3.3 Including the t_2 -term

In the particle-hole ladder considered so far, the t_2 -term does not contribute as there is no way for the t_2 -processes to lead to an exchange of a fermionic and a bosonic dimer (which is what is described by the ph-ladder diagrams) without taking into account bosonic background interactions. As these are not included in the approach, we hence lose the effects of the t_2 -terms. Nevertheless, close to the RK-point, we can substitute the original t_2 flip-terms in the Hamiltonian by effective t_2 exchange interactions. We will then find that these effective exchange interactions reproduce the correct terms that we expect the original t_2 interaction to contribute to the functional expression for the spectral function in the exchange channel. This approach effectively takes into account bosonic background plaquette flips and should again be valid close to the RK-point.

First, we need to argue which physical processes including t_2 -terms we expect to contribute to the expression of the spectral function by an overall exchange of two dimers, which is essentially determined by the functional average $\langle F_{q_2, \eta_2} D_{q_1+p, \eta_1} \bar{D}_{q_2+p, \eta_2} \bar{F}_{q_1, \eta_1} \rangle$. Observe that the two dimer species exchange their respective orientation in the course of the process. Since the t_2 -term is not an exchange term, we conclude that there cannot be a first order contribution by t_2 to this functional average. Possible contributions to $\langle F_{q_2, \eta_2} D_{q_1+p, \eta_1} \bar{D}_{q_2+p, \eta_2} \bar{F}_{q_1, \eta_1} \rangle$ that involve t_2 hence arise from diagrams that necessarily feature more than one (possibly purely bosonic) interaction line. In other words, the t_2 -terms contribute to produce *induced* effective exchanges at higher order. We show some possibilities of such induced exchanges in Fig.(9) The crucial step is now to substitute $H_{t_2} \rightarrow \tilde{H}_{t_2}$ with

$$\tilde{H}_{t_2} = -t_2 \sum_i F_{i,y}^\dagger D_{i+\hat{y},x}^\dagger D_{i,y} F_{i+\hat{y},x} + 7 \text{ terms}, \quad (3.60)$$

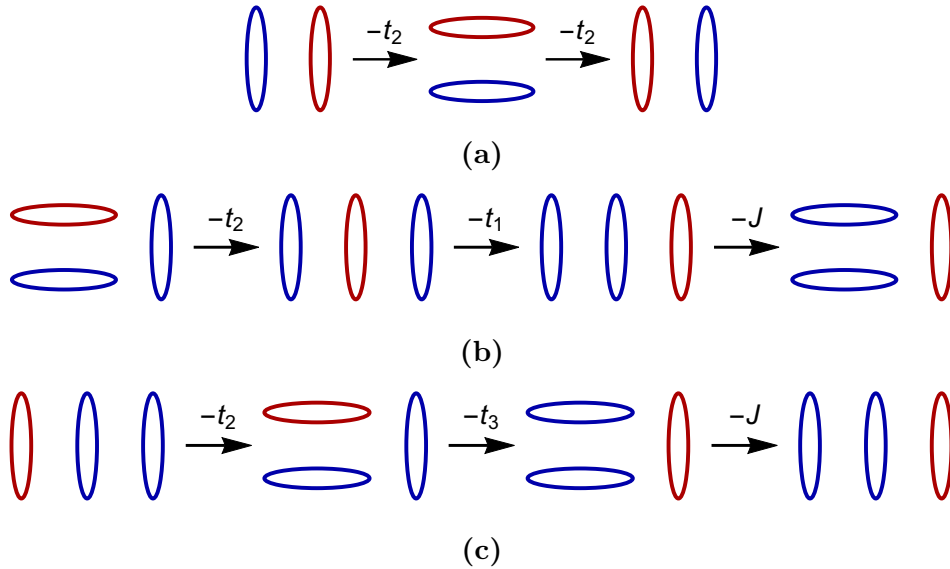


Figure 9: A number of possible effective exchanges induced by the t_2 -term. In (a), two t_2 -flips combine to form an effective t_1 -exchange. In (b), a t_2 -flip combines with a t_1 -exchange and a subsequent J -plaquette flip which resets the bosonic background to its starting configuration. We are left with an overall t_3 -exchange. In (c), a new effective exchange is induced by combining t_2 - with a t_3 -exchange and the necessary J -plaquette flip.

where the 7 terms not displayed are generated from the first one by application of the lattice symmetry group. Note that these exchange terms project on configurations which explicitly violate the hard-core constraint. This should however not affect the validity of our approach, as we assumed a translational invariant dimer density and the effective terms of Eq.(3.60) should be viewed in a mean field sense. Nevertheless, an important property of \tilde{H}_{t_2} is its blockdiagonality with respect to the spaces of constraint-fulfilling and non-constraint configurations: Let \mathcal{C} denote all possible hard-core dimer configurations (including fermionic dimers) on the lattice, then for every $c \in \mathcal{C}$, $\tilde{c} \notin \mathcal{C}$

$$\langle \tilde{c} | \tilde{H}_{t_2} | c \rangle = 0. \quad (3.61)$$

This feature is crucial to ensure that Eq.(3.34) remains valid, i.e. the self energies $\Sigma_{f/b}(\mathbf{q}, i\omega_q)$ of both dimer species must stay purely imaginary.

It is then possible to convince oneself that the effective exchanges involving t_2 -terms are induced exactly by the first-order exchange interaction of \tilde{H}_{t_2} from Eq.(3.61). With this substitution we effectively included bosonic plaquette flips that are necessary to bring back the bosonic background configuration into its original state from before the t_2 flip, compare Fig.(9). This is necessary, as the background must be left unaltered in order to obtain a contribution to $\langle F_{q_2, \eta_2} D_{q_1+p, \eta_1} \bar{D}_{q_2+p, \eta_2} \bar{F}_{q_1, \eta_1} \rangle$. Diagrammatically, we can illustrate the situation in real space via Fig.(10). The vertex $\Gamma_{\tilde{t}_2}$ of the effective first order t_2 -exchange is generated by the original Γ_{t_2} and a J -flip of a bosonic plaquette. This effective vertex can then be inserted into the particle-hole ladder diagrams at every step just like a bare exchange term. One can check that the possible real space processes in Fig.(9) can indeed

be represented in terms of ladder diagrams which feature Γ_{t_1} , Γ_{t_3} and the $\Gamma_{\tilde{t}_2}$ from Fig.(10). We can insert \tilde{H}_{t_2} from Eq.(3.60) into the ph-ladder approach which yields new bare vertices

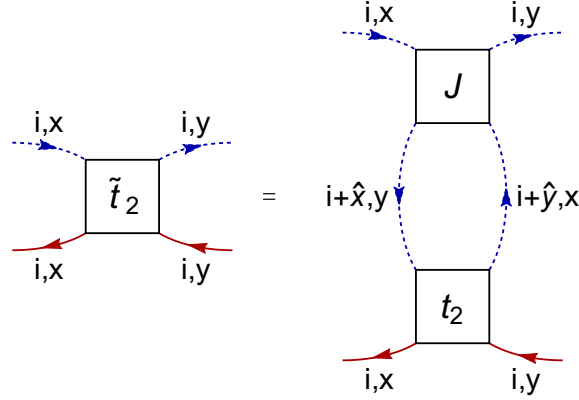


Figure 10: Effective vertex for the t_2 -interaction terms which includes a bosonic plaquette flip J in order to render the original Γ_{t_2} into an exchange interaction.

$$\begin{aligned} \Gamma^{xyxy}(p) &= \frac{t_3}{\beta N} (e^{i(p_x+p_y)} + e^{ip_x} + e^{i(p_y-2p_x)} + e^{-2ip_x} + e^{2ip_y} + e^{i(2p_y-p_x)} + e^{-ip_y} + e^{-i(p_x+p_y)}) \\ &\quad + \frac{t_2}{\beta N} (1 + e^{ip_x}) (1 + e^{-ip_y}) \\ \Gamma^{yxyx}(p) &= \Gamma^{xyxy}(-p) \end{aligned} \tag{3.62}$$

which have to be inserted into the matrix equation from Eq.(3.56) in order to obtain the effective vertex $\tilde{\Gamma}$.

3.4 The hard-core constraint

The way we defined our many-body theory, we included the hard-core constraint only in a mean field way via the chemical potential which fixes the average density of a given dimer species. As described above, this was done in a way such that the overall average density for a given link on the lattice is just 1/4. In this section we argue how one can systematically implement the hard-core constraint into this functional setting under the assumption of a translationally invariant RK-like background structure by making use of the known classical dimer-dimer correlations. In first order, the argument reduces to the one already encountered in the mean field description of Sec.(2.3.2) which will allow us to make progress by a simple substitution of the vertex parameters t_i with their effective values induced by the constraint.

The action S of Eq.(3.7) does not contain any interaction terms that disfavour the occupation of a single site by multiple dimers. Adding such terms (which could in principle be done by considering a strong on-site repulsion and suitable nearest neighbour interaction terms) is expected to change the effective interaction which is generated by the t_i .

This change can be imagined to be due to a change in the densities of the dimers which participate in a t_i -interaction process. Just like in the case of the mean-field theory from above, a given t_i -process can occur only if two dimers are positioned in a suitable way relative to each other. In our current average constraint, the probability of this to happen is given just by the product of the corresponding probabilities of a dimer occupying one of the respective sites involved in the process, namely $1/4 \times 1/4$. Remembering our initial assumption $t_i/J \ll 1$, we note that we are expanding around the RK-point where the exact wavefunction is the RK equal weight superposition state of all dimer coverings on the square lattice. A rigorous treatment of the hard-core constraint via additional terms in the action should therefore enforce the realization of the RK-like bosonic background. In this case, the probability of having two dimers in a position that allows for a t_i process and hence the product of the corresponding effective average occupations numbers is then given by the classical dimer-dimer correlation function. In our approach, the Feynman diagram of a bare t_i interaction process is simply given by

$$G_f^0(q_1)G_b^0(p+q_1)\Gamma^{\eta_1\eta_2\eta_1\eta_2}(p)G_f^0(q_2)G_b^0(p+q_2). \quad (3.63)$$

After summation over the external momenta and frequencies q_1 and q_2 , the contribution to the spectral function of this simple diagram is just $\psi(i\omega_p)\Gamma^{\eta_1\eta_2\eta_1\eta_2}(p)\psi(i\omega_p)$, where the function $\psi(i\omega_p)$ is proportional to the total dimer density $n_{D,i,\eta} = 1/4$ on a given link (i, η) , see Eq.(3.37). We illustrate the process in real space in Fig.(11). Implementing the constraint in a more rigorous way, we have to change the density of the dimers on the link to the right of the interaction line in Fig.(11) to the value of the classical dimer correlation function under the assumption that the link to the left of the interaction line is occupied. Similar to the MFT from Sec.(2.3.2), this leads us to the replacements

$$t_1 \rightarrow \frac{4}{2}t_1 = 2t_1 \quad (3.64)$$

$$t_2 \rightarrow 2t_2 \quad (3.65)$$

$$t_3 \rightarrow \frac{4}{\pi}t_3 \quad (3.66)$$

for every bare interaction line. By this procedure, we effectively substitute the density $1/4$ on a given link by the conditional density (i.e. conditional probability) $1/2$ or $1/\pi$ on the same link. Attention has to be paid only for the effective t_2 -exchange from Sec.(3.3), which projects on non-constraint configurations. In that case, we substitute with the classical probability for an original t_2 -process to occur, which leads to Eq.(3.65). Note that although we make use of a classical correlation function, we expect this substitution to be valid in our theory, as expectation values in the exactly solvable RK-model correspond to expectation values of the classical dimer problem at $T = \infty$. It is also evident that the replacements Eq.(3.64), (3.65) and (3.66) implement the constraint at first order in the interaction parameters t_i . For a general real space m-rung ph-ladder diagram of Fig.(12), one would have to substitute the product of the dimer densities of every rung by the classical probability of having all the links occurring in the rungs occupied with dimers. As shown in Fig.(12), in every step of the ladder process the usual factor $1/4$ is replaced by the classical conditional probability of having the corresponding link occupied given that

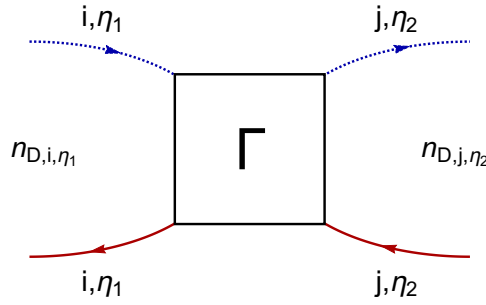


Figure 11: Simplest Feynman diagram featuring the bare vertex in first order. Summing over the two external frequencies $i\omega_1$ and $i\omega_2$ leads to a contribution proportional to $\propto n_{D,i,\eta_1} \cdot n_{D,j,\eta_2}$. Implementing the hard-core dimer constraint, one of these densities has to be substituted by the conditional density obtained from the classical dimer correlations.

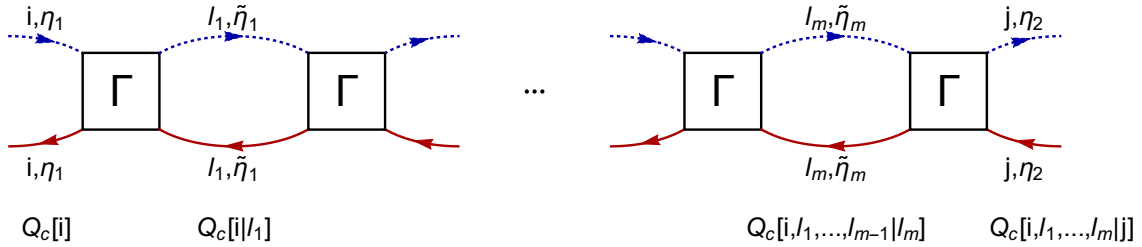


Figure 12: m -rung real space ladder diagram. In every step of the process, the average density $Q_c[i] = 1/4$ on a given link (for abbreviation of notation we assume $i = (i, \eta)$ to contain the orientation as well) is replaced by the conditional classical probability $Q_c[i, l_1, \dots, l_n | l_{n+1}]$ of finding a dimer on link l_{n+1} given that there are dimers on the links i, l_1, \dots, l_n .

all the links from the previous steps are occupied. In the notation $i = (i, \eta)$, the overall factor multiplying the diagram is hence

$$4^{m+2} Q_c[i] \cdot Q_c[i|l_1] \left(\prod_{n=1}^{m-1} Q_c[i, l_1, \dots, l_n | l_{n+1}] \right) Q_c[i, l_1, \dots, l_m | j] = 4^{m+2} Q_c[i, l_1, \dots, l_m, j]. \quad (3.67)$$

This way, the whole interaction process is taken into account by the hard-core constraint. In principle, given the RK-like background, this scheme allows to implement the constraint exactly if we introduce the factors from Eq.(3.67) into all diagrams of our ph-ladder approach. Note that if one wants to go beyond first order in the constraint, these additional factors cannot be attached to the vertices t_i in a simple manner anymore as it was possible in Eq.(3.64), (3.65) and (3.66). For every bare interaction line one would have to consider the "history" of the interaction process. At first order on the other hand, we only consider the corresponding bare interaction line of the next step in a given process. Hence we discard the preceding process and are only interested in the next link relative to the current one, which depends now only on t_i . The full constraint is of course hard to implement and in the following we are content with the first order replacements of Eq.(3.64), (3.65) and

(3.66) that have to be made in all the results of the next section, Sec.(3.5).

At this point we remark that we actually expect this first order replacement to yield better results as compared to including the complete correlation $Q_c[i, l_1, \dots, l_m, j]$. The reason is the following: In our diagrammatic expansion, we did not include the bosonic interaction terms proportional to V and J , as there is no quadratic term in the theory that would allow to treat them within perturbation theory. Thus, the way our theory is set up as of now, the background configuration of bosonic dimers is static, which leads to the correlations $Q_c[i, l_1, \dots, l_m, j]$ of a given ladder process. This way, we lose track of the possible rearrangements of the bosonic background always in between two interactions with the fermionic dimer. This rearrangement occurs without a cost in energy at the RK-point. Therefore, for a given ladder process, the background does not necessarily need to be set up in a configuration that allows for all the steps in the ladder-process to occur, described by $Q_c[i, l_1, \dots, l_m, j]$. Instead, the background needs to be set up such that the first exchange in that process can happen, corresponding to $Q_c[i, l_1]$. After that, the bosonic background can rearrange via the RK-term and then needs to be set up such that the second exchange can occur, corresponding to $Q_c[l_1, l_2]$. This line of reasoning applies to every step in a given ladder-process and we therefore arrive at the first order replacement of the $Q_c[i, l_1, \dots, l_m, j]$ -version. This first order replacement then, by the arguments just given, effectively includes the bosonic background interactions and is hence expected to yield good results.

3.5 Results

We present and analyze the results for the spectral function obtained by the derivations of the previous section. From the spectral function we can infer a dispersion $\varepsilon(\mathbf{p})$ for the inserted holes, as well as the corresponding quasiparticle-residuuum $\mathcal{Z}(\mathbf{p})$. We compare the results for the dispersion with the mean field theory from Sec.(2.3.2) and check the agreement of both dispersion and quasiparticle residuum with results from exact diagonalization that were kindly provided by M. Punk and S. Huber.

3.5.1 Symmetries

We begin with the analysis of the symmetry properties that the spectral function resulting from the ph-ladder approach exhibits. We insert the solution Eq.(3.59) for the effective vertex into the expression from Eq.(3.35) for the electron propagator \mathcal{G}_c and use the analytic continuation procedure from Eq.(3.28) to obtain the spectral function via Eq.(3.27). In the following we confine ourselves to the parameter regime of $t_i/J \ll 1$, where we believe our Ansatz to be valid.

We can consider the system to be filled with electrons (i.e. vanishing doping relative to half-filling) in the beginning. Upon injecting holes into the system, the highest electronic states become unoccupied. In a dual description, we insert holes into their lowest lying energy states. Hence, to obtain the spectral function and thus the dispersion for the holes from our electronic spectral function we have to make the replacement

$$\mathcal{A}(\mathbf{p}, \omega_p) \rightarrow \mathcal{A}(-\mathbf{p}, -\omega_p). \quad (3.68)$$

One can now prove that the spectral function is symmetric under momentum-inversion $\mathbf{p} \rightarrow -\mathbf{p}$. We can show this explicitly by applying $\mathbf{p} \rightarrow -\mathbf{p}$ to the matrix equation Eq.(3.59). Taking into consideration the form of the vector $\vec{\Gamma}(\mathbf{p})$ from Eq.(3.55) we note that this transformation effectively acts as $\Gamma^{\eta_1 \eta_2 \eta_1 \eta_2}(-\mathbf{p}) = \Gamma^{\eta_2 \eta_1 \eta_2 \eta_1}(\mathbf{p})$, i.e. as an exchange of dimer orientations. We denote this as $\vec{\Gamma}(-\mathbf{p}) = \vec{\Gamma}^{\eta_1 \leftrightarrow \eta_2}(\mathbf{p})$. The same argument holds true for the matrix \mathcal{M} from Eq.(3.57), i.e. $\mathcal{M}(-\mathbf{p}, i\omega_p) = \mathcal{M}^{\eta_1 \leftrightarrow \eta_2}(\mathbf{p}, i\omega_p)$. Under momentum-inversion, Eq.(3.59) hence becomes

$$\vec{\Gamma}(-\mathbf{p}, i\omega_p) = \vec{\Gamma}^{\eta_1 \leftrightarrow \eta_2}(\mathbf{p}) [\mathcal{M}^{\eta_1 \leftrightarrow \eta_2}(\mathbf{p})]^{-1} = \vec{\Gamma}^{\eta_1 \leftrightarrow \eta_2}(\mathbf{p}, i\omega_p). \quad (3.69)$$

To insert this relation into the expression for the electronic propagator $\mathcal{G}_c(\mathbf{p}, i\omega_p)$, we write Eq.(3.35) in a short form as

$$\mathcal{G}_c(\mathbf{p}) = \frac{1}{4\beta V} \sum_{\eta_1, \eta_2} f^{\eta_1, \eta_2}(\mathbf{p}) \Lambda^{\eta_1, \eta_2}(\mathbf{p}, i\omega_p), \quad (3.70)$$

where $f^{\eta_1, \eta_2}(\mathbf{p}) = (1 + e^{-ip\eta_1})(1 + e^{ip\eta_2})$ and $\Lambda^{\eta_1, \eta_2}(\mathbf{p}, i\omega_p)$ contains the effective vertex. We then see readily that $f^{\eta_1, \eta_2}(-\mathbf{p}) = f^{\eta_1 \leftrightarrow \eta_2}(\mathbf{p})$ which together with the property Eq.(3.69) of the vertex directly implies that $\mathcal{G}_c(-\mathbf{p}, i\omega_p) = \mathcal{G}_c(\mathbf{p}, i\omega_p)$. This symmetry of the propagator then leads to the same symmetry of the spectral function,

$$\mathcal{A}(-\mathbf{p}, \omega_p) = \mathcal{A}(\mathbf{p}, \omega_p). \quad (3.71)$$

The spectral function for holes with momentum \mathbf{p} and frequency ω_h is thus $\mathcal{A}_h(\mathbf{p}, \omega_h) = \mathcal{A}(\mathbf{p}, -\omega_h)$ in terms of the electronic spectral function we already calculated. Later on, we want to compare the hole part of the numerically determined spectral function with this analytic hole spectral function for $T = 0$.

To continue with our analysis we see that the matrix equation from Eq.(3.59) can be solved exactly and the resulting analytic form of the spectral function at zero temperature is

$$\mathcal{A}(\mathbf{p}, \omega_p) = \frac{2\gamma}{\pi} \frac{8\mathcal{Z}_0(\mathbf{p}) (16(\gamma^2 + \omega_p^2) + K_1(\mathbf{p})) + 2K_2(\mathbf{p}) (4\omega_p - t_1 \cos(p_x) - t_1 \cos(p_y))}{[16(\gamma^2 - \omega_p^2) + 8\omega_p t_1 (\cos(p_x) + \cos(p_y)) + K_1(\mathbf{p})]^2 + [8\gamma (4\omega_p - t_1 \cos(p_x) - t_1 \cos(p_y))]^2}, \quad (3.72)$$

where $\mathcal{Z}_0(\mathbf{p}) = \frac{1}{4} [\cos^2(p_x/2) + \cos^2(p_y/2)]$ from before. We further introduced a finite width $\gamma > 0$ which can be done by replacing $i\omega_p \rightarrow \omega_p + i\gamma$ in the analytic continuation procedure for the retarded Green's function. The functions $K_1(\mathbf{p})$ and $K_2(\mathbf{p})$ only depend on momentum and on the t_i and we have given their explicit form in the Appendix of [34]. For our current purposes it suffices to note that K_1 is quadratic in the parameters t_i while K_2 is linear, i.e.

$$K_1(\mathbf{p}) = \sum_{i,j \in \{1,2,3\}} t_i t_j g_{i,j}(\mathbf{p}) \quad (3.73)$$

$$K_2(\mathbf{p}) = \sum_{i \in \{1,2,3\}} t_i h_i(\mathbf{p}). \quad (3.74)$$

For a given value of \mathbf{p} in the BZ, the spectral function $\mathcal{A}(\mathbf{p}, \omega_p)$ from Eq.(3.72) is made up of a sum of Lorentzians (or delta functions for $\gamma \rightarrow 0$), typical examples are shown in Fig.(13). The pure composition from delta functions allows to make use of the relation $\mathcal{A}(\mathbf{p}, \omega_p) = \mathcal{Z}(\mathbf{p})\delta(\varepsilon(\mathbf{p}) - \omega_p)$ in order to extract the dispersion $\varepsilon(\mathbf{p})$ as well as the quasiparticle residuum $\mathcal{Z}(\mathbf{p})$ of the fermionic quasiparticles. The general approach is as follows: For a given \mathbf{p} in the BZ we fit a sum of Lorentzians to the function $\mathcal{A}_h(\mathbf{p}, \omega_h)$. We then note the position and the weight of the leftmost peak (which can also be zero) and associate the peak-position $\omega_{\text{peak}}(\mathbf{p}) = \varepsilon(\mathbf{p})$ with the dispersion and in the same fashion the weight with the quasiparticle residuum.

We start by writing the spectral function from Eq.(3.72) as a sum of two Lorentzians,

$$\mathcal{A}(\mathbf{p}, \omega_p) = \mathcal{Z}_1(\mathbf{p}) \frac{1}{\pi} \frac{\gamma}{(\omega_p - \omega_1)^2 + \gamma^2} + \mathcal{Z}_2(\mathbf{p}) \frac{1}{\pi} \frac{\gamma}{(\omega_p - \omega_2)^2 + \gamma^2}, \quad (3.75)$$

where ω_1 and ω_2 mark the positions of the peaks on the frequency axis and $\mathcal{Z}_{1,2}$ correspond to the respective peak-weights. Expressed within a single fraction we obtain

$$\mathcal{A}(\mathbf{p}, \omega_p) = \frac{\gamma}{\pi} \frac{\mathcal{Z}_1(\mathbf{p}) [(\omega_p - \omega_2)^2 + \gamma^2] + \mathcal{Z}_2(\mathbf{p}) [(\omega_p - \omega_1)^2 + \gamma^2]}{[(\omega_p - \omega_1)^2 + \gamma^2] [(\omega_p - \omega_2)^2 + \gamma^2]}. \quad (3.76)$$

At width $\gamma \rightarrow 0$, the denominator of this expression has its zeroes at the peak positions ω_1 and ω_2 , i.e.

$$(\mathcal{A}(\mathbf{p}, \omega_p))^{-1} \propto [(\omega_p - \omega_1)^2 + \gamma^2] [(\omega_p - \omega_2)^2 + \gamma^2] \xrightarrow{\gamma \rightarrow 0} (\omega_p - \omega_1)^2 (\omega_p - \omega_2)^2. \quad (3.77)$$

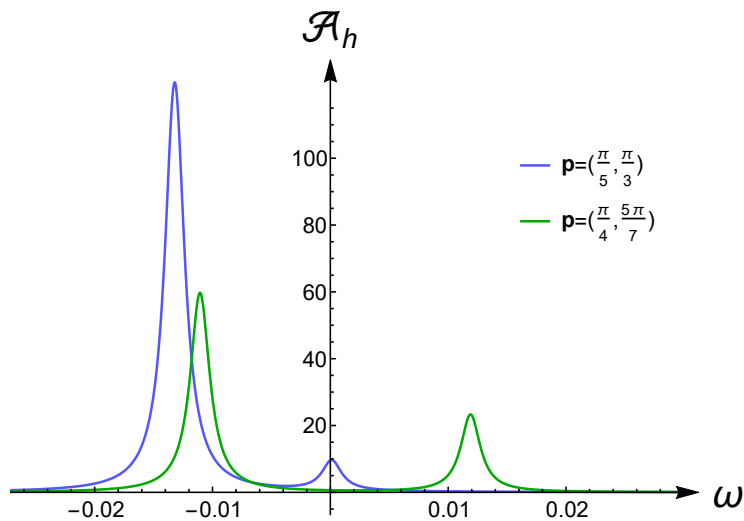


Figure 13: Typical form of the spectral function at given points in momentum space, for a parameter set $t_1 = t_3 = 0.01$, $t_2 = 0$. $\mathcal{A}_h(\omega)$ is generally composed of delta functions (or Lorentzians) whose norm and position on the ω -axis depend on \mathbf{p} . The leftmost peak at a given momentum \mathbf{p} corresponds to the low energy spectral peak of the holes.

Hence we can find the exact peak positions of our spectral function from Eq.(3.72) by finding the zeroes of the denominator at $\gamma = 0$. This leads to the condition

$$-16\omega_p^2 + 8\omega_p t_1 (\cos(p_x) + \cos(p_y)) + K_1(\mathbf{p}) = 0 \quad (3.78)$$

which is solved by the positions

$$\omega_{1,2} = \frac{1}{4}t_1 (\cos(p_x) + \cos(p_y)) \pm \frac{1}{4}\sqrt{t_1^2 (\cos(p_x) + \cos(p_y))^2 + K_1(\mathbf{p})} \quad (3.79)$$

for the delta peaks. Furthermore, it is easy to check that Eq.(3.75) implies

$$\mathcal{Z}_1(\mathbf{p}) \left(1 - \frac{\gamma^4}{[(\omega_1 - \omega_2)^2 + \gamma^2]^2} \right) = \pi\gamma\mathcal{A}(\mathbf{p}, \omega_1) - \pi\gamma\mathcal{A}(\mathbf{p}, \omega_2) \frac{\gamma^2}{(\omega_1 - \omega_2)^2 + \gamma^2}, \quad (3.80)$$

which, assuming $\omega_1 \neq \omega_2$, implies

$$\mathcal{Z}_1(\mathbf{p}) = \lim_{\gamma \rightarrow 0} [\gamma\pi\mathcal{A}(\mathbf{p}, \omega_1)] \quad (3.81)$$

and correspondingly for the weight \mathcal{Z}_2 of the second peak. As explained above, the spectral function for the holes is given by $\mathcal{A}_h(\mathbf{p}, \omega_h) = \mathcal{A}(\mathbf{p}, -\omega_h)$, so the leftmost peak of the hole spectral function and hence the dispersion is given by

$$\varepsilon(\mathbf{p}) = -\omega_1(\mathbf{p}) = -\frac{1}{4}t_1 (\cos(p_x) + \cos(p_y)) - \frac{1}{4}\sqrt{t_1^2 (\cos(p_x) + \cos(p_y))^2 + K_1(\mathbf{p})}. \quad (3.82)$$

The quasiparticle residuum is then given by the weight of the corresponding peak, i.e.

$$\mathcal{Z}(\mathbf{p}) = \mathcal{Z}_1(\mathbf{p}) = \lim_{\gamma \rightarrow 0} [\gamma\pi\mathcal{A}(\mathbf{p}, \omega_1(\mathbf{p}))]. \quad (3.83)$$

At this point we can make a simple consistency check for the form of our spectral function from Eq.(3.72) by considering the non-interacting limit $t_i = 0$. Accordingly, we obtain $\omega_1 = 0 = \varepsilon(\mathbf{p})$ from Eq.(3.82) and

$$\mathcal{Z}_{\{t_i=0\}} = \lim_{\gamma \rightarrow 0} [\gamma \pi \mathcal{A}_{\{t_i=0\}}(\mathbf{p}, 0)] = \lim_{\gamma \rightarrow 0} \gamma \pi \frac{2\gamma}{\pi} \frac{8\mathcal{Z}_0(\mathbf{p}) \cdot 16\gamma^2}{(16\gamma^2)^2} = \mathcal{Z}_0(\mathbf{p}) \quad (3.84)$$

as required.

As a next step, we consider the behaviour of the spectral function under a total sign change of the Hamiltonian implemented by $t_i \rightarrow -t_i$. To this end we extend our notation and write $\mathcal{A}(\mathbf{p}, \omega_p) = \mathcal{A}_{\{t_i\}}(\mathbf{p}, \omega_p)$ for a given set of parameters $\{t_i\}$. One can then consider the behaviour of the expression in Eq.(3.72) for the spectral function under $t_i \rightarrow -t_i, \omega_p \rightarrow -\omega_p$. Using that under this transformation the functions K_1 and K_2 change like $K_1(\mathbf{p}) \rightarrow K_1(\mathbf{p})$ (K_1 quadratic in the t_i) and $K_2(\mathbf{p}) \rightarrow -K_2(\mathbf{p})$ (K_2 linear in the t_i), one can readily see from Eq.(3.72) that $\mathcal{A}_{\{-t_i\}}(\mathbf{p}, -\omega_p) = \mathcal{A}_{\{t_i\}}(\mathbf{p}, \omega_p)$ and hence

$$\mathcal{A}_{\{-t_i\}}(\mathbf{p}, \omega_p) = \mathcal{A}_{\{t_i\}}(\mathbf{p}, -\omega_p). \quad (3.85)$$

This relation maps a dimer model with parameter set $\{-t_i\}$ back to the model with $\{t_i\}$ by inverting the frequency axis. Recalling that in order to compute dispersion and quasiparticle residuum we consider the leftmost peak of the hole spectral function, we note that for a transformation $t_i \rightarrow -t_i$ the role of the two peaks are interchanged, i.e. the initially rightmost peak becomes the leftmost and its weight the corresponding quasiparticle residuum. It hence suffices to calculate the complete spectral function for a given parameter set $\{t_i\}$.

Finally, we use this mapping to prove that the normalization relation from Eq.(3.42) for the spectral function holds true for the analytic results obtained here. We consider a fixed set of parameter $\{t_i\}$ and want to compute the sum $\mathcal{Z}_1(\mathbf{p}) + \mathcal{Z}_2(\mathbf{p})$ of the two peaks via Eq.(3.81). To this end, we calculate

$$\mathcal{A}(\mathbf{p}, \omega_{1,2}) = \frac{2\gamma}{\pi} \frac{8\mathcal{Z}_0 [16\gamma^2 + 16\omega_{1,2}^2 + K_1] \pm 2K_2 \sqrt{t_1^2 (\cos(p_x) + \cos(p_y))^2 + K_1}}{(16\gamma^2)^2 + 64\gamma^2 (t_1^2 (\cos(p_x) + \cos(p_y))^2 + K_1)} \quad (3.86)$$

and therefore

$$\begin{aligned} \mathcal{A}(\mathbf{p}, \omega_1) + \mathcal{A}(\mathbf{p}, \omega_2) &= \frac{2\gamma}{\pi} \frac{8\mathcal{Z}_0}{(16\gamma^2)^2 + 64\gamma^2 (t_1^2 (\cos(p_x) + \cos(p_y))^2 + K_1)} \times \\ &\times \left[32\gamma^2 + 2K_1 + 16\omega_1^2 + 16\omega_2^2 \right] = \\ &= \frac{16\gamma}{\pi} \mathcal{Z}_0 \frac{32\gamma^2 + 4 [t_1^2 (\cos(p_x) + \cos(p_y))^2 + K_1]}{16\gamma^2 \{16\gamma^2 + 4 [t_1^2 (\cos(p_x) + \cos(p_y))^2 + K_1]\}}. \end{aligned} \quad (3.87)$$

The added weight of the two peaks can hence be determined by

$$\begin{aligned} \sum_{i=1,2} \mathcal{Z}_i(\mathbf{p}) &= \lim_{\gamma \rightarrow 0} [\gamma \pi (\mathcal{A}(\mathbf{p}, \omega_1) + \mathcal{A}(\mathbf{p}, \omega_2))] = \\ &= \mathcal{Z}_0 \lim_{\gamma \rightarrow 0} \frac{32\gamma^2 + 4 [t_1^2 (\cos(p_x) + \cos(p_y))^2 + K_1]}{16\gamma^2 + 4 [t_1^2 (\cos(p_x) + \cos(p_y))^2 + K_1]}. \end{aligned} \quad (3.88)$$

For $t_1^2 (\cos(p_x) + \cos(p_y))^2 + K_1 \neq 0$ (i.e. $\omega_1 \neq \omega_2$) when the two energy bands generated by the two delta peaks are non-degenerate, we obtain from Eq.(3.88) the desired relation

$$\sum_{i=1,2} \mathcal{Z}_i(\mathbf{p}) = \mathcal{Z}_0(\mathbf{p}). \quad (3.89)$$

For $\omega_1 = \omega_2$ there remains only one peak and the resulting spectral function is again $\mathcal{Z}(\mathbf{p}) = \frac{1}{2} \sum_{i=1,2} \mathcal{Z}_i(\mathbf{p}) = \mathcal{Z}_0(\mathbf{p})$.

For a given parameter set $\{t_i\}$ and the mapping between $\{t_i\}$ and $\{-t_i\}$ from above we thus arrive at the relation

$$\mathcal{Z}_{\{t_i\}}(\mathbf{p}) + \mathcal{Z}_{\{-t_i\}}(\mathbf{p}) = \mathcal{Z}_0(\mathbf{p}) \quad (3.90)$$

and within the ph-ladder approach the quasiparticle residuum of a set of interaction parameters can be computed directly from the corresponding residuum of the sign-inverted parameter set. One can further derive the following relations from Eq.(3.82) for the dispersion and Eq.(3.86) which determines the quasiparticle residuum:

$$\varepsilon_{\{c \cdot t_i\}}(\mathbf{p}) = c \cdot \varepsilon_{\{t_i\}}(\mathbf{p}) \quad (3.91)$$

$$\mathcal{Z}_{\{c \cdot t_i\}}(\mathbf{p}) = \mathcal{Z}_{\{t_i\}}(\mathbf{p}) \quad (3.92)$$

Again we simply used the scaling behaviour of the functions $K_1(\mathbf{p})$ and $K_2(\mathbf{p})$. As a consequence, it suffices to consider the model on an arbitrary half-sphere in the (t_1, t_2, t_3) -parameter space.

3.5.2 Dispersion and residuum

In Fig.(14) we show the hole spectral function in the upper right quarter of the BZ for various values of the interaction parameters t_i . As a consequence of the form of the bare bosonic and fermionic propagators, the resulting spectral function consists of delta functions (or Lorentzians once we introduce a finite width γ). We show \mathcal{A}_h for different values of t_1, t_2, t_3 at a fixed ω . The structure of the spectral function is clearly visible and generally consists of a pocket around $\mathbf{p} = 0$ and another pocket located roughly around $\mathbf{p} = (\pi/2, \pi/2)$ and symmetry related points. This coincides with our expectations from the dispersion of the mean field analysis as well as from exact diagonalization, which both feature the two pockets that can be identified here as well. Note again that the existence of the $(\pi/2, \pi/2)$ -pocket is just what we expect in the pseudogap phase of high- T_c cuprates, where experiments feature so-called Fermi-arcs. From the viewpoint of our dimer model, these arcs arise due to a fractionalized Fermi liquid structure. The fermionic quasiparticles, corresponding to the insertion of holes into the bosonic dimer background, form the pocket of size p (the doping) around $(\pi/2, \pi/2)$ and lead to a spectral function that correspondingly forms the Fermi-arc we want to describe. Experimentally, these Fermi-arcs are detected by the use of ARPES measurements (see Sec.(1)) which provide direct access to the hole-part of the spectral function that we evaluated here in an analytical approach.

We also see from Fig.(14) that the spectral function carries a quasiparticle residuum \mathcal{Z} that corresponds to the norm of the delta (or Lorentz) peaks one can see throughout the BZ. At this point, our diagrammatic Ansatz goes beyond the mean field approach which only allowed to approximate the dispersion of the system's fermionic quasiparticles. An

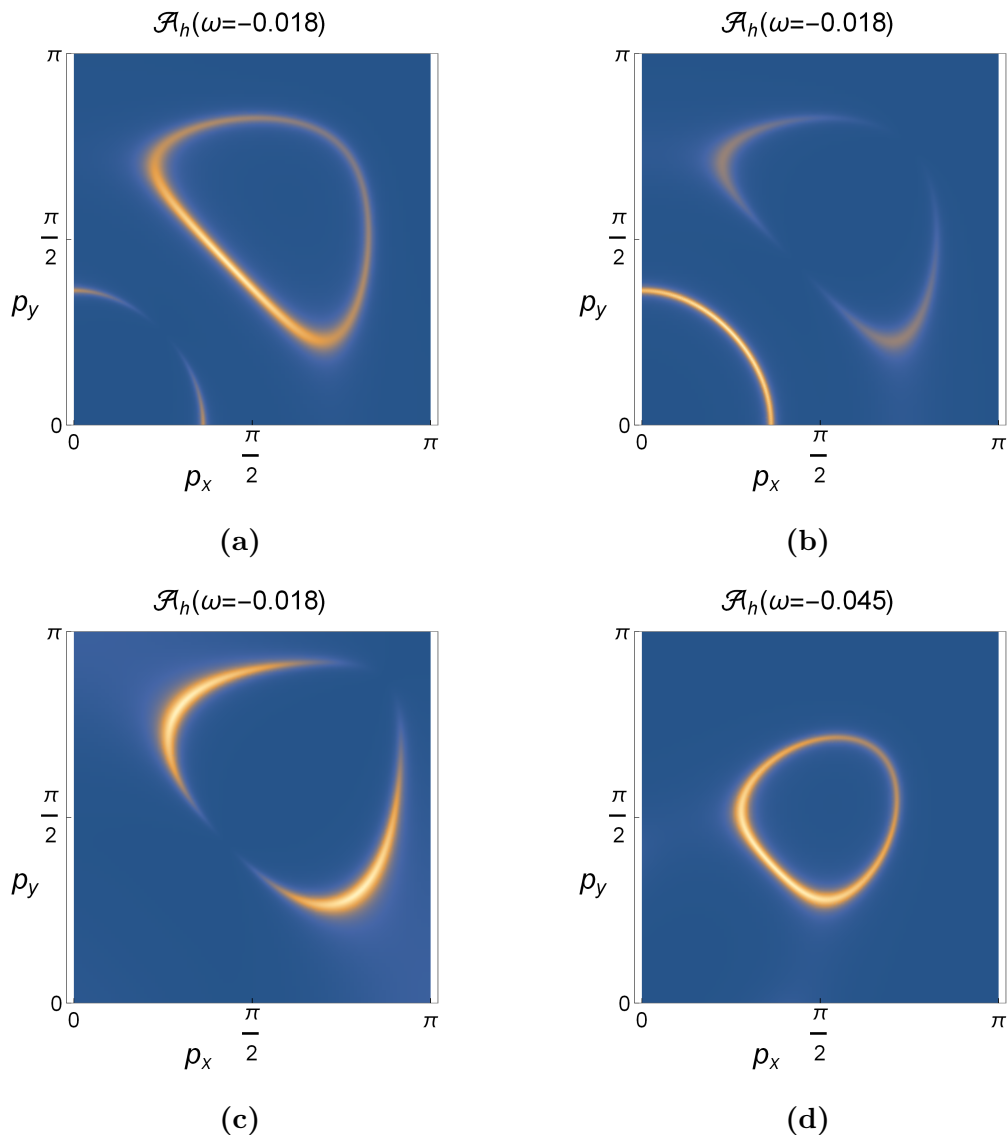


Figure 14: The hole spectral function $\mathcal{A}_h(\mathbf{p}, \omega)$ in the upper right corner of the BZ at a fixed Fermi level $\omega = \varepsilon_F$ (measured in units of J) that illustrates the structure of $\mathcal{A}_h(\mathbf{p}, \omega)$ for a selection of parameters t_i . For better visibility, the delta functions were broadened into Lorentzian peaks of finite width γ . The corresponding parameter values shown in (a)-(d) are (a) $t_1 = t_2 = 0, t_3 = -0.02$ (b) $t_1 = t_2 = 0, t_3 = 0.02$ (c) $t_1 = -0.02, t_2 = -0.01, t_3 = 0.02$ (d) $t_1 = -0.01, t_2 = 0.03, t_3 = -0.02$

interesting feature which can be seen e.g. in Fig.(14a) is the decrease of the spectral function in the area of the second magnetic BZ, i.e. towards the backside of the pocket. As proposed by [1], this decrease towards (π, π) can be imagined to be the reason for the experimentally observed, non-closed structure of the fermi-arcs in the second magnetic BZ. According to this reasoning, the comparatively small quasiparticle weight along the pocket's backside avoids its detection in ARPES experiments. Fig.(14) then shows that we can qualitatively obtain this crucial behaviour of the spectral function within our diagrammatic approach.

Next, we analyze dispersion and quasiparticle residuum of \mathcal{A}_h separately according to the relation $\mathcal{A}_h(\mathbf{p}, \omega_h) = \mathcal{Z}(\mathbf{p}) \delta(\varepsilon(\mathbf{p}) - \omega_h)$ as this makes a quantitative comparison with exact diagonalization results accessible. We show the 2D dispersion for various values of the parameters t_1, t_2, t_3 within the topright corner of the BZ next to the corresponding dispersions obtained by exact diagonalization of a 6×6 dimer model in Fig.(15) and (16). For the small values of the interaction parameters that were chosen here, the particle-hole ladder seems to be in good agreement with the numerical results. This can be made more explicit by plotting certain line cuts of the dispersion along a given path within the BZ in Fig.(17). The quantitative agreement is very good and shows that the diagrammatic approach indeed captures the essential features of the model as long as a homogeneous, i.e. RK-like bosonic background system can be assumed. It can further be observed from these line cuts (and analytically proven using the exact form of the dispersion with the function $K_1(\mathbf{p})$) that the mean-field dispersions obtained by the Ansatz from Sec.(2.3.2) in [1] exactly match the dispersion obtained from the ladder diagrams.

The residuum $\mathcal{Z}(\mathbf{p})$ resulting from Eq.(3.83) of our approach is evaluated again in the domain $(0, \pi) \times (0, \pi)$ and displayed in Fig.(18) and (19) next to the corresponding ED residua. Just like for the dispersion we find good agreement of our approach with the exact result. Again, the quantitative agreement can be shown to be quite accurate via the line cuts in Fig.(20), which indicates that for the region of small t_i in parameter space we have found reliable analytical access to the dimer model at hand. Notice in particular, that including the t_2 term according to the prescription from Sec.(3.3) provides a good fit to the numerical data, see e.g. Fig.(16b) and (19b).

Focusing on the case $t_2 = 0$ for a moment, Fig.(15) shows that we can obtain identical dispersions for different parameter sets. The dispersion seems to be invariant under $t_3 \rightarrow -t_3$ which can as well be understood from the analytic expression Eq.(3.82) by considering the properties of K_1 from Eq.(3.73) together with $g_{i,j}(\mathbf{p}) \propto \delta_{i,j}$ for $t_2 = 0$. From the perspective of the mean field dispersion there is no telling apart of such a pair of parameters sets. Our results then show that the two parameter sets can be distinguished by the quasiparticle residuum. In fact, $\mathcal{Z}_{t_1, t_2=0, t_3}(\mathbf{p})$ and $\mathcal{Z}_{t_1, t_2=0, -t_3}(\mathbf{p})$ have similar features, see e.g. Fig.(18a) and (18c) where in both cases the residuum vanishes along the BZ boundaries from (π, π) to $(\pi, 0)$ or $(0, \pi)$. The crucial difference comes in the behaviour around the point $(\pi/3, \pi/3)$. For a parameter set with $t_3 > 0$, the quasiparticle residuum is large in a region which can be approximated by $[0, \pi/3] \times [0, \pi/3]$ and decreases sharply when crossing the boundary to the outside of this region in the BZ. For $t_3 < 0$ it is the other way round, within $[0, \pi/3] \times [0, \pi/3]$ the residuum is highly suppressed and rises sharply outside. Towards the BZ boundary both cases converge again and eventually exactly match on the boundary. We note that the point $(\pi/3, \pi/3)$ was chosen deliberately to characterize the behaviour of the quasiparticle residuum, as at this specific point in the BZ the gap between the two induced electronic energy bands closes exactly. This can be checked easily by evaluating $2 \Delta\varepsilon(\pi/3, \pi/3) = \sqrt{t_1^2 (\cos(\pi/3) + \cos(\pi/3))^2 + K_1(\pi/3, \pi/3)} = 0$ for $t_2 = 0$. The residuum line cuts in Fig.(20) show that going along the BZ diagonal, the quasiparticle residuum can behave discontinuously right at the point $(\pi/3, \pi/3)$ with either a discontinuous drop or rise, see e.g. Fig.(20a-d). This may look suspicious at first sight, as we would not expect to obtain such discontinuous behaviour of the spectral peaks in this approach. The explanation for this feature then relies on $(\pi/3, \pi/3)$ being a gap closing point. We recall

that the determination of the quasiparticle residuum via Eq.(3.83) involved the assignment of the residuum to the weight of the leftmost peak of $\mathcal{A}_h(\mathbf{p}, \omega_h)$. The weight and position of each of the two peaks that constitute \mathcal{A}_h behave continuously throughout the whole BZ, but the assignment to the leftmost peak does not. Therefore, at a band touching point like $(\pi/3, \pi/3)$ the relative position of the two peaks can change in a perfectly continuous way while in the assignment of Eq.(3.83) we change the peak which we consider to be the left one. Hence the quasiparticle residuum defined by Eq.(3.83) may feature a discontinuity at that point. For the specific cases shown in Fig.(20a-d) we encounter a large peak and one with weight zero which invert their relative position on the frequency axis at $(\pi/3, \pi/3)$. Observe that although there is a weight-zero peak, i.e. one of the peaks is not actually present, we still consider it as a peak that contributes to the residuum if it is positioned to the left of the other peak. This is to make sure that the dispersion does not feature any discontinuities: Assume we have such a zero-weight peak at an energy $\omega = \omega_1$ located at a given point (k_0, k_0) on the BZ-diagonal. Moving away infinitesimally from the diagonal by a vector $\boldsymbol{\delta}$, we obtain an infinitesimally weighted peak at an infinitesimally shifted energy $\omega = \omega_1 + c \cdot |\boldsymbol{\delta}|$. Therefore, if we did not consider the weight-zero peak as a contributing peak, the leftmost peak at a point infinitesimally shifted away from the BZ-diagonal would correspond to an energy $\varepsilon(\mathbf{k}_0 + \boldsymbol{\delta}) = \omega_1 + c \cdot |\boldsymbol{\delta}|$ while at \mathbf{k}_0 we would have to take the position $\varepsilon(\mathbf{k}_0) = \omega_2$ of the second peak and would hence obtain a discontinuous dispersion upon crossing the BZ-diagonal.

Note that moving away from the $t_2 = 0$ -hyperplane in parameter space, the band degeneracy at $(\pi/3, \pi/3)$ is lifted and this specific point of the BZ in general no longer features a discontinuous residuum. Nonetheless, discussing the special case $t_2 = 0$ was worthwhile as it leads to insights on the behaviour of our results.

As a summarizing statement, the computed spectral function from Eq.(3.72) behaves perfectly continuous, possible discontinuities in the quasiparticle residuum arise from the discontinuous way of assigning the residuum to the weight of one of the two peaks in the spectral function \mathcal{A}_h . The dispersion must be continuous everywhere while band touching points in the BZ may be viewed as sources of discontinuity for the quasiparticle residuum. One way of characterizing a model obtained from a given parameter set with $t_2 = 0$ is to note how $\mathcal{Z}(\mathbf{p})$ behaves when crossing the band touching point of our model at $(\pi/3, \pi/3)$ going from the Γ -point $(0, 0)$ towards (π, π) . For $t_3 > 0$ we encounter a sharp drop of an initially large quasiparticle residuum while for $t_3 < 0$ the initially suppressed residuum makes a positive jump at $(\pi/3, \pi/3)$.

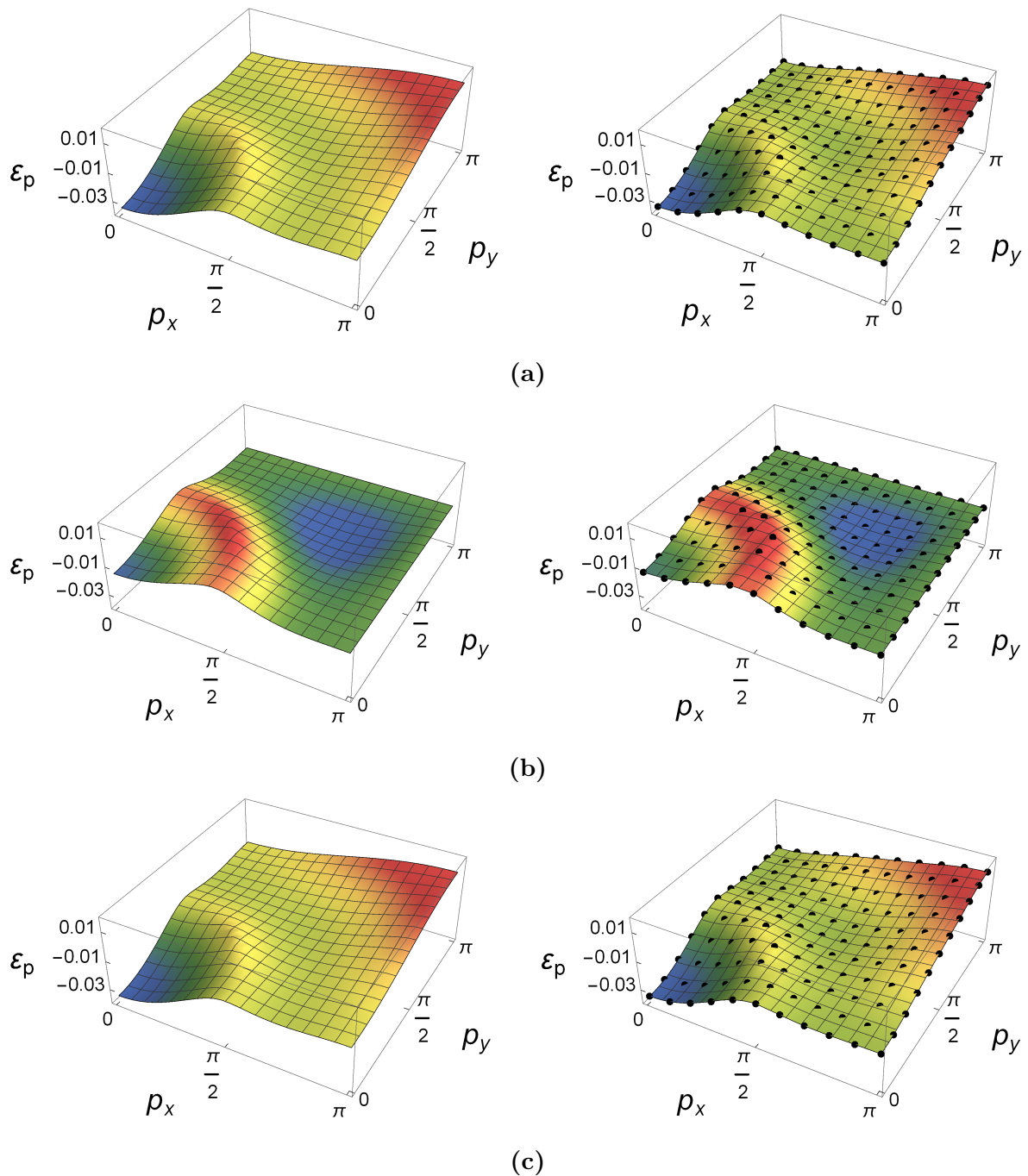


Figure 15: Comparison between analytical results and exact diagonalization of the hole-dispersion for different values of t_1, t_2, t_3 . The dispersions shown in the left column correspond to the analytical dispersion from Eq.(3.82) (which matches the mean field dispersion from Eq.(2.30)), those in the right column to ED results. The parameter values are (a) $t_1 = t_3 = 0.01, t_2 = 0$ (b) $t_1 = -t_3 = -0.01, t_2 = 0$ (c) $t_1 = -t_3 = 0.01, t_2 = 0$. The dispersions to the right are taken from exact diagonalization on a 6×6 square lattice with twisted boundary conditions. Notice the invariance of $\varepsilon(\mathbf{p})$ under $t_3 \rightarrow -t_3$ for $t_2 = 0$, see (a) and (b).

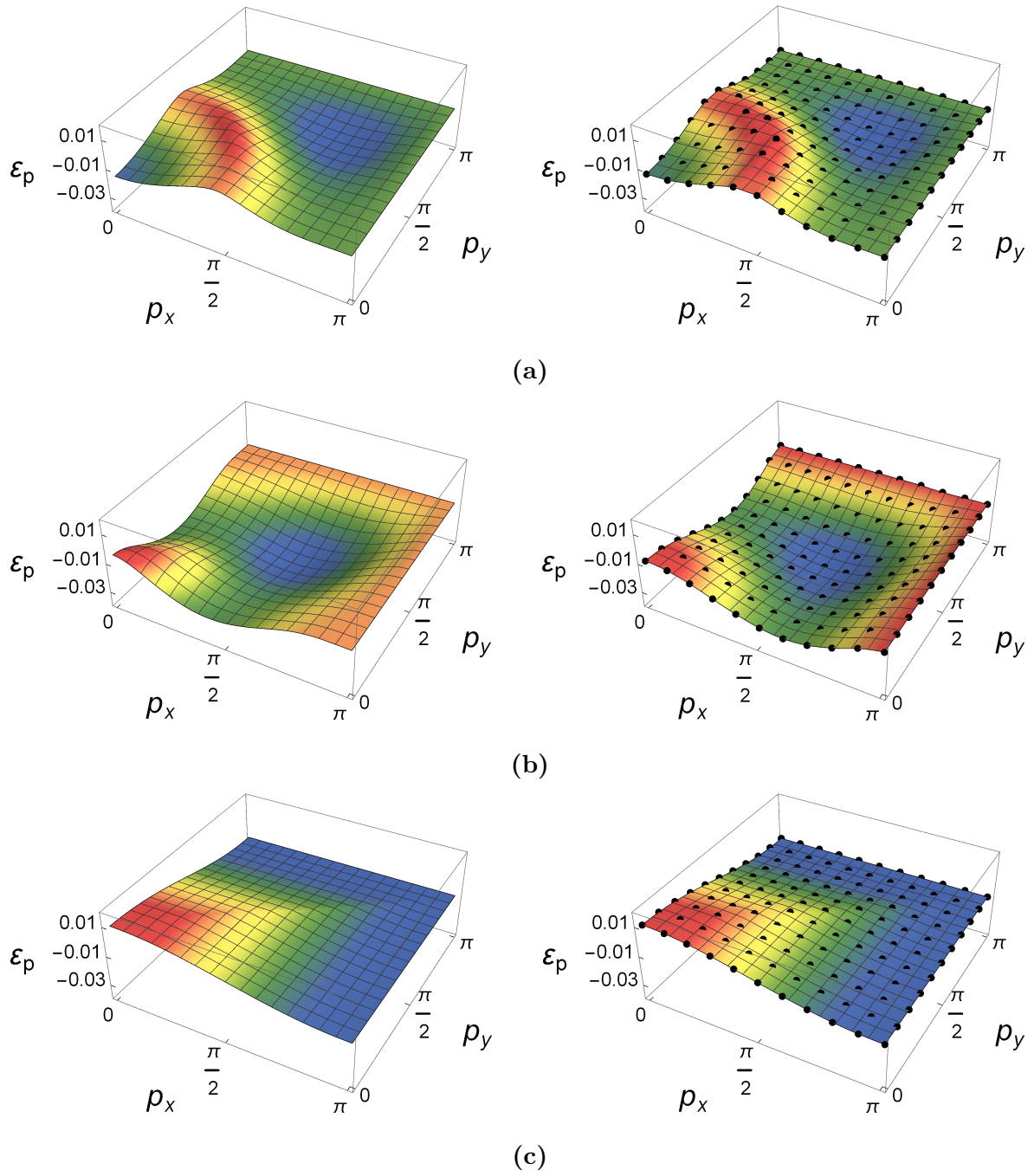


Figure 16: Continuation of Fig.(15) for the parameter sets (a) $t_1 = t_3 = -0.01, t_2 = 0$
 (b) $t_1 = -0.01, t_2 = -0.02, t_3 = 0.01$ (c) $t_1 = -0.01, t_2 = t_3 = 0$.

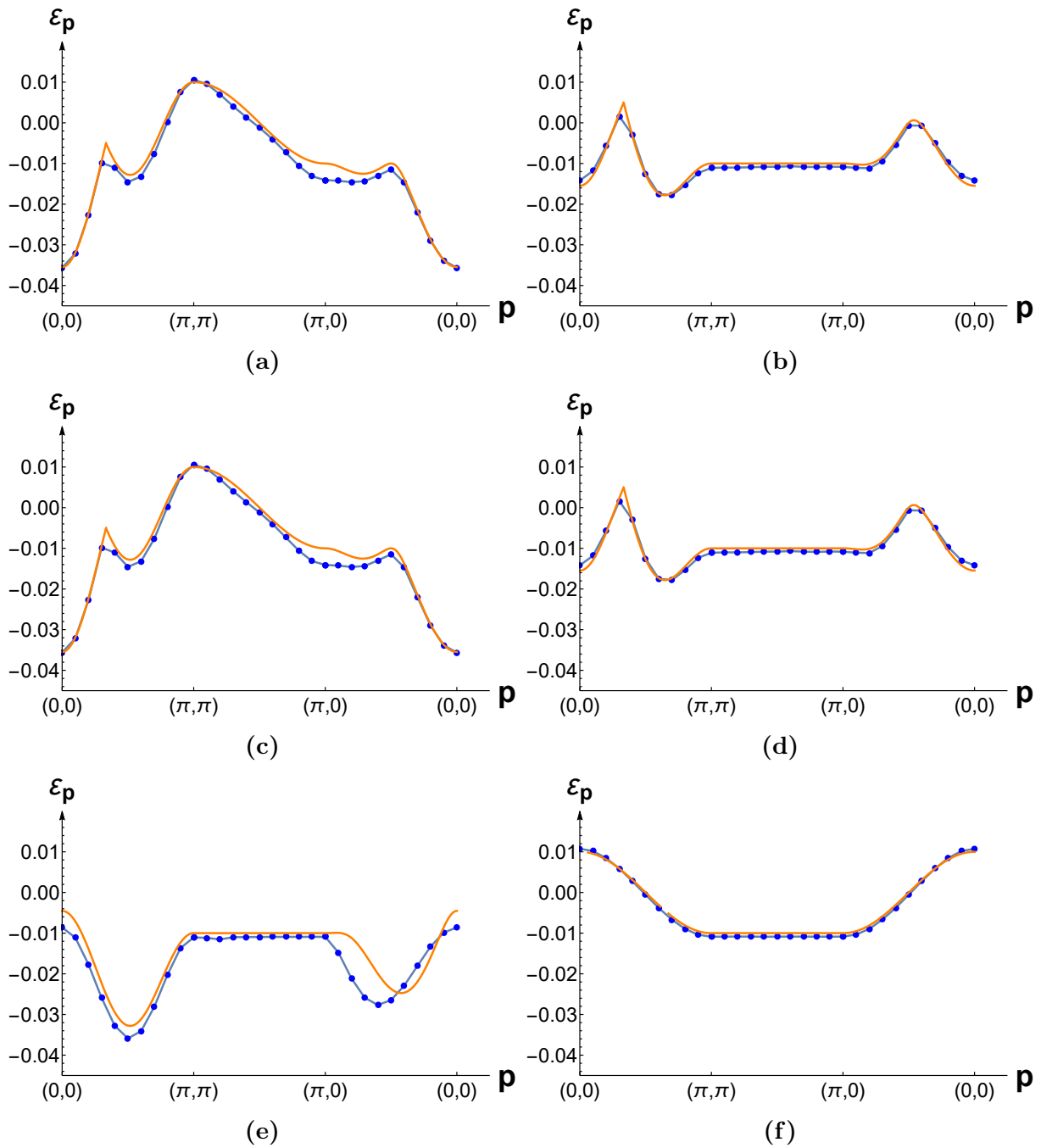


Figure 17: Line cuts of the dispersion $\varepsilon(\mathbf{p})$ along a given path in the BZ. Blue dotted line: exact diagonalization results; Red: results from the analytic ladder approach. We find excellent agreement of our calculations with numerical predictions. Parameter values (a) $t_1 = t_3 = 0.01, t_2 = 0$ (b) $t_1 = -t_3 = -0.01, t_2 = 0$ (c) $t_1 = -t_3 = 0.01, t_2 = 0$ (d) $t_1 = t_3 = -0.01, t_2 = 0$ (e) $t_1 = -0.01, t_2 = -0.02, t_3 = 0.01$ (f) $t_1 = -0.01, t_2 = t_3 = 0$.

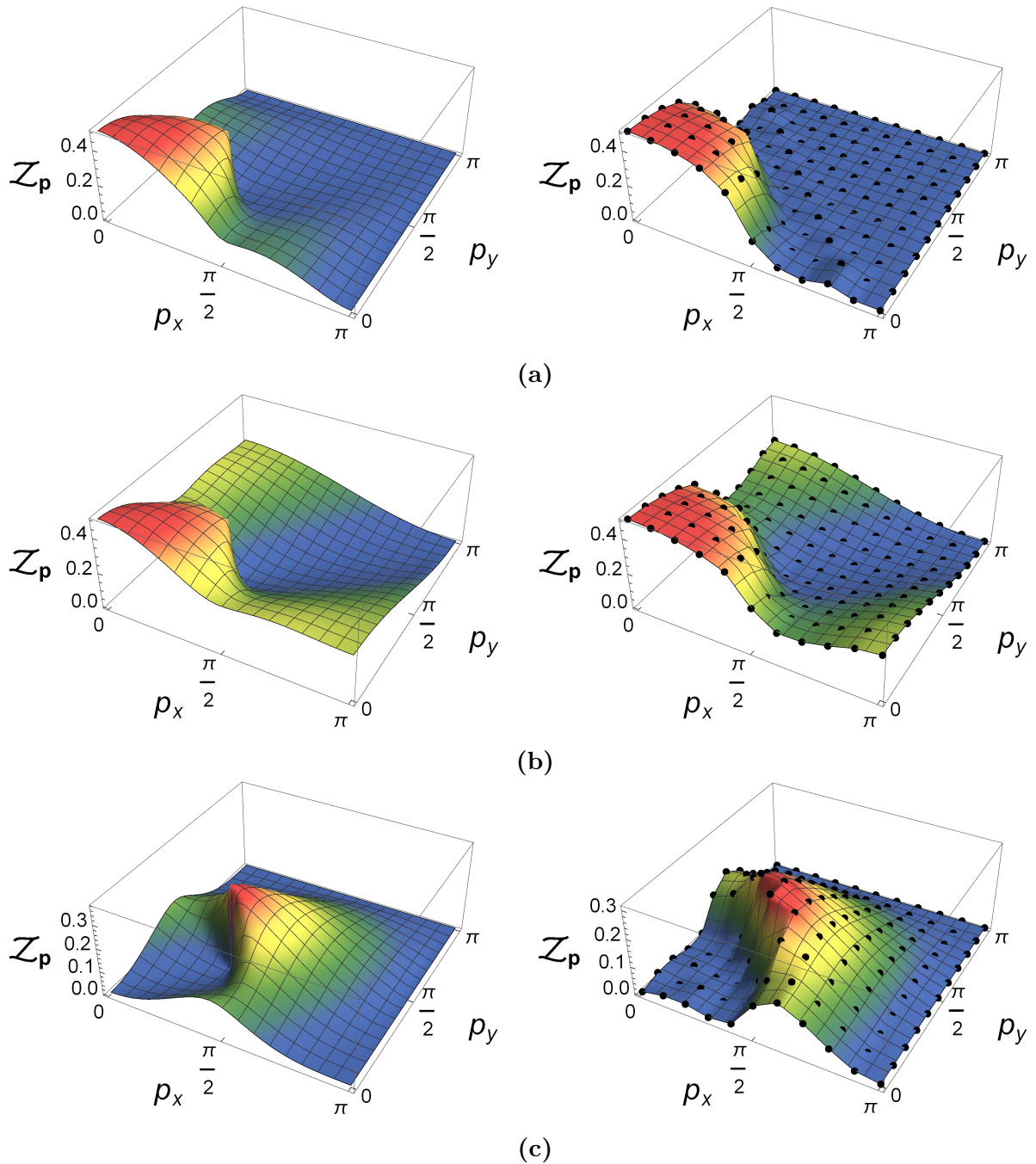


Figure 18: Comparison between analytical results and exact diagonalization of the quasi-particle residuum for different values of t_1, t_2, t_3 . The left column corresponds to the analytical calculation, the right column to ED results. The parameter values are (a) $t_1 = t_3 = 0.01, t_2 = 0$ (b) $t_1 = -t_3 = -0.01, t_2 = 0$ (c) $t_1 = -t_3 = 0.01, t_2 = 0$. The residuums to the right are taken from exact diagonalization on a 6×6 square lattice with twisted boundary conditions.

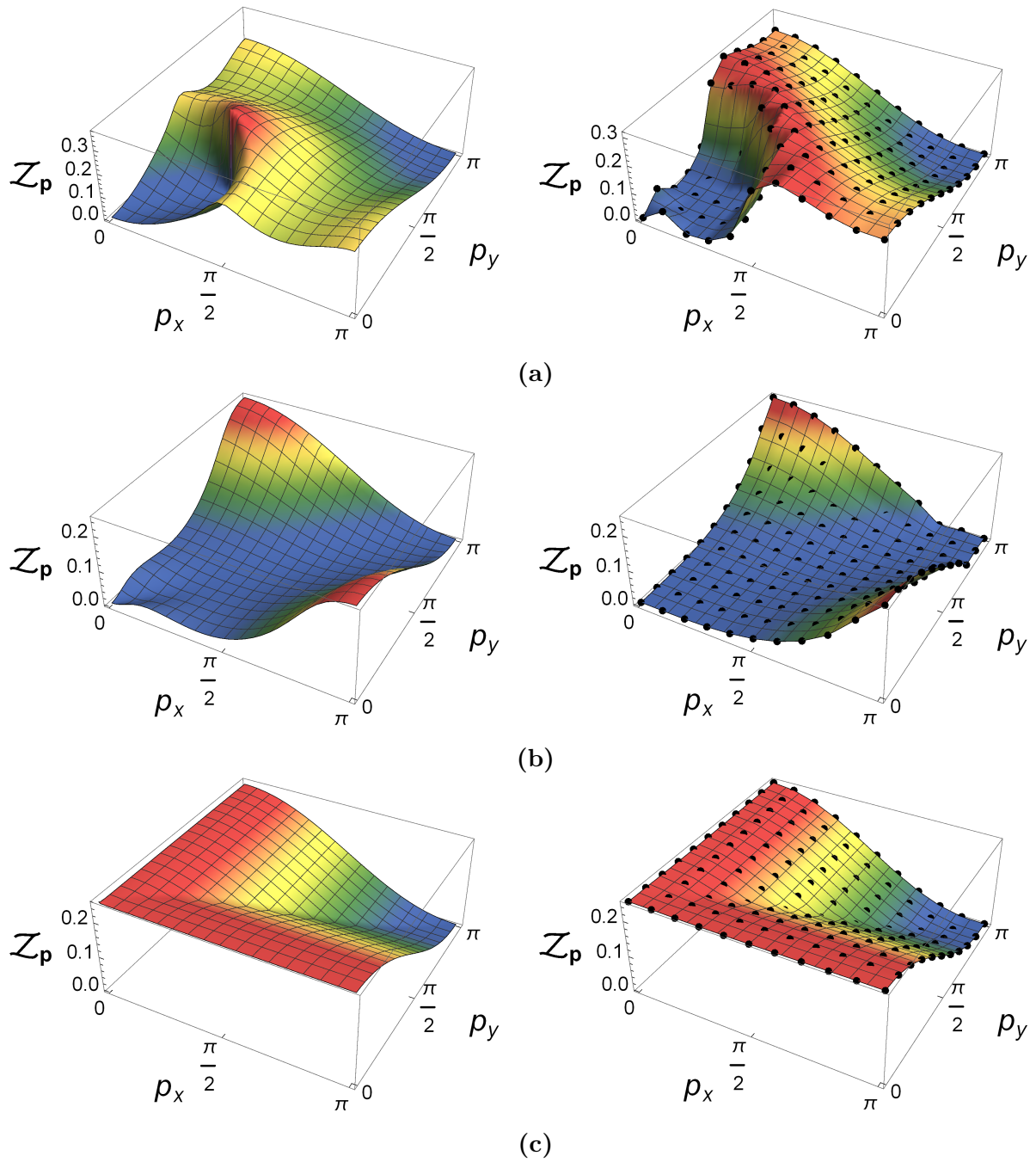


Figure 19: Continuation of Fig.(18) for the parameter sets (a) $t_1 = t_3 = -0.01, t_2 = 0$ (b) $t_1 = -0.01, t_2 = -0.02, t_3 = 0.01$ (c) $t_1 = -0.01, t_2 = t_3 = 0$.

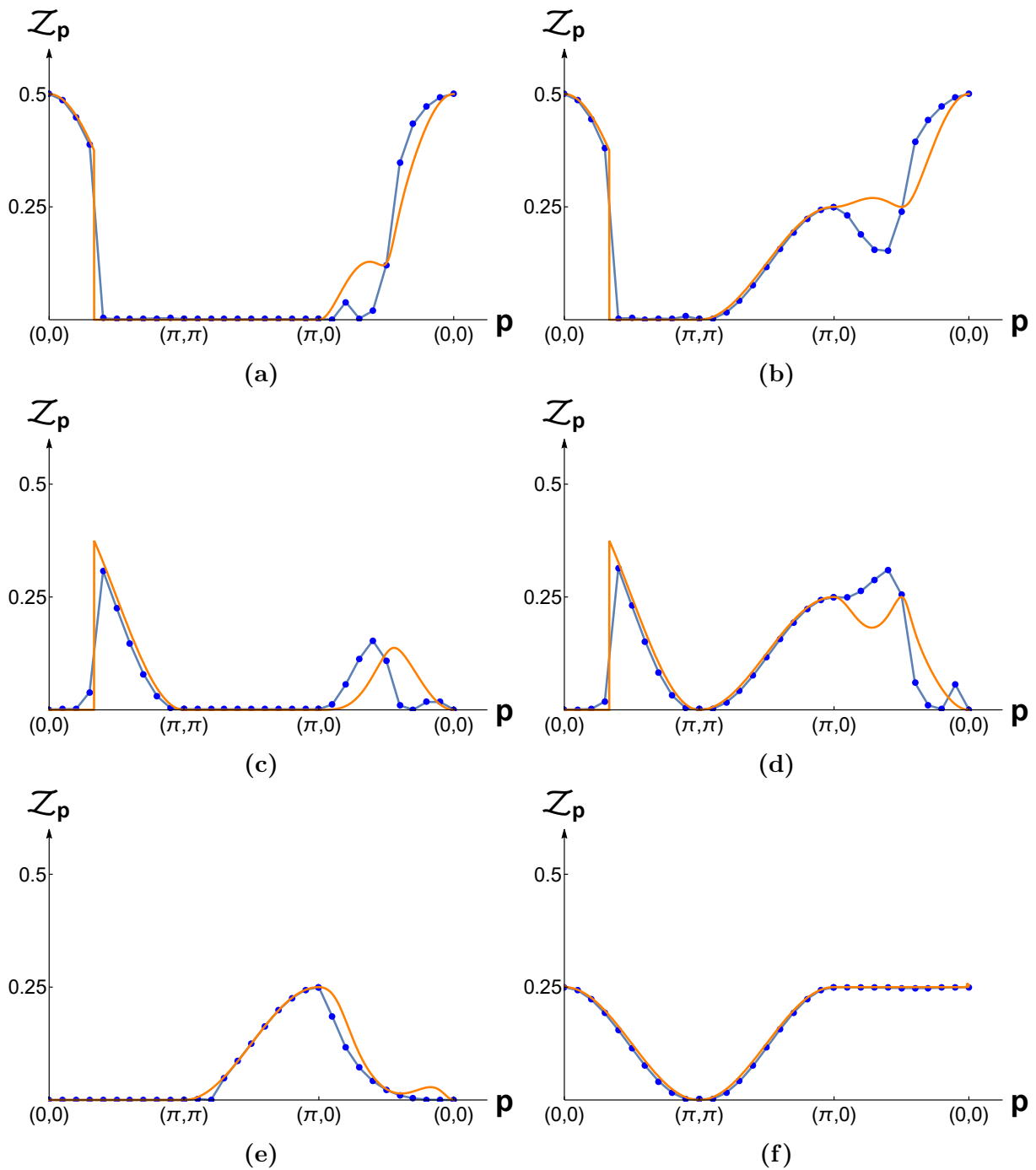


Figure 20: Line cuts of the quasiparticle residuum $\mathcal{Z}(\mathbf{p})$ along a given path in the BZ. Blue dotted line: exact diagonalization results; Red: results from the analytic ladder approach. We find excellent agreement of our calculations with numerical predictions. Parameter values (a) $t_1 = t_3 = 0.01, t_2 = 0$ (b) $t_1 = -t_3 = -0.01, t_2 = 0$ (c) $t_1 = -t_3 = 0.01, t_2 = 0$ (d) $t_1 = t_3 = -0.01, t_2 = 0$ (e) $t_1 = -0.01, t_2 = -0.02, t_3 = 0.01$ (f) $t_1 = -0.01, t_2 = t_3 = 0$.

3.5.3 Discussion

In the previous section we proved that the dispersion resulting from our diagrammatic approach and the dispersion from the mean field approach of Sec.(2.3.2) coincide exactly. The only difference comes in the interpretation of the two respective dispersions. In the mean field approach we effectively describe non-interacting fermionic dimers on an otherwise empty square lattice with hopping parameters t_i . In contrast, the diagrammatic approach assigns the dispersion not to the fermionic dimers but to the holes that are inserted into the system. There is of course a correspondence, as in our dimer picture the insertion of holes corresponds to the creation of fermionic dimers and thus the dispersions match exactly, yet the mean field approach disregards the bosonic background and hence misses that the resulting dispersion should be assigned to the holes as opposed to the fermionic dimers. Due to the correct assignment in the diagrammatic approach it is possible to compute the quasiparticle residuum via the ph-ladder as well. In the mean field case the spectral function of the fermionic excitations, i.e. the fermionic dimers, is given by the standard form $\mathcal{A}_0(\mathbf{p}, \omega_p) = \frac{1}{\pi} \frac{\gamma}{(\omega_p - \varepsilon(\mathbf{p}))^2 + \gamma^2}$ for non-interacting particles which results in $\mathcal{Z}(\mathbf{p}) = 1$ for the quasiparticle residuum. A non-interacting mean field model for the fermionic dimers can therefore not provide a realistic estimate for the actual quasiparticle residuum of the full dimer model, not even for vanishing interaction parameters $t_i = 0$. Thus, a realistic model for the spectral function must explicitly take into account the bosonic dimers.

Moreover, the preceding analysis and results provide clear indication that the quasiparticle residuum is generated only by the terms H_{t_1} , H_{t_2} and H_{t_3} in the Hamiltonian. In general, the spectral function takes the form

$$\mathcal{A}(\mathbf{p}, \omega) = \mathcal{Z}(\mathbf{p})\delta(\omega - \varepsilon(\mathbf{p})) + \mathcal{A}_{incoh.}(\mathbf{p}, \omega), \quad (3.93)$$

where the first term corresponds to the coherent part while $\mathcal{A}_{incoh.}(\mathbf{p}, \omega)$ denotes the incoherent contribution. In our calculations of the preceding sections we found access only to the coherent spectral peak because of two reasons: First, we assumed the self-energy in the full dimer propagators G_f and G_b to be negligible due to the effects of the hard-core constraint, which prevents the emergence of a dispersion in the two-point functions. Second, we did not explicitly take into account the underlying H_{RK} and only included the fermion-boson interaction terms of H_{t_i} within a ladder approach that leads to a sharp bound state. Since this approach provided a very good estimate of the coherent part of the spectrum in the regime $t_i \ll J$, we conclude that the coherent part is indeed produced exclusively by the terms H_{t_i} . The underlying Hamiltonian H_{RK} is then expected to provide an incoherent contribution to the spectral function and can be obtained by numerical investigation.

An analytical approach to the incoherent part can be found by again restoring to a mean field model in which the fermionic degrees of freedom are decoupled from the bosonic background. As explained above, this Ansatz will miss the coherent residuum, but as it is in principle feasible to treat the H_{RK} -Hamiltonian with means of a mean field decoupling as well, it is thinkable to apply a bosonic mean field decoupling to both parts of the full Hamiltonian, therefore effectively describing two non-interacting quasiparticle-modes, one bosonic, the other fermionic. With this inclusion of the H_{RK} term, such a two-mode approximation provides a way of computing the incoherent part of the spectral function while omitting the coherent contribution from H_{t_i} . This approach was carried out in [34].

4 Exact solution of a two-species quantum dimer model for pseudogap metals

Having examined diagrammatic techniques in the previous sections, we take a step back and examine an extended version of the model at hand by looking for choices of parameters that allow for exact ground state solutions. As stated in a condensed version of the following sections that can be found in [23], we are able to identify a line in parameter space where the exact ground state wave functions can be constructed at an arbitrary density of fermionic dimers. At this exactly solvable line the ground state has a huge degeneracy, which can be interpreted as a flat band of fermionic excitations. Perturbing around the exactly solvable line, this degeneracy is lifted and the ground state is a fractionalized Fermi liquid with a small pocket Fermi surface in the low doping limit.

4.1 Extending the dimer model

In this section we extend the dimer model under investigation by adding a new interaction term which corresponds to an energy offset for every pair of fermionic and bosonic dimers within a flippable plaquette configuration. The corresponding new term in the Hamiltonian is thus

$$H_{v_1} = v_1 \sum_i F_{i,x}^\dagger D_{i+y,x}^\dagger D_{i+y,x} F_{i,x} + 3 \text{ terms.} \quad (4.1)$$

Our dimer model is then given by the total Hamiltonian

$$H = H_{RK} + H_1 + H_{v_1}. \quad (4.2)$$

In the next step, we identify a line in parameters space which allows to rewrite the Hamiltonian from Eq.(4.2) as a sum of projectors. As the model then takes a form similar to the Original RK Hamiltonian at the RK point $J = V$, we shall speak of an RK-line in parameter space in the following. Inserting the choice

$$\begin{aligned} v_1 &= t_2 = -t_1 \\ t_3 &= 0 \end{aligned} \quad (4.3)$$

into Eq.(4.2), it turns out the total Hamiltonian can be expressed graphically as

$$\begin{aligned} H = & J \sum_{\text{plaq}} \left(\left| \begin{array}{c} \text{blue} \\ \text{blue} \end{array} \right\rangle - \left| \begin{array}{c} \text{blue} \\ \text{blue} \end{array} \right\rangle \right) \left(\left\langle \begin{array}{c} \text{blue} \\ \text{blue} \right| - \left\langle \begin{array}{c} \text{blue} \\ \text{blue} \right| \right) + \\ & + v_1 \sum_{\text{plaq}} \left(\left| \begin{array}{c} \text{red} \\ \text{blue} \end{array} \right\rangle + \left| \begin{array}{c} \text{blue} \\ \text{red} \end{array} \right\rangle - \left| \begin{array}{c} \text{blue} \\ \text{red} \end{array} \right\rangle - \left| \begin{array}{c} \text{red} \\ \text{blue} \end{array} \right\rangle \right) \left(\left\langle \begin{array}{c} \text{red} \\ \text{blue} \right| + \left\langle \begin{array}{c} \text{blue} \\ \text{red} \right| - \left\langle \begin{array}{c} \text{blue} \\ \text{red} \right| - \left\langle \begin{array}{c} \text{red} \\ \text{blue} \right| \right) \end{aligned} \quad (4.4)$$

As claimed, this is a pure sum of projectors onto single plaquette configurations. Since the model now also contains mixed fermion-boson projectors, we can ask whether the ground state of the implied model can be determined exactly as well. Furthermore, the similar structure to the original RK-Hamiltonian leads to think that the corresponding exact ground state will be a generalized version of the RK RVB-state encountered before. Naively, one would expect that the ground state of H at the RK line is an equal weight

superposition of all dimer configurations at a fixed density of fermionic dimers. This is only true if a single fermion is present, however, since the equal weight superposition is not antisymmetric under the exchange of two fermionic dimers. In the following section, we provide a calculation which yields the exact ground state of Eq.(4.4), we examine its properties and show that a perturbative computation of the dispersion $\varepsilon(\mathbf{p})$ in the parameters t_i solidifies the assumed presence of a fractionalized Fermi liquid (FL*) phase in the quantum dimer model.

4.2 Exact ground states

As a consequence of the special form of Eq.(4.4), the Hamiltonian is positive definite, i.e. $\langle \psi | H | \psi \rangle \geq 0$ for all wavefunctions ψ . The ground state can hence be determined by the condition

$$H |\psi_0\rangle = E_0 |\psi_0\rangle = 0, \quad (4.5)$$

which we want to solve for $|\psi_0\rangle$ in an arbitrary sector of the (conserved) number of fermionic dimers N_f . In the following, we restrict our calculation to the case $N_f = 2$. The generalization to higher fermion numbers will then be straightforward.

We assume the ground state to be a common eigenstate of H_{RK} and $H_1 + H_{v_1}$. As we already know that the bosonic part H_{RK} is minimized by an equal weight superposition of all (bosonic) dimer coverings, we can define the basic states

$$\begin{aligned} |(i_1, \eta_1), (i_2, \eta_2)\rangle &\equiv \mathcal{N} \cdot F_{i_1, \eta_1}^\dagger F_{i_2, \eta_2}^\dagger \sum_{c \in \mathcal{C}_{(i_1, \eta_1), (i_2, \eta_2)}} D_{i_3(c), \eta_3(c)}^\dagger \cdots D_{i_{N/2}(c), \eta_{N/2}(c)}^\dagger |0\rangle = \\ &= \mathcal{N} \cdot F_{i_1, \eta_1}^\dagger F_{i_2, \eta_2}^\dagger |0\rangle_{(i_1, \eta_1), (i_2, \eta_2)} \otimes \left\{ \sum_{c \in \mathcal{C}_{(i_1, \eta_1), (i_2, \eta_2)}} |c\rangle \right\} \end{aligned} \quad (4.6)$$

where the sum runs over all possible bosonic configurations $|c\rangle$ covering the lattice

$$\mathcal{R}_{(i_1, \eta_1), (i_2, \eta_2)} = \left(\mathbb{Z}^{\sqrt{N}} \times \mathbb{Z}^{\sqrt{N}} \right) \setminus \{i_1, i_1 + \hat{\eta}_1, i_2, i_2 + \hat{\eta}_2\}, \quad (4.7)$$

i.e. all sites except those already occupied by fermionic dimers. For later convenience, we choose to normalize $|(i_1, \eta_1), (i_2, \eta_2)\rangle$ with respect to the number of all possible bosonic dimer configurations N_t on the entire lattice $\mathbb{Z}^{\sqrt{N}} \times \mathbb{Z}^{\sqrt{N}}$, therefore setting $\mathcal{N} \equiv \frac{1}{\sqrt{N_t}}$. The norm of such a state is hence given by

$$\| |(i_1, \eta_1), (i_2, \eta_2)\rangle \|^2 = \frac{1}{N_t} \sum_{c \in \mathcal{C}_{(i_1, \eta_1), (i_2, \eta_2)}} = \frac{N_{(i_1, \eta_1), (i_2, \eta_2)}}{N_t} = Q_c[(i_1, \eta_1), (i_2, \eta_2)], \quad (4.8)$$

i.e. the classical dimer correlation function. $N_{(i_1, \eta_1), (i_2, \eta_2)}$ labels the number of all classical configurations with two dimers fixed at (i_1, η_1) and (i_2, η_2) . Featuring the mentioned equal weight superposition of bosonic dimer coverings, these states are zero energy eigenstates of H_{RK} by construction and thus constitute our building blocks for minimizing the remaining part $H_1 + H_{v_1}$ of the full Hamiltonian. Note that with the correlations of Eq.(4.8) we implicitly enforce the hard-core constraint, as any constraint violating configuration c yields a vanishing norm $Q_c[c] = 0$.

For a given plaquette, we further define the plaquette states

$$|\phi_l\rangle = \left| \begin{array}{c} \color{red}{\circ} \color{blue}{\circ} \\ \color{blue}{\circ} \color{red}{\circ} \end{array} \right\rangle_l + \left| \begin{array}{c} \color{blue}{\circ} \color{red}{\circ} \\ \color{red}{\circ} \color{blue}{\circ} \end{array} \right\rangle_l - \left| \begin{array}{c} \color{blue}{\circ} \\ \color{red}{\circ} \end{array} \right\rangle_l - \left| \begin{array}{c} \color{red}{\circ} \\ \color{blue}{\circ} \end{array} \right\rangle_l = \left(F_{l,y}^\dagger D_{l+\hat{x},y}^\dagger + 3 \text{ terms} \right) |0\rangle_l, \quad (4.9)$$

where the label l refers to the lower left site index of the plaquette under consideration and marks the restriction to the four sites constituting the plaquette. Within that notation, we can define the projector

$$P_l = |\phi_l\rangle \langle \phi_l| \otimes \prod_{p \neq l} \mathbb{1}_p \quad (4.10)$$

and write the v_1 -part of the Hamiltonian from Eq.(4.4) as

$$H_1 + H_{v_1} = \sum_l P_l. \quad (4.11)$$

Finally, we define the state

$$|\phi_l, (i, \eta)\rangle = \frac{1}{\sqrt{N_{(l,\tau),(l+\hat{\tau},\tau),(i,\eta)}}} F_{i,\eta}^\dagger |0\rangle_{(i,\eta)} \otimes |\phi_l\rangle \otimes \left\{ \sum_{c \in \mathcal{C}_{(l,\tau),(l+\hat{\tau},\tau),(i,\eta)}} |c\rangle \right\}, \quad (4.12)$$

which fixes the plaquette l in the state $|\phi_l\rangle$ as well as a fermionic dimer at (i, η) . The corresponding norm is

$$\| |\phi_l, (i, \eta)\rangle \|^2 = \langle \phi_l | \phi_l \rangle = 4. \quad (4.13)$$

With these definitions we can derive the exact ground state in the following. We start with a general expansion

$$|\psi_0\rangle = \sum_{i_1, \eta_1, i_2, \eta_2} A_{(i_1, \eta_1), (i_2, \eta_2)} |(i_1, \eta_1), (i_2, \eta_2)\rangle \quad (4.14)$$

for the supposed ground state $|\psi_0\rangle$. We apply the Hamiltonian Eq.(4.11) to this expansion to obtain

$$H |\psi_0\rangle = v_1 \sum_l \sum_{i_1, \eta_1, i_2, \eta_2} A_{(i_1, \eta_1), (i_2, \eta_2)} P_l |(i_1, \eta_1), (i_2, \eta_2)\rangle. \quad (4.15)$$

Note that P_l acts nontrivially only on plaquettes containing a single fermionic dimer and thus

$$P_l |(i_1, \eta_1), (i_2, \eta_2)\rangle = (\delta_{l, i_1} + \delta_{l+\hat{\eta}_1, i_1} + \delta_{l, i_2} + \delta_{l+\hat{\eta}_2, i_2}) P_l |(i_1, \eta_1), (i_2, \eta_2)\rangle. \quad (4.16)$$

Furthermore, we note that

$$\begin{aligned}
 \delta_{l,i_1} P_l |(i_1, \eta_1), (i_2, \eta_2)\rangle &= \frac{1}{\sqrt{N_t}} \sum_{c \in \mathcal{C}_{(l, \eta_1), (i_2, \eta_2)}} |\phi_l\rangle \langle \phi_l| F_{l, \eta_1}^\dagger F_{i_2, \eta_2}^\dagger \left(|0\rangle_{(l, \eta_1), (i_2, \eta_2)} \otimes |c\rangle \right) = \\
 &= \frac{1}{\sqrt{N_t}} \sum_{c' \in \mathcal{C}_{(l, \eta_1), (i_2, \eta_2), (l+\hat{\eta}_1, \eta_1)}} |\phi_l\rangle \langle \phi_l| F_{l, \eta_1}^\dagger F_{i_2, \eta_2}^\dagger D_{l+\hat{\eta}_1, \eta_1}^\dagger \left(|0\rangle_{(l, \eta_1), (i_2, \eta_2), (l+\hat{\eta}_1, \eta_1)} \otimes |c'\rangle \right) = \\
 &= (-1)^{s_{\eta_1}} \frac{1}{\sqrt{N_t}} F_{i_2, \eta_2}^\dagger |0\rangle_{(i_2, \eta_2)} \otimes |\phi_l\rangle \otimes \left\{ \sum_{c' \in \mathcal{C}_{(l, \eta_1), (i_2, \eta_2), (l+\hat{\eta}_1, \eta_1)}} |c'\rangle \right\} = \\
 &= (-1)^{s_{\eta_1}} \sqrt{\frac{N_{(l, \eta_1), (l+\hat{\eta}_1, \eta_1), (i_2, \eta_2)}}{N_t}} |\phi_l, (i_2, \eta_2)\rangle = \\
 &= (-1)^{s_{\eta_1}} \sqrt{Q_c [(l, \eta_1), (l+\hat{\eta}_1, \eta_1), (i_2, \eta_2)]} |\phi_l, (i_2, \eta_2)\rangle.
 \end{aligned} \tag{4.17}$$

In the second equality, we have used that the projection onto $|\phi_l\rangle$ is nonzero only if $|c\rangle = D_{l+\hat{\eta}_1, \eta_1}^\dagger |0\rangle_{(l+\hat{\eta}_1, \eta_1)} \otimes |c'\rangle$ with $|c'\rangle \in \mathcal{C}_{(l, \eta_1), (i_2, \eta_2), (l+\hat{\eta}_1, \eta_1)}$. In the third equality we then used

$$\langle \phi_l| F_{l, \eta}^\dagger D_{l+\hat{\eta}, \eta}^\dagger |0\rangle_{(l, \eta), (l+\hat{\eta}, \eta)} = (-1)^{s_\eta} \tag{4.18}$$

together with the definition

$$s_\eta = \begin{cases} 1, & \text{for } \eta = y \\ 0, & \text{for } \eta = x \end{cases}. \tag{4.19}$$

Again, Eq.(4.17) resorts to classical correlations and effectively projects onto the physical space of hard-core configurations. We proceed in an analogous manner for the remaining three terms of Eq.(4.16) and hence obtain

$$\begin{aligned}
 \delta_{l+\hat{\eta}_1, i_1} P_l |(i_1, \eta_1), (i_2, \eta_2)\rangle &= \delta_{l+\hat{\eta}_1, i_1} (-1)^{s_{\eta_1}} \sqrt{Q_c [(l, \eta_1), (l+\hat{\eta}_1, \eta_1), (i_2, \eta_2)]} |\phi_l, (i_2, \eta_2)\rangle \\
 \delta_{l, i_2} P_l |(i_1, \eta_1), (i_2, \eta_2)\rangle &= \delta_{l, i_2} (-1)^{s_{\eta_2}} \sqrt{Q_c [(l, \eta_2), (l+\hat{\eta}_2, \eta_2), (i_1, \eta_1)]} |(i_1, \eta_1), \phi_l\rangle \\
 \delta_{l+\hat{\eta}_2, i_2} P_l |(i_1, \eta_1), (i_2, \eta_2)\rangle &= \delta_{l+\hat{\eta}_2, i_2} (-1)^{s_{\eta_2}} \sqrt{Q_c [(l, \eta_2), (l+\hat{\eta}_2, \eta_2), (i_1, \eta_1)]} |(i_1, \eta_1), \phi_l\rangle.
 \end{aligned} \tag{4.20}$$

Inserting this into Eq.(4.16) and (4.15) we obtain

$$\begin{aligned}
 \sum_l \sum_{i_1, \eta_1, i_2, \eta_2} A_{(i_1, \eta_1), (i_2, \eta_2)} P_l |(i_1, \eta_1), (i_2, \eta_2)\rangle &= \\
 &= \sum_{l, \eta_1, i_2, \eta_2} [A_{(l, \eta_1), (i_2, \eta_2)} + A_{(l+\hat{\eta}_1, \eta_1), (i_2, \eta_2)}] (-1)^{s_{\eta_1}} \sqrt{Q_c [(l, \eta_1), (l+\hat{\eta}_1, \eta_1), (i_2, \eta_2)]} |\phi_l, (i_2, \eta_2)\rangle \\
 &+ \sum_{i_1, \eta_1, l, \eta_2} [A_{(i_1, \eta_1), (l, \eta_2)} + A_{(i_1, \eta_1), (l+\hat{\eta}_2, \eta_2)}] (-1)^{s_{\eta_2}} \sqrt{Q_c [(l, \eta_2), (l+\hat{\eta}_2, \eta_2), (i_1, \eta_1)]} |(i_1, \eta_1), \phi_l\rangle
 \end{aligned} \tag{4.21}$$

We consider now the first term of Eq.(4.21) and carry out the sum over η_1 . We note that $Q_c [(l, \eta_1), (l+\hat{\eta}_1, \eta_1), (i_2, \eta_2)]$ is independent of η_1 . This is clear, as for every configuration

$(l, \eta_1) \otimes (l + \hat{\eta}_1, \eta_1) \otimes \mathcal{B}$ with some background configuration \mathcal{B} , there exists a configuration $(l, \bar{\eta}_1) \otimes (l + \hat{\eta}_1, \bar{\eta}_1) \otimes \mathcal{B}$ with the l -plaquette flipped. The prefactor multiplying $|\phi_l, (i_2, \eta_2)\rangle$ in the first term of Eq.(4.21) is thus

$$\left[A_{(l,x),(i_2,\eta_2)} - A_{(l,y),(i_2,\eta_2)} + A_{(l+\hat{y},x),(i_2,\eta_2)} - A_{(l+\hat{x},y),(i_2,\eta_2)} \right] \sqrt{Q_c[(l,x), (l+\hat{y},x), (i_2,\eta_2)]}. \quad (4.22)$$

We can proceed in the same manner with the second term of Eq.(4.21). For the ground state $|\psi_0\rangle$, we demand that the coefficients for both terms vanish and therefore arrive at the conditions

$$\begin{aligned} A_{(l,x),(i_2,\eta_2)} - A_{(l,y),(i_2,\eta_2)} + A_{(l+\hat{y},x),(i_2,\eta_2)} - A_{(l+\hat{x},y),(i_2,\eta_2)} &= 0 \\ A_{(i_1,\eta_1),(l,x)} - A_{(i_1,\eta_1),(l,y)} + A_{(i_1,\eta_1),(l+\hat{y},x)} - A_{(i_1,\eta_1),(l+\hat{x},y)} &= 0. \end{aligned} \quad (4.23)$$

We can solve these conditions by a simple product Ansatz

$$A_{(i_1,\eta_1),(i_2,\eta_2)} = a_{i_1,\eta_1} a_{i_2,\eta_2}, \quad (4.24)$$

which leads to

$$a_{i_m,x} - a_{i_m,y} + a_{i_m+\hat{y},x} - a_{i_m+\hat{x},y} = 0, \quad (4.25)$$

for $m = 1, 2$. At this point, the generalization to an arbitrary number of fermions in the system is now straightforward and can simply be done by extending Eq.(4.25) to $m = 1, \dots, N_f$. We introduce the lattice momenta \mathbf{p}_m and make the Ansatz

$$a_{i_m,\eta_m} = a_{i_m,\eta_m}(\mathbf{p}_m) = C_{\eta_m}(\mathbf{p}_m) e^{i\mathbf{p}_m \cdot \mathbf{i}_m}, \quad (4.26)$$

which upon insertion into Eq.(4.25) leads to

$$C_x(\mathbf{p}_m) = C_y(\mathbf{p}_m) \frac{1 + e^{ip_{m,x}}}{1 + e^{ip_{m,y}}}. \quad (4.27)$$

The factors $C_\eta(\mathbf{p})$ can be interpreted as weight factors for the two possible dimer orientations. We can thus parametrize the possible ground states on the RK-line via

$$|\psi_0\rangle = |\mathbf{p}_1, \mathbf{p}_2\rangle = \sum_{i_1,\eta_1,i_2,\eta_2} a_{i_1,\eta_1}(\mathbf{p}_1) a_{i_2,\eta_2}(\mathbf{p}_2) |(i_1, \eta_1), (i_2, \eta_2)\rangle \quad (4.28)$$

or more generally via $|\psi_0\rangle = |\mathbf{p}_1, \dots, \mathbf{p}_{N_f}\rangle$ for arbitrary fermion number N_f .

We now wish to normalize the state given in Eq.(4.28). To this end, we make the following choice for the factors $C_\eta(\mathbf{p})$:

$$\begin{aligned} C_y &= \frac{2}{\sqrt{N}} \frac{1 + e^{ip_y}}{\sqrt{|1 + e^{ip_y}|^2 + |1 + e^{ip_x}|^2}} \\ C_x &= \frac{2}{\sqrt{N}} \frac{1 + e^{ip_x}}{\sqrt{|1 + e^{ip_y}|^2 + |1 + e^{ip_x}|^2}}, \end{aligned} \quad (4.29)$$

which fulfill the ground state condition of Eq.(4.27) and obey the normalization $|C_x(\mathbf{p})|^2 + |C_y(\mathbf{p})|^2 = \frac{4}{N}$. We evaluate

$$\begin{aligned}
 & \langle \mathbf{p}_1, \mathbf{p}_2 | \mathbf{p}_1, \mathbf{p}_2 \rangle = \\
 & = \sum_{i_1, \eta_1, i_2, \eta_2, j_1, \tau_1, j_2, \tau_2} a_{i_1, \eta_1}(\mathbf{p}_1) a_{i_2, \eta_2}(\mathbf{p}_2) a_{j_1, \tau_1}^*(\mathbf{p}_1) a_{j_2, \tau_2}^*(\mathbf{p}_2) \langle (j_1, \tau_1), (j_2, \tau_2) | (i_1, \eta_1), (i_2, \eta_2) \rangle = \\
 & = \sum_{i_1, \eta_1, i_2, \eta_2, j_1, \tau_1, j_2, \tau_2} a_{i_1, \eta_1}(\mathbf{p}_1) a_{i_2, \eta_2}(\mathbf{p}_2) a_{j_1, \tau_1}^*(\mathbf{p}_1) a_{j_2, \tau_2}^*(\mathbf{p}_2) \times \\
 & \quad \times [\delta_{(j_1, \tau_1), (i_1, \eta_1)} \delta_{(j_2, \tau_2), (i_2, \eta_2)} - \delta_{(j_1, \tau_1), (i_2, \eta_2)} \delta_{(j_2, \tau_2), (i_1, \eta_1)}] Q_c [(i_1, \eta_1), (i_2, \eta_2)] = \\
 & = \sum_{i_1, \eta_1, i_2, \eta_2} [|a_{i_1, \eta_1}(\mathbf{p}_1)|^2 |a_{i_2, \eta_2}(\mathbf{p}_2)|^2 - \\
 & \quad - a_{i_1, \eta_1}(\mathbf{p}_1) a_{i_1, \eta_1}^*(\mathbf{p}_2) a_{i_2, \eta_2}(\mathbf{p}_2) a_{i_2, \eta_2}^*(\mathbf{p}_1)] Q_c [(i_1, \eta_1), (i_2, \eta_2)]. \tag{4.30}
 \end{aligned}$$

In the following, we treat this norm in the low doping limit that we describe as $N \rightarrow \infty$, which is the limit we are interested in and in which we expect to find the FL* phase. The second term of Eq.(4.30) then reads

$$\sum_{\eta_1, \eta_2} C_{\eta_1}(\mathbf{p}_1) C_{\eta_1}^*(\mathbf{p}_2) C_{\eta_2}(\mathbf{p}_1) C_{\eta_2}^*(\mathbf{p}_2) \sum_{i_1, i_2} e^{i(\mathbf{p}_1 - \mathbf{p}_2) \cdot (i_1 - i_2)} Q_c [(i_1, \eta_1), (i_2, \eta_2)] \tag{4.31}$$

and contains the Fourier transform of the classical dimer correlation function. It was shown in [38, 41] that the classical dimer correlations decrease algebraically like

$$Q_c [(0, x), ((X, Y), x)] = \frac{1}{16} + \frac{1}{2\pi^2} \left[(-1)^{X+Y} \frac{Y^2 - X^2}{R^4} + (-1)^X \frac{1}{R^2} \right], \tag{4.32}$$

where $R^2 = X^2 + Y^2$. Employing the abbreviated notation $i_1 = (i_1, \eta_1)$ for the links of the lattice, the algebraic decay of these correlations then ensures that in a large system, the Fourier transformed classical dimer correlations take the form

$$\frac{1}{N^2} \sum_{i_1, i_2} e^{i\mathbf{p}(i_1 - i_2)} Q_c [i_1, i_2] \rightarrow \frac{1}{4} \delta_{\mathbf{p}, 0} + \mathcal{O}(\log(N)/N), \tag{4.33}$$

i.e. a Kronecker delta with corrections of maximum order $\mathcal{O}(\log(N)/N)$, depending on the chosen momentum point \mathbf{p} . As $|\mathbf{p}_1, \mathbf{p}_2\rangle$ is antisymmetric, $\langle \mathbf{p}, \mathbf{p} | \mathbf{p}, \mathbf{p} \rangle = 0$ and the second term of Eq.(4.30) only contains finite momentum Fourier transforms of the classical correlations and can be discarded in the low doping limit. We are now left only with the first term, which, also in the limit $N \rightarrow \infty$, using Eq.(4.29) and again neglecting corrections of order $\mathcal{O}(\log(N)/N)$ evaluates to

$$\langle \mathbf{p}_1, \mathbf{p}_2 | \mathbf{p}_1, \mathbf{p}_2 \rangle = 1. \tag{4.34}$$

We can easily generalize this to higher fermion numbers. Employing again the compact notation $i = (i, \eta)$ and defining the states

$$|i_1, \dots, i_{N_f}\rangle = |(i_1, \eta_1), \dots, (i_{N_f}, \eta_{N_f})\rangle \tag{4.35}$$

in analogy to Eq.(4.6), we can write down a relation for the matrix elements that are needed in order to compute the normalization of the ground states $|\mathbf{p}_1, \dots, \mathbf{p}_{N_f}\rangle$,

$$\langle j_1, \dots, j_{N_f} | i_1, \dots, i_{N_f} \rangle \propto \sum_{P \in \text{Perm}(N_f)} (-1)^{\sigma(P)} \delta_{i_1, j_{P_1}} \delta_{i_2, j_{P_2}} \cdots \delta_{i_{N_f}, j_{P_{N_f}}}. \quad (4.36)$$

For every permutation other than the trivial (non-)permutation, the corresponding contribution to the analogue of Eq.(4.30) involves a finite momentum Fourier transform of classical dimer correlations of N_f dimers. As we saw in Sec.(2.2), the (long-range) dimer correlations can be constructed from a quadratic field theory using Grassmann variables. Wick's theorem then ensures that Fourier transforms of higher order correlation functions still contribute corrections of maximum order $\mathcal{O}(\log(N)/N)$ in the low doping limit, which is now described as

$$N_f = \text{const.}, \quad N \rightarrow \infty. \quad (4.37)$$

The remaining contribution of the trivial permutation then yields

$$\begin{aligned} & \langle \mathbf{p}_1, \dots, \mathbf{p}_{N_f} | \mathbf{p}_1, \dots, \mathbf{p}_{N_f} \rangle = \\ & = \sum_{i_1, \eta_1, \dots, i_{N_f}, \eta_{N_f}} |a_{i_1, \eta_1}(\mathbf{p}_1)|^2 \cdots |a_{i_{N_f}, \eta_{N_f}}(\mathbf{p}_{N_f})|^2 Q_c [(i_1, \eta_1), \dots, (i_{N_f}, \eta_{N_f})] = 1, \end{aligned} \quad (4.38)$$

again in the limit of Eq.(4.37).

To summarize this section, we note that we can indeed find the normalized exact ground states of the Hamiltonian from Eq.(4.4) on the RK-line in any fermion number sector (where normalization only holds for $N_f \ll N_b$) with the specific form

$$|\mathbf{p}_1, \dots, \mathbf{p}_{N_f}\rangle = \sum_{i_1, \eta_1, \dots, i_{N_f}, \eta_{N_f}} a_{i_1, \eta_1}(\mathbf{p}_1) \cdots a_{i_{N_f}, \eta_{N_f}}(\mathbf{p}_{N_f}) |(i_1, \eta_1), \dots, (i_{N_f}, \eta_{N_f})\rangle. \quad (4.39)$$

Here, $|(i_1, \eta_1), \dots, (i_{N_f}, \eta_{N_f})\rangle$ is given by Eq.(4.6) while

$$a_{i, \eta}(\mathbf{p}) = \frac{2}{\sqrt{N}} \frac{1 + e^{ip_\eta}}{\sqrt{|1 + e^{ip_x}|^2 + |1 + e^{ip_y}|^2}} e^{i\mathbf{p} \cdot \mathbf{i}}. \quad (4.40)$$

Note that although the normalization to unity only holds in the low doping limit Eq.(4.37), the states of Eq.(4.39) are exact ground states for every choice of bosonic and fermionic dimer numbers. The replacement $Q_c [(i_1, \eta_1), \dots, (i_{N_f}, \eta_{N_f})] \rightarrow 1/4^{N_f}$, which corresponds to treating the fermionic dimers independently of each other and which is approximately valid only in said low doping limit, was not used in the derivation of the ground states of Eq.(4.39). Note as well that the normalization to unity does hold exactly for any system size, in particular for small lattices, in the sector of one fermionic dimer in the system, as can be shown by a straightforward calculation.

Furthermore, the lattice momenta $\mathbf{p}_1, \mathbf{p}_2$ in the ground states of Eq.(4.28) may take arbitrary values in the first Brillouin zone, save $\mathbf{p}_1 = \mathbf{p}_2$, which corresponds to a ground state degeneracy of $N(N-1)/2$. For an arbitrary number N_f of fermionic dimers there

are $N!/((N - N_f)!N_f!)$ possibilities to choose the momenta $(\mathbf{p}_1, \dots, \mathbf{p}_{N_f})$. It is important to emphasize that the states $|\mathbf{p}_1, \dots, \mathbf{p}_{N_f}\rangle$ are in general not linearly independent and the number of possible momenta $(\mathbf{p}_1, \dots, \mathbf{p}_{N_f})$ does not correspond to the ground state degeneracy in sectors with a large density of fermionic dimers. This can be deduced from the fact that the number of possible choices for the N_f momenta exceeds the number of states in the Hilbert space for large N_f . However, in the low doping limit of Eq.(4.37), the states $|\mathbf{p}_1, \dots, \mathbf{p}_{N_f}\rangle$ not only become normalized as shown above, but indeed orthonormal and the ground state degeneracy is indeed obtained via the above relation. Orthogonality can be shown in similar fashion as normalization, as for two sets of momenta $(\mathbf{q}_1, \dots, \mathbf{q}_{N_f}) \neq (\mathbf{p}_1, \dots, \mathbf{p}_{N_f})$ all terms arising from the evaluation of the matrix elements will now contain a finite momentum Fourier transform of Q_c .

4.3 Ground state properties

4.3.1 Perturbations around RK-Line

In the following we want to study how small perturbations in the parameters t_i around the RK-line change the ground state structure. As expected, the huge ground state degeneracy will be lifted and the fermions will acquire a dispersion. The perturbative ground state in the vicinity of the RK line is then unique and similar to a Fermi gas, where the lowest energy momentum states \mathbf{p}_m will be filled with N_f fermions. We show that in the limit of Eq.(4.37), the corresponding first order ground state energy can be written as a sum of the supposed single fermion ground state energies. For simplicity, we concentrate on perturbations in the exchange interactions t_1 and t_3 in the following. Flip interactions like t_2 could however be included in a similar manner with an analogous evaluation of the arising matrix elements that yield the perturbative energy.

Restricting again to the case $N_f = 2$, the energy in first order perturbation theory reads

$$E = \langle \mathbf{p}_1, \mathbf{p}_2 | \Delta H_{t_i} | \mathbf{p}_1, \mathbf{p}_2 \rangle, \quad (4.41)$$

with

$$\Delta H_{t_i} = -\delta t_i \sum_{s=1}^{S_{t_i}} \sum_{j,\eta} F_{j+r_{t_i}^{s,\eta}, \eta+\eta_{t_i}}^\dagger D_{j,\eta}^\dagger D_{j+r_{t_i}^{s,\eta}, \eta+\eta_{t_i}} F_{j,\eta}. \quad (4.42)$$

Here, $r_{t_i}^{s,\eta}$ and η_{t_i} correspond to displacement vector and relative change in orientation for a given t_i process which starts with a fermionic dimer with orientation η . Note that the sum over the possible displacement vectors corresponding to a given t_i depends on the orientation index η and runs from 1 to $S_{t_1} = 2$, $S_{t_3} = 8$. For the energy of Eq.(4.41) we thus obtain

$$\begin{aligned} \Delta E = & -\delta t_i \sum_{s=1}^{S_{t_i}} \sum_{j,\eta} \sum_{i_1,\eta_1, i_2,\eta_2} \sum_{l_1,\tau_1, l_2,\tau_2} a_{i_1,\eta_1}(\mathbf{p}_1) a_{i_2,\eta_2}(\mathbf{p}_2) a_{l_1,\tau_1}^*(\mathbf{p}_1) a_{l_2,\tau_2}^*(\mathbf{p}_2) \times \\ & \times \left\langle (l_1, \tau_1), (l_2, \tau_2) \left| F_{j+r_{t_i}^{s,\eta}, \eta+\eta_{t_i}}^\dagger D_{j,\eta}^\dagger D_{j+r_{t_i}^{s,\eta}, \eta+\eta_{t_i}} F_{j,\eta} \right| (i_1, \eta_1), (i_2, \eta_2) \right\rangle. \end{aligned} \quad (4.43)$$

In order to evaluate the matrix elements we again introduce $i_1 = (i_1, \eta_1)$ as abbreviated notation for a link index which contains emanating site and orientation. We then get

$$\begin{aligned} & \left\langle l_1, l_2 \left| F_{j+r_{t_i}^{s,j}}^\dagger D_j^\dagger D_{j+r_{t_i}^{s,j}} F_j \right| i_1, i_2 \right\rangle = \\ & = \delta_{j,i_1} \left(\delta_{l_1, i_1+r_{t_i}^{s,i_1}} \delta_{l_2, i_2} - \delta_{l_2, i_1+r_{t_i}^{s,i_1}} \delta_{l_1, i_2} \right) \times Q_c[i_1, i_2, i_1 + r_{t_i}^{s,i_1}] + \\ & \quad + \delta_{j,i_2} \left(\delta_{l_2, i_2+r_{t_i}^{s,i_2}} \delta_{l_1, i_1} - \delta_{l_1, i_2+r_{t_i}^{s,i_2}} \delta_{l_2, i_1} \right) \times Q_c[i_1, i_2, i_2 + r_{t_i}^{s,i_2}], \end{aligned} \quad (4.44)$$

and therefore for the energy

$$\begin{aligned} \Delta E = & -\delta t_i \sum_{s=1}^{S_{t_i}} \sum_{i_1, i_2} t_i \left(a_{i_1}(\mathbf{p}_1) a_{i_2}(\mathbf{p}_2) a_{i_1+r_{t_i}^{s,i_1}}^*(\mathbf{p}_1) a_{i_2}^*(\mathbf{p}_2) - a_{i_1}(\mathbf{p}_1) a_{i_2}(\mathbf{p}_2) a_{i_1+r_{t_i}^{s,i_1}}^*(\mathbf{p}_2) a_{i_2}^*(\mathbf{p}_1) \right) \\ & \times Q_c[i_1, i_2, i_1 + r_{t_i}^{s,i_1}] + \\ & - \delta t_i \left(a_{i_1}(\mathbf{p}_1) a_{i_2}(\mathbf{p}_2) a_{i_1}^*(\mathbf{p}_1) a_{i_2+r_{t_i}^{s,i_2}}^*(\mathbf{p}_2) - a_{i_1}(\mathbf{p}_1) a_{i_2}(\mathbf{p}_2) a_{i_1}^*(\mathbf{p}_2) a_{i_2+r_{t_i}^{s,i_2}}^*(\mathbf{p}_1) \right) \times \\ & \times Q_c[i_1, i_2, i_2 + r_{t_i}^{s,i_2}]. \end{aligned} \quad (4.45)$$

We analyze this expression term by term once more in leading order in the low doping limit. The first term then yields

$$\begin{aligned} & -\delta t_i \sum_{s=1}^{S_{t_i}} \sum_{i_1, i_2} \left(|C_{i_2}(\mathbf{p}_2)|^2 C_{i_1}(\mathbf{p}_1) C_{i_1+r_{t_i}^{s,i_1}}^*(\mathbf{p}_1) e^{-ir_{t_i}^{s,i_1} \cdot \mathbf{p}_1} \right) Q_c[i_1, i_2, i_1 + r_{t_i}^{s,i_1}] = \\ & = -\delta t_i \sum_{s=1}^{S_{t_i}} \sum_{i_1} C_{i_1}(\mathbf{p}_1) C_{i_1+r_{t_i}^{s,i_1}}^*(\mathbf{p}_1) e^{-ir_{t_i}^{s,i_1} \cdot \mathbf{p}_1} Q_c[i_1, i_1 + r_{t_i}^{s,i_1}] = \\ & = -\delta t_i \sum_{\eta_1} \frac{(1 + e^{ip_1, \eta_1})(1 + e^{-ip_1, \eta_1 + \eta_{t_i}})}{|1 + e^{ip_1, y}|^2 + |1 + e^{ip_1, x}|^2} \sum_{s=1}^{S_{t_i}} \left[e^{-ir_{t_i}^{s, \eta_1} \cdot \mathbf{p}_1} \right] Q_c[(0, \eta_1) | r_{t_i}^{s, \eta_1}] \equiv \varepsilon(\mathbf{p}_1). \end{aligned} \quad (4.46)$$

Correspondingly, the third term evaluates to

$$-\delta t_i \sum_{\eta_2} \frac{(1 + e^{ip_2, \eta_2})(1 + e^{-ip_2, \eta_2 + \eta_{t_i}})}{|1 + e^{ip_2, y}|^2 + |1 + e^{ip_2, x}|^2} \sum_{s=1}^{S_{t_i}} \left[e^{-ir_{t_i}^{s, \eta_2} \cdot \mathbf{p}_2} \right] Q_c[(0, \eta_2) | r_{t_i}^{s, \eta_2}] = \varepsilon(\mathbf{p}_2). \quad (4.47)$$

The second and the last term of Eq.(4.45) again contain Fourier transforms of classical dimer correlations and tend to zero in the limit under consideration. In this limit, the energy resulting from Eq.(4.45) is hence a sum

$$\Delta E(\mathbf{p}_1, \mathbf{p}_2) = \varepsilon(\mathbf{p}_1) + \varepsilon(\mathbf{p}_2) \quad (4.48)$$

of the single particle contributions from \mathbf{p}_1 and \mathbf{p}_2 . We show an example for $\varepsilon(\mathbf{p})$ together with exact diagonalization results in Fig.(21). For $|\delta t_i| \ll |v_1|, J$, we find good agreement. Note the formation of hole-pockets around $(\pi/2, \pi/2)$ at a finite density of fermionic dimers

for perturbations in δt_i . This shows that close to the RK-line, the eigenstates found above indeed yield a realistic description of the dimer model.

Again, generalization to higher fermion numbers N_f can be done via generalization of the arising matrix elements in the evaluation of the first order perturbative ground state energy ΔE . In particular, ΔE can be calculated by using the relation

$$\begin{aligned} & \left\langle l_1, \dots, l_{N_f} \left| F_{j+r}^\dagger D_j^\dagger D_{j+r} F_j \right| i_1, \dots, i_{N_f} \right\rangle = \\ & = \sum_{k=1}^{N_f} \delta_{j,i_k} \sum_{P \in \pi_{N_f}} (-1)^{\sigma(P)} \delta_{i_1, l_{P(1)}} \cdot \dots \cdot \delta_{i_{k+r}, l_{P(k)}} \cdot \dots \cdot \delta_{i_{N_f}, l_{P(N_f)}} Q_C[i_1, \dots, i_k, i_k + r, \dots, i_{N_f}]. \end{aligned} \quad (4.49)$$

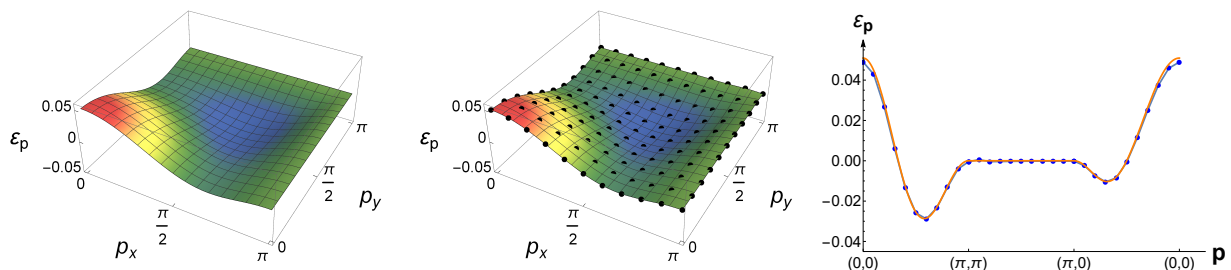


Figure 21: Comparison between $\varepsilon(\mathbf{p})$ (left) from Eq.(4.46) and ED (middle) for $\delta t_3 = -0.02$, $\delta t_{i \neq 3} = 0$, $J = V = 1$. To the right: corresponding line cut along a given path in the BZ (blue: ED, orange: $\varepsilon(\mathbf{p})$).

4.3.2 Fractionalized Fermi liquid structure

The preceding results demonstrate that in the low doping limit the energy of a state $|\mathbf{p}_1, \dots, \mathbf{p}_{N_f}\rangle$ can be expressed as the sum $\sum_{i=1}^{N_f} \varepsilon(\mathbf{p}_i)$ of the single particle energies, indicating a system with Fermi-liquid like behaviour. In this section we further show that in the same limit, the states $|\mathbf{p}_1, \dots, \mathbf{p}_{N_f}\rangle$ can be constructed using creation and annihilation operators that fulfill canonical fermionic anticommutation relations.

We start by defining the vacuum state of the theory to be the usual RK state given by the solution of the RK-model, i.e. $|0^*\rangle = |\text{RK}\rangle$. We add the star in this notation to make clear the difference to the vacuum state $|0\rangle$ used in the previous sections and to suggest this to be the ground state upon which the FL* is built. By defining the operator

$$f_{\mathbf{p}}^\dagger = \sum_{i,\eta} a_{i,\eta}(\mathbf{p}) F_{i,\eta}^\dagger D_{i,\eta}, \quad (4.50)$$

we can express the possible ground states along the RK-line as

$$\left| \mathbf{p}_1, \dots, \mathbf{p}_{N_f} \right\rangle = \prod_{i=1}^{N_f} f_{\mathbf{p}_i}^\dagger |0^*\rangle. \quad (4.51)$$

We aim to show that the corresponding Hamiltonian

$$H = \sum_{\mathbf{p}} \varepsilon(\mathbf{p}) f_{\mathbf{p}}^\dagger f_{\mathbf{p}} \quad (4.52)$$

describes the model in the vicinity of the RK-line as a system of non-interacting fermionic excitations. We hence need to show that the canonical anticommutation relations

$$\{f_{\mathbf{p}_1}^\dagger, f_{\mathbf{p}_2}\} = \delta_{\mathbf{p}_1, \mathbf{p}_2} \quad (4.53)$$

are satisfied in the limit of Eq.(4.37).

Note that since the relation of Eq.(4.53) is an operator identity, we require specification of the Hilbert space on which Eq.(4.53) is supposed to hold. In usual fermionic theories, the corresponding canonical anticommutation relations must hold on the Fock space spanned by the set of states $\{\prod_{i=1}^{N_f} c_{\mathbf{k}_i}^\dagger |0\rangle\}$. In complete analogy we hence demand that for the FL* model, Eq.(4.53) should hold on the corresponding Hilbert space spanned by the states $\{\prod_{i=1}^{N_f} f_{\mathbf{k}_i}^\dagger |0^*\rangle\}$. Thus, even though the operators defined by Eq.(4.50) clearly do not constitute fermionic operators on a Hilbert space built upon a completely empty lattice $|0\rangle$, we still might prove them to be fermionic within our relevant Hilbert space. The quantity we aim to compute is now

$$\{f_{\mathbf{p}_1}^\dagger, f_{\mathbf{p}_2}\} |0^*\rangle, \quad (4.54)$$

and we want to show that this expression yields $\delta_{\mathbf{p}_1, \mathbf{p}_2} |0^*\rangle$. We can easily compute

$$\{f_{\mathbf{p}_1}^\dagger, f_{\mathbf{p}_2}\} = \sum_{i, \eta} a_{i, \eta}(\mathbf{p}_1) a_{i, \eta}^*(\mathbf{p}_2) \left(F_{i, \eta}^\dagger F_{i, \eta} + D_{i, \eta}^\dagger D_{i, \eta} \right) = \sum_{i, \eta} a_{i, \eta}(\mathbf{p}_1) a_{i, \eta}^*(\mathbf{p}_2) \hat{N}_{i, \eta}, \quad (4.55)$$

where $\hat{N}_{i, \eta}$ corresponds to the total dimer number operator in the link (i, η) . From this we deduce

$$\begin{aligned} \|\{f_{\mathbf{p}_1}^\dagger, f_{\mathbf{p}_2}\} |0^*\rangle\|^2 &= \sum_{i, \eta, j, \tau} a_{i, \eta}(\mathbf{p}_1) a_{i, \eta}^*(\mathbf{p}_2) a_{j, \tau}^*(\mathbf{p}_1) a_{j, \tau}(\mathbf{p}_2) \left\langle 0^* \left| \hat{N}_{j, \tau} \hat{N}_{i, \eta} \right| 0^* \right\rangle = \\ &= \sum_{i, \eta, j, \tau} a_{i, \eta}(\mathbf{p}_1) a_{i, \eta}^*(\mathbf{p}_2) a_{j, \tau}^*(\mathbf{p}_1) a_{j, \tau}(\mathbf{p}_2) Q_c[(i, \eta), (j, \tau)] \propto \\ &\propto \frac{1}{N^2} \sum_{i, \eta, j, \tau} e^{i(\mathbf{p}_1 - \mathbf{p}_2) \cdot (i - j)} Q_c[(i, \eta), (j, \tau)] \rightarrow \frac{1}{4} \delta_{\mathbf{p}_1, \mathbf{p}_2} + \mathcal{O}(\log(N)/N), \end{aligned} \quad (4.56)$$

which reduces to the desired form after again making use of the correlation function in large systems sizes. The appearance of the total dimer number operator $\hat{N}_{i, \eta}$ in Eq.(4.55) then ensures that the preceding result remains valid in the excited states of the FL*, provided that Eq.(4.37) be fulfilled.

Beyond this limit, we now show that the relation found in Eq.(4.56) is indeed true exactly for arbitrary N_f/N when the momenta $\mathbf{p}_1, \mathbf{p}_2$ lie on the BZ diagonal. For that purpose, consider the state

$$\{f_{\mathbf{p}_1}^\dagger, f_{\mathbf{p}_2}\} |0^*\rangle = \sum_{i,\eta} a_{i,\eta}(\mathbf{p}_1) a_{i,\eta}^*(\mathbf{p}_2) \hat{N}_{i,\eta} |0^*\rangle. \quad (4.57)$$

If this state is to vanish, we need the prefactor of every basic configuration $|c\rangle$ on the lattice to vanish. Here, $|c\rangle$ represents a purely bosonic covering of the lattice as we apply $\{f, f^\dagger\}$ to $|0^*\rangle$. Furthermore, we restrict to configurations of the topological sector with winding number zero. The corresponding prefactor is given by

$$d_c \equiv \langle c | \{f_{\mathbf{p}_1}^\dagger, f_{\mathbf{p}_2}\} |0^*\rangle = \sum_{(i,\eta) \in \{(j,\tau) | \hat{N}_{j,\tau}|c\rangle = |c\rangle\}} a_{i,\eta}(\mathbf{p}_1) a_{i,\eta}^*(\mathbf{p}_2), \quad (4.58)$$

where the sum runs over all links that are occupied by a dimer in the configuration $|c\rangle$. Assume now we have some configuration $|c_0\rangle$ where the value d_{c_0} has already been calculated. Upon flipping a plaquette $(l, \nu), (l + \hat{\nu}, \nu)$ in $|c_0\rangle$ we obtain a new state $|c_1\rangle$ with corresponding prefactor

$$\begin{aligned} \Delta d &= d_{c_1} - d_{c_0} = \\ &= a_{l,\bar{\nu}}(\mathbf{p}_1) a_{l,\bar{\nu}}^*(\mathbf{p}_2) + a_{l+\hat{\nu},\bar{\nu}}(\mathbf{p}_1) a_{l+\hat{\nu},\bar{\nu}}^*(\mathbf{p}_2) - a_{l,\nu}(\mathbf{p}_1) a_{l,\nu}^*(\mathbf{p}_2) - a_{l+\hat{\nu},\nu}(\mathbf{p}_1) a_{l+\hat{\nu},\nu}^*(\mathbf{p}_2). \end{aligned} \quad (4.59)$$

One can then compute the prefactors of all configurations within a given winding number sector by starting from a given configuration $|c_0\rangle$ and subsequently going through all possible plaquette flips on the lattice. This reasoning corresponds to going the Ergodic theorem "backwards", i.e. instead of computing the desired correlation function as an average over an ensemble, we introduce a dynamics in the form of plaquette flips and compute the correlation of interest along the course of the plaquette flips.

Demanding that the prefactors d_c vanish for all configurations in a winding number sectors then amounts to finding a starting configuration $|c_0\rangle$ for which $d_{c_0} = 0$ and showing that Δd from Eq.(4.59) vanishes. For the latter, we plug the known form of $a_{i,\eta}(\mathbf{p})$ into Eq.(4.59) to obtain

$$\begin{aligned} \Delta d &= e^{i(\mathbf{p}_1 - \mathbf{p}_2) \cdot l} [C_{\bar{\nu}}(\mathbf{p}_1) C_{\bar{\nu}}^*(\mathbf{p}_2) + e^{i(\mathbf{p}_1 - \mathbf{p}_2) \cdot \hat{\nu}} C_{\bar{\nu}}(\mathbf{p}_1) C_{\bar{\nu}}^*(\mathbf{p}_2) \\ &\quad - C_{\nu}(\mathbf{p}_1) C_{\nu}^*(\mathbf{p}_2) - e^{i(\mathbf{p}_1 - \mathbf{p}_2) \cdot \hat{\nu}} C_{\nu}(\mathbf{p}_1) C_{\nu}^*(\mathbf{p}_2)] \\ &\propto (1 + e^{ip_{1,x}})(1 + e^{-ip_{2,x}}) + e^{i(\mathbf{p}_1 - \mathbf{p}_2) \cdot \hat{y}} (1 + e^{ip_{1,x}})(1 + e^{-ip_{2,x}}) \\ &\quad - (1 + e^{ip_{1,y}})(1 + e^{-ip_{2,y}}) - e^{i(\mathbf{p}_1 - \mathbf{p}_2) \cdot \hat{x}} (1 + e^{ip_{1,y}})(1 + e^{-ip_{2,y}}) \end{aligned} \quad (4.60)$$

which reduces to zero for $p_{1/2,x} = p_{1/2,y}$. Now, for a starting configuration which corresponds to a columnar VBS state, which is part of the possible zero winding number configurations on the square lattice, we can easily calculate $d_{c_0} = 0$ for $\mathbf{p}_1 \neq \mathbf{p}_2$ on the diagonal. Hence, for two momenta $\mathbf{p}_1, \mathbf{p}_2$ on the BZ diagonal, $\{f_{\mathbf{p}_1}^\dagger, f_{\mathbf{p}_2}\} = \delta_{\mathbf{p}_1, \mathbf{p}_2}$ holds exactly; for every other pair of momenta it is valid in the limit considered before.

We can relate the relation we have just shown with the fourier transform of the classical dimer correlation function to obtain an exact result. For $\mathbf{p}_1, \mathbf{p}_2$ on the BZ diagonal we can

write

$$\begin{aligned} \delta_{\mathbf{p}_1, \mathbf{p}_2} &= \sum_c |d_c|^2 = \|\{f_{\mathbf{p}_1}^\dagger, f_{\mathbf{p}_2}\} |0^*\rangle\|^2 = \\ &= \frac{4}{N^2} \sum_{i, \eta, j, \tau} e^{i(\mathbf{p}_1 - \mathbf{p}_2) \cdot (i - j)} Q_c[(i, \eta), (j, \tau)] = \frac{4}{N} \sum_{i, \eta, \tau} e^{i(\mathbf{p}_1 - \mathbf{p}_2) \cdot i} Q_c[(0, \eta), (i, \tau)] \end{aligned} \quad (4.61)$$

We have thus found an exact sum rule for the Fourier transform of the classical dimer correlations on the BZ diagonal.

Finally, we show the relation between the creation operator $f_{\mathbf{p}}^\dagger$ of the excitations on the RK line and the actual electron annihilation operator $c_{\mathbf{p}}$. From the form Eq.(2.25) for the electron operator in dimer basis we infer

$$c_{\mathbf{p}, \alpha} = \sum_{i, \eta} \frac{\varepsilon_{\alpha, \beta}}{2\sqrt{N}} e^{-i\mathbf{p} \cdot i} (1 + e^{-ip_\eta}) F_{i, \eta, \beta}^\dagger D_{i, \eta}. \quad (4.62)$$

Suppressing the electronic spin index and comparing this expression with the definition of the operator $f_{\mathbf{p}}^\dagger$ from Eq.(4.50) it immediately follows that

$$f_{\mathbf{p}}^\dagger = \mathcal{K}(\mathbf{p}) c_{-\mathbf{p}}, \quad (4.63)$$

with

$$\mathcal{K}(\mathbf{p}) = 4 \frac{1}{\sqrt{|1 + e^{ip_x}|^2 + |1 + e^{ip_y}|^2}}. \quad (4.64)$$

This relation is particularly useful because it shows that the Fermi surface of fermionic dimers directly translates to the electronic Fermi surface. Moreover, from the fact that the $f_{\mathbf{p}}^\dagger$ fermions form a free Fermi gas, we can deduce that the electron spectral function in the vicinity of the RK line takes the form $\mathcal{A}(\mathbf{p}, \omega) = \mathcal{Z}(\mathbf{p}) \delta(\omega - \varepsilon(\mathbf{p}))$ with quasiparticle weight $\mathcal{Z}(\mathbf{p}) = \frac{1}{4} [\cos^2(p_x/2) + \cos^2(p_y/2)]$, which we already encountered in Eq.(3.38) of our diagrammatic approach at the noninteracting point $t_i = 0$, which is of course part of the RK line as well. This can be seen from the relation

$$\mathcal{Z}(\mathbf{p}) = |\langle \mathbf{p} | c_{-\mathbf{p}} | 0^* \rangle|^2 = \left| \left\langle 0^* \left| f_{\mathbf{p}} \frac{1}{\mathcal{K}(\mathbf{p})} f_{\mathbf{p}}^\dagger \right| 0^* \right\rangle \right|^2 = \left| \frac{1}{\mathcal{K}(\mathbf{p})} \right|^2. \quad (4.65)$$

On the RK line, the electron spectral function thus only features a coherent peak but no incoherent background due to the normalization of Eq.(3.42). Perturbing away from the RK line, incoherent weight appears, but not within first order perturbation theory. Numerical results in the vicinity of the RK-line obtained by exact diagonalization confirm this result.

4.4 Summary

In summary, see [23], we provided an exact ground state solution for the dimer model introduced in Ref. [1] on a particular line in parameter space for arbitrary densities of fermionic dimers. At this line the ground state is massively degenerate and can be interpreted as a fermionic flat band. Perturbing away from the exactly solvable line lifts this degeneracy

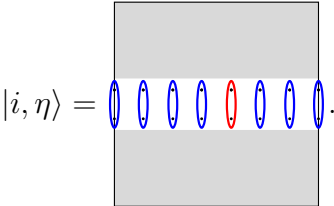
and we were able to show that the ground state is a fractionalized Fermi liquid, at least in the limit of small fermionic dimer densities. In this limit the ground state can be constructed by applying canonical fermion creation operators to a suitably chosen vacuum state and the energy of these fermions is additive. Moreover, these fermionic operators are directly related to electron creation operators in the restricted Hilbert space of our model. Even though we limited the discussion to spinless fermionic dimers, our construction can be easily generalized to spin-1/2 fermionic dimers. We also note that the very same construction works for other lattice geometries as well, such as a triangular lattice, where we expect that the fractionalized Fermi liquid ground state is stable over a wider parameter regime. Indeed, the $U(1)$ spin liquid in the RK model is unstable towards confining VBS states away from the special RK point $J = V$. On non-bipartite lattices an extended Z_2 spin liquid phase exists, however [26]. Analogous considerations hold for the fractionalized Fermi liquid phase discussed here [45, 46]. In conclusion, our results provide a rare example of a strongly correlated, fermionic lattice model in two dimensions, which is exactly solvable and potentially relevant for the description of the metallic pseudogap phase in underdoped cuprates.

5 Finite size effects in the quantum dimer model

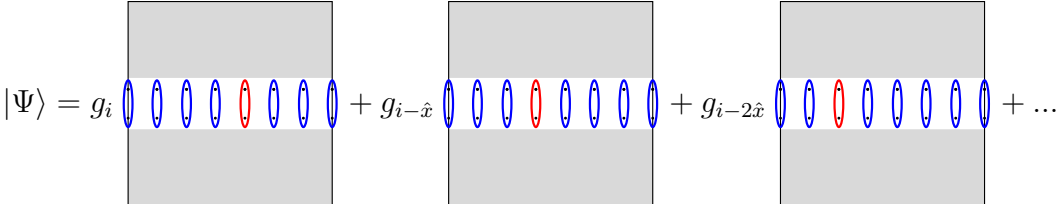
Up to now, we have focused exclusively on parameter regimes which allow to assume an RK-like bosonic background configuration. Away from the perturbative regime in the vicinity of the RK-line this assumption will no longer be valid and the effective dimer correlations in the neighbourhood of fermionic dimers will be altered. We return to the question raised in Sec.(2.3.2) whether we can deduce these effective correlations, at least for some simple models. In the following we consider a simplified dimer model with one fermionic dimer which features the t_1 interaction only, in order to go beyond the scope of small interaction parameters t_i and to examine finite size effects in the 6×6 case. We compute the ground state and its properties in the strong coupling limit $t_1/J \rightarrow \infty$ and examine a simple variational approach to compute properties of the model at intermediate interaction strength.

5.1 The strong coupling limit

The model under consideration is now $H = H_{RK} + H_{t_1}$ and we consider $t_1 > 0$, $V = J \rightarrow 0$, leaving only a small strength of the RK Hamiltonian. Our aim is to explain the dispersion obtained from exact diagonalization shown in Fig.(22). The building blocks of which the supposed ground state will consist of are the states

$$|i, \eta\rangle = F_{i, \eta}^\dagger \prod_{j_{\bar{\eta}}=i_{\bar{\eta}}+\hat{\eta}}^{i_{\bar{\eta}}-\hat{\eta}} D_{(j_{\bar{\eta}}, i_{\eta}), \eta}^\dagger |0\rangle \otimes \sum_c |c\rangle$$

(5.1)

Here, the fermionic dimer is located on the (i, η) site and is part of a "lane" of bosonic dimers across the whole system in the direction perpendicular to the orientation of the fermionic dimer. Gray shaded areas correspond to an equal weight sum over all possible bosonic configurations on the corresponding part of the lattice. The Ansatz for the ground state of the Hamiltonian is then made up of a sum over the possible positions of the fermionic dimer within the lane, as well as shifting the lane as a whole in the perpendicular direction,

$$|\Psi\rangle = \sum_i g_i |i, y\rangle,$$

(5.2)

The same Ansatz can of course be made using a lane which wraps around the \hat{y} -direction of the lattice.

Note that the motivation for such an Ansatz for the ground state is that the formation of a lane of parallel bosonic dimers is disfavored by H_{RK} , but since we consider H_{RK} to be small, we infer that the energy cost of such a lane will disappear in the limit where H_{RK} vanishes and hence we aim to minimize the energy via the t_1 -interaction. The natural way to define a state with overall momentum \mathbf{p} is then

$$|\Psi_{\mathbf{p}}\rangle = \sum_i \frac{1}{\sqrt{N}} e^{i\mathbf{p}\cdot\mathbf{i}} |i, y\rangle, \quad (5.3)$$

which upon projection on H_{t_1} yields

$$H_{t_1} |\Psi_{\mathbf{p}}\rangle = -2t_1 \cos(p_x) |\Psi_{\mathbf{p}}\rangle. \quad (5.4)$$

We can proceed analogously with the fermionic dimer oriented in the x direction which results in the overall dispersion

$$\varepsilon(\mathbf{p}) = \min[-2t_1 \cos(p_x), -2t_1 \cos(p_y)]. \quad (5.5)$$

This dispersion, although matching the numerical outcome exactly at the Γ -point in the BZ in the limit $J \rightarrow 0$, does otherwise not look very similar to the result from Fig.(22). Clearly, we have thus far found eigenstates of the Hamiltonian H_{t_1} for every momentum \mathbf{p} , but, apart from the Γ point, not the lowest possible ones. The crucial aspect to find the ground state for every momentum in the BZ is to find the right partitioning of a given momentum \mathbf{p} into a part carried by the fermionic dimer, as well as a part carried by the bosonic background. That is to say that, as opposed to the case of a dominating H_{RK} where all the momentum of a given state is attached to the fermionic dimer, in the limit of a dominating t_1 -interaction the momentum is divided into bosonic background momentum as well as fermionic momentum. We can then construct the ground state as shown in the following.

Consider again the basic states of Eq.(5.1), but now we will implement a momentum \mathbf{p} into the bosonic background of the gray shaded area. For that purpose, we consider the background part in the state of Eq.(5.1), $\sum_c |c\rangle$. This was constructed as an equal weight superposition. We now introduce weights into this sum like $\sum_c w(c) |c\rangle$. The RK-Hamiltonian forces the system to implement an equal weight superposition of the bosonic dimers outside the t_1 -dominated lane across the system. If we go to a momentum point away from the Γ -point, it might be energetically favourable for the system outside the lane to assume a non-equal weight superposition in order to keep a vanishing momentum of the fermionic dimer. Our Ansatz for the basic building blocks of the ground state should therefore be a minimal violation of the equal weight Ansatz,

$$\sum_c w(c) |c\rangle \equiv |\mathcal{B}_c\rangle, \quad (5.6)$$

where the $w(c)$ have to be determined by minimizing the corresponding energy expectation value.

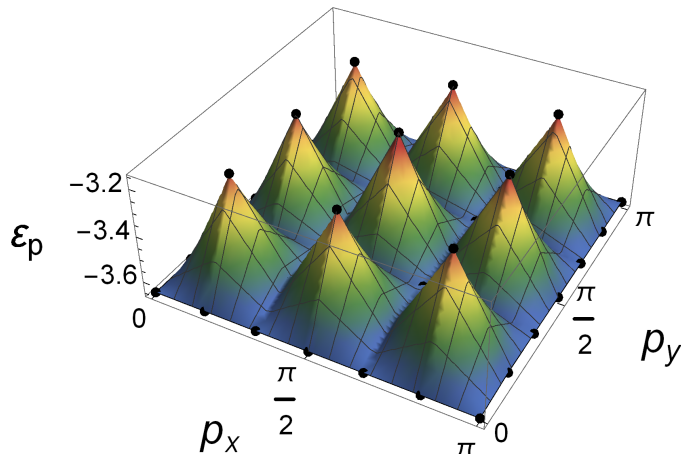


Figure 22: Dispersion from ED on a 6×6 lattice for $V = J = 0.1$, $t_1 = 2.0$. At the physical momenta $p_{x,y} = -\pi + \frac{\pi}{3} \cdot n$ with $n \in \{0, \dots, 5\}$, the corresponding energies $\varepsilon(\mathbf{p})$ almost coincide. At $V = J = 0$ they match exactly. By use of twisted boundary conditions we also included non-lattice momenta, which are marked by the appearance of cones in the ground state energy.

Observe that our Ansatz for the bosonic background is now in general no longer translational invariant. We thus can construct the states

$$|i, \eta, p_{\hat{\eta}}\rangle = F_{i,\eta}^\dagger \prod_{j_{\hat{\eta}}=i_{\hat{\eta}}+\hat{\eta}}^{i_{\hat{\eta}}-\hat{\eta}} D_{(j_{\hat{\eta}}, i_{\eta}), \eta}^\dagger |0\rangle \otimes \sum_{n=0}^{L-1} e^{ip_{\hat{\eta}} \cdot n} \left(\hat{T}_{\hat{\eta}} \right)^n |\mathcal{B}_C\rangle, \quad (5.7)$$

where we defined the translation operator $\hat{T}_{\hat{\eta}}$ that shifts a given dimer configuration by one lattice constant into the $\hat{\eta}$ -direction. L is the length of the system, i.e. $N = L^2$ on the square lattice. This state carries a momentum $p_{\hat{\eta}} \cdot \hat{\eta}$ in the $\hat{\eta}$ -direction. The estimate for the ground state wavefunction at a given lattice momentum $\mathbf{p} = \sum_{\eta} p_{\eta} \cdot \hat{\eta}$ other than the Γ -point is then given by

$$|\Phi_{\eta, \mathbf{p}}\rangle \equiv \sum_i e^{ip_{\eta} \cdot i_{\eta}} |i, \eta, p_{\hat{\eta}}\rangle, \quad (5.8)$$

i.e. by delocalizing the fermion over the lane. We assume that the background $|\mathcal{B}_C\rangle$ is not invariant under translations on the lattice, i.e. $\hat{T}_{\hat{\eta}} |\mathcal{B}_C\rangle \neq |\mathcal{B}_C\rangle$. Under this assumption, $|\Phi_{\eta, \mathbf{p}}\rangle$ is an eigenstate of the translation operator,

$$\hat{T}_{x/y} |\Phi_{\eta, \mathbf{p}}\rangle = e^{ip_{x/y}} |\Phi_{\eta, \mathbf{p}}\rangle \quad (5.9)$$

and therefore carries a momentum \mathbf{p} , where the part $p_{\hat{\eta}}$ parallel to the fermion lane is attached to the bosonic background. Note that for the case of the fermionic dimer fixed in

the η -direction, the only non-trivial momentum component is the $\bar{\eta}$ -component. Next, we determine the correct normalization of $|\Phi_{\eta,\mathbf{p}}\rangle$ by computing

$$\begin{aligned} \langle \Phi_{\eta,\mathbf{p}} | \Phi_{\eta,\mathbf{p}} \rangle &= \sum_i \langle i, \eta, p_{\bar{\eta}} | i, \eta, p_{\bar{\eta}} \rangle = N \sum_{n,m=0}^{L-1} e^{ip_{\bar{\eta}}(n-m)} \langle \mathcal{B}_C | \left(\hat{T}_{\bar{\eta}}^\dagger \right)^m \left(\hat{T}_{\bar{\eta}} \right)^n | \mathcal{B}_C \rangle = \\ &= N \sum_{n,m=0}^{L-1} e^{ip_{\bar{\eta}}(n-m)} \sum_{c,c'} w^*(c') w(c) \langle c' | \left(\hat{T}_{\bar{\eta}}^\dagger \right)^m \left(\hat{T}_{\bar{\eta}} \right)^n | c \rangle. \end{aligned} \quad (5.10)$$

One possible approximation we could apply at this point is to set

$$w(c) = \begin{cases} 1, & c \in \mathcal{C} \\ 0, & \text{else} \end{cases}, \quad (5.11)$$

i.e. an equal weight sum over all configurations contained in a set \mathcal{C} . From here, the simplest approach is to assume that \mathcal{C} contains only a single configuration $|c\rangle$, i.e. $\mathcal{C} = \{|c\rangle\}$. Equivalently, \mathcal{C} contains all configurations but one, i.e. $\mathcal{C} = (\bigcup_{c'} \{|c'\rangle\}) \setminus \{|c\rangle\}$, were we will assume a non-translational invariant state $|c\rangle$, i.e. $\hat{T}_{\bar{\eta}} |c\rangle \neq |c\rangle$ in order to fulfill $\hat{T}_{\bar{\eta}} |\mathcal{B}_C\rangle \neq |\mathcal{B}_C\rangle$. For these two cases, the normalization from Eq.(5.10) becomes

$$N \sum_{n,m=0}^{L-1} e^{ip_{\bar{\eta}}(n-m)} (|\mathcal{C}| - 1 + \delta_{n,m}), \quad (5.12)$$

which, for $p_{\bar{\eta}} \neq 0$, evaluates to

$$\langle \Phi_{\eta,\mathbf{p}} | \Phi_{\eta,\mathbf{p}} \rangle = N \cdot L, \quad (5.13)$$

The normalized ground state estimate wave function for the chosen \mathcal{C} is hence

$$|\Phi_{\eta,\mathbf{p}}\rangle \rightarrow \frac{1}{\sqrt{N \cdot L}} \sum_i e^{ip_{\eta} i_{\eta}} |i, \eta, p_{\bar{\eta}}\rangle = \frac{1}{\sqrt{N \cdot L}} \sum_{i_{\eta}} e^{ip_{\eta} i_{\eta}} \left\{ \sum_{i_{\bar{\eta}}} |i, \eta, p_{\bar{\eta}}\rangle \right\}. \quad (5.14)$$

This state is a sum over non-overlapping terms which consist of a tensor product of the lane-part and the background part of the system. The sum then runs over the position i_{η} of the lane and different positions of the lane have vanishing matrix elements with respect to the Hamiltonian. Thus, to compute the corresponding ground state energy, we can write

$$\langle H_{RK} + H_{t_1} \rangle = \langle H_{t_1} + H_{RK} \rangle_{\text{lane}} + \frac{1}{L} \sum_{n,m=0}^{L-1} e^{ip_{\bar{\eta}}(n-m)} \langle \mathcal{B}_C | \left(\hat{T}_{\bar{\eta}}^\dagger \right)^m H_{RK} \left(\hat{T}_{\bar{\eta}} \right)^n | \mathcal{B}_C \rangle, \quad (5.15)$$

which separates into two parts that only depend on the lane or the background, respectively. $\langle H_{t_1} \rangle_{\text{lane}}$ only depends on the delocalized fermion which we assume to have a vanishing momentum along the direction of the lane. The expression $\langle H_{t_1} + H_{RK} \rangle_{\text{lane}}$ thus evaluates to $\langle H_{t_1} \rangle_{\text{lane}} = -2t_1 + V(L-2)$. Here, the part proportional to $V = J$ is due to the parallel bosonic dimers in the lane which constitute a chain of flippable plaquettes. We thus obtain

a finite energy offset between Γ -point and finite lattice momenta by the second term of Eq.(5.15). Note that at the Γ -point, $|\mathcal{B}_C\rangle \rightarrow |RK\rangle$ and this energy offset vanishes as it should. The offset can now be related to the state $|c\rangle$ via

$$\begin{aligned} & \frac{1}{L} \sum_{n,m=0}^{L-1} e^{ip_{\bar{\eta}}(n-m)} \langle \mathcal{B}_C | \left(\hat{T}_{\bar{\eta}}^\dagger \right)^m H_{RK} \left(\hat{T}_{\bar{\eta}} \right)^n | \mathcal{B}_C \rangle = \\ & = \frac{1}{L} \sum_{n,m=0}^{L-1} e^{ip_{\bar{\eta}}(n-m)} \langle c | \left(\hat{T}_{\bar{\eta}}^\dagger \right)^m H_{RK} \left(\hat{T}_{\bar{\eta}} \right)^n | c \rangle = \langle c | H_{RK} | c \rangle = V N_{fp}(c), \end{aligned} \quad (5.16)$$

where translational invariance of H_{RK} was used and where $N_{fp}(c)$ denotes the number of flippable plaquettes in the configuration $|c\rangle$. Finding the best approximate ground state now reduces to minimizing the energy offset Eq.(5.16) with respect to the configuration $|c\rangle$. In other words, we need to find the single hard-core covering of the gray shaded area from Eq.(5.1) with the lowest possible number of flippable plaquettes in the sector of winding number zero. Note that there may be more than one configuration with the minimal number of flippable plaquettes.

We compare the dispersion obtained from ED for a 6×6 lattice with our estimate

$$\langle H \rangle_{\Phi_{\eta,\mathbf{p}}} = -2t_1 + V(L-2) + (1 - \delta_{\mathbf{p},0}) V \min_c [N_{fp}(c)] \quad (5.17)$$

for the ground state energy at the possible lattice momenta $p_{x,y} = -\pi + \frac{\pi}{3} \cdot n$ with $n \in \{0, \dots, 5\}$, assumed to be valid for large t_1 (at fixed length L) in Fig.(23). The minimization over c can be done numerically by counting the number of flippable plaquettes in all the configurations possible on a 6×4 lattice with open boundary conditions in the y - and periodic boundary conditions in the x -direction, which corresponds to the gray shaded area of Eq.(5.1) in the 6×6 case. This process results in $\min_c [N_{fp}(c)] = 2$. Eq.(5.17) then yields an upper bound for the difference between the energies at $\mathbf{p} = 0$ and $\mathbf{p} \neq 0$ for small V/t_1 . In particular, in the limit $V = J \rightarrow 0$, Eq.(5.17) shows that the ground state energies coincide independent of momentum, providing an explanation for the numerical results of Fig.(22).

We shortly discuss how the background state at non-vanishing momentum, determined by \mathcal{C} , could qualitatively look like beyond the approximation of a single bosonic configuration. To that end, we note that we have to choose \mathcal{C} such that

$$\langle H \rangle_{\mathbf{p}} - \langle H \rangle_{\mathbf{p}=0} = \frac{\sum_{n,m=0}^{L-1} e^{ip_{\bar{\eta}}(n-m)} \langle \mathcal{B}_C | \left(\hat{T}_{\bar{\eta}}^\dagger \right)^m H_{RK} \left(\hat{T}_{\bar{\eta}} \right)^n | \mathcal{B}_C \rangle}{\sum_{n,m=0}^{L-1} e^{ip_{\bar{\eta}}(n-m)} \langle \mathcal{B}_C | \left(\hat{T}_{\bar{\eta}}^\dagger \right)^m \left(\hat{T}_{\bar{\eta}} \right)^n | \mathcal{B}_C \rangle}, \quad (5.18)$$

i.e. the energy shift from the Γ -point to finite momenta, is minimized. In principle, we hence want to maximize the norm of $\sum_{n=0}^{L-1} e^{ip_{\bar{\eta}}n} \left(\hat{T}_{\bar{\eta}} \right)^n | \mathcal{B}_C \rangle$ while minimizing its energy expectation value. A scheme for maximizing the norm of Eq.(5.10) can be given by defining equivalence classes on the set of all possible configurations. We can define an equivalence relation between two configurations via

$$|c\rangle \sim |c'\rangle \Leftrightarrow \exists n \in \mathbb{N} : \hat{T}_{\bar{\eta}}^n |c'\rangle = |c\rangle. \quad (5.19)$$

Thus, there will be $N_{\mathfrak{E}}$ equivalence classes \mathfrak{E}_i into which the set of all dimer configurations can be subdivided. Assume we construct the set \mathcal{C} from before such that $\mathcal{C} = \{|c_1\rangle, \dots, |c_M\rangle\}$ with $c_i \in \mathfrak{E}_i$. Then in the norm of Eq.(5.10), $\langle c' | (\hat{T}_{\bar{\eta}})^{n-m} | c \rangle = \delta_{c',c} \delta_{n,m}$ and the norm is proportional to the number M of configurations in \mathcal{C} . If we continue to add more states to \mathcal{C} than the number of different equivalence classes, the norm of Eq.(5.10) is no longer directly proportional to M , but contains terms like $\cos(p_{\bar{\eta}} n)$ with $n \in \mathbb{N}$. Thus, upon adding more states to \mathcal{C} , the norm will begin to decrease again after some point. On the other hand, the more states \mathcal{C} contains, the closer we get to the RK-state, where for every configuration with a given flippable plaquette, \mathcal{C} would contain the corresponding configuration with that plaquette flipped. Hence, upon adding configurations to \mathcal{C} beyond the number of equivalence classes, we expect the total number of flippable plaquettes without a flipped counterpart configuration within \mathcal{C} , and thus the numerator of Eq.(5.18), to decrease. There should thus exist an optimal \mathcal{C} which balances norm and energy expectation value such that Eq.(5.18) becomes minimal.

Let us note further, that the energy cost of developing a lane throughout the system is proportional to the system length L via $V(L-2)$ according to Eq.(5.17). Thus, for large system sizes, the formation of such a lane is highly disfavored and the attachment of the momentum to the fermionic dimer should be restored. The loss of the Fermi-liquid like behaviour at high values of the t -parameter that is observed in the 6×6 ED can thus be attributed to finite size effects, as the crucial parameter in the system is $\frac{t_1}{VL}$ instead of $\frac{t_1}{V}$, as we have just shown.

Furthermore, in the dispersion shown in Fig.(22), we also included non-lattice momenta via the twisted boundary conditions. We have shown that the attachment of momentum to the bosonic background works for the case of lattice momenta. Therefore, we conclude that the cone-structure of the ground state energy at non-physical momenta visible in Fig.(22) arises because non-lattice momenta cannot be attached to the background. For any given momentum point \mathbf{p} we can write $\mathbf{p} = \mathbf{p}_b + \mathbf{p}_f$, where \mathbf{p}_b corresponds to the lattice momentum closest to \mathbf{p} . The momentum \mathbf{p}_b can be attached to the background by the construction we have examined above. The difference \mathbf{p}_f then has to be attached to the fermion again, which explains the symmetry of the cones appearing in Fig.(22).

5.2 Variational ansatz

So far we have considered the small- ($t_1/V \rightarrow 0$) as well as the strong- ($t_1/VL \rightarrow \infty$) coupling limit of the dimer model with perturbations around both. We can ask whether we can determine the ground state wavefunction of the dimer model at least at some specific point in the BZ approximately at intermediate coupling strengths. We will continue to pursue a variational Ansatz for the ground state at $\mathbf{p} = 0$ for every value of t_1 in the dimer model considered above. The reasoning behind this approach is that, depending on the value of t_1 , the dimer correlations in the vicinity of the fermionic dimer are effectively changed. While at $t_1 = 0$, these correlations correspond exactly to the classical dimer equal weight correlations, at $VL/t_1 \rightarrow 0$ the fermionic dimer forces the bosonic dimers to form a lane of parallel dimers as described above. At intermediate interaction strength we thus expect to find a mix of both, where with increasing t_1 the probability of finding bosonic dimers parallel to the fermionic dimer increases as well.

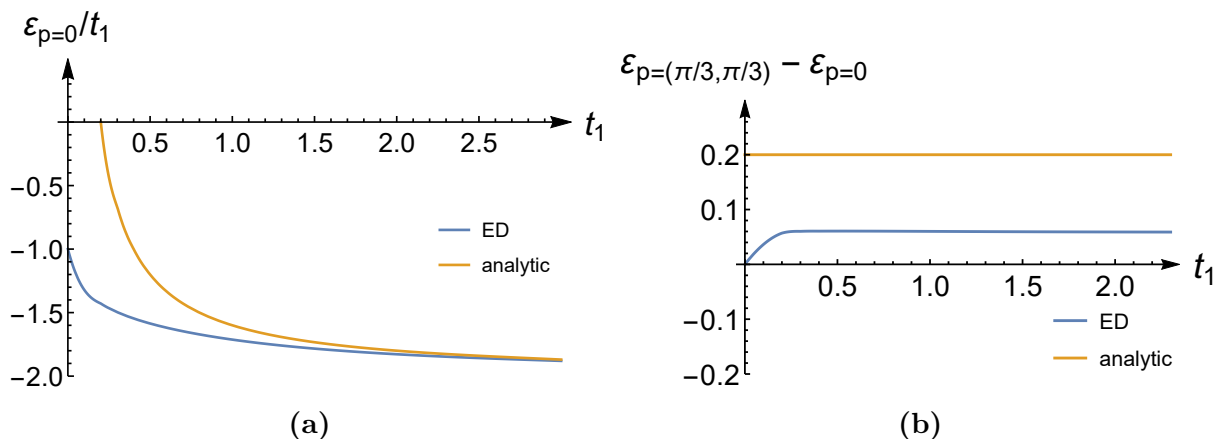


Figure 23: Comparison between ED and the wave function considered above for $V = J = 0.1$. (a) shows the ground state energy at $\mathbf{p} = 0$ as a function of t_1 ; blue: ED, orange: analytical Ansatz from Eq.(5.17). The results give a good match for dominating t_1 as expected. (b) shows the ground state energy difference between $\mathbf{p} = 0$ and $\mathbf{p} = (\pi/3, \pi/3)$ as a function of t_1 ; blue: ED, orange: Ansatz from Eq.(5.17). Eq.(5.17) only gives a very rough upper bound for this energy difference, but captures correctly that above a certain value of t_1 this difference stays constant, indicating lane formation.

The Ansatz is the following: Consider a single fermionic dimer among otherwise bosonic dimers. We denote the probability of finding a bosonic dimer parallel and next to the fermionic one by P . This is the probability of finding the fermionic dimer in a position to conduct a t_1 -exchange. This probability then depends on t_1 and has to fulfill the boundary conditions $P(t_1 \rightarrow 0) = 1/2$ and $P(t_1 \rightarrow \infty) = 1$. The goal is to find a functional form for $P(t_1)$ by minimizing the corresponding energy expectation value via a variational principle. We write down the energy function

$$E(P(t_1)) = -2t_1P(t_1) + \Delta E_V(P(t_1)) \quad (5.20)$$

for the energy of a $\mathbf{p} = 0$ ground state. The first term in Eq.(5.20) originates from the the fermionic dimer interacting with the background via t_1 . The second term captures the energy cost of setting the dimer correlations to $P(t_1)$. The task is to find $\Delta E_V(P(t_1))$ and minimize Eq.(5.20) with respect to P .

Consider the fermionic dimer at a given link. In accordance with the physical picture from before, we will evaluate ΔE_V by considering the fermionic dimer as part of a lane with parallel bosonic dimers. But now we assume the length of this lane to be variable, i.e. not necessarily extended over the whole lattice size. We denote the probability of adding a new rung to the lane by $\tilde{P}(t_1)$. Note that this is different from $P(t_1)$, as here we already assume that there is a lane present and $\tilde{P}(t_1)$ determines its average length. Intuitively, we expect \tilde{P} to be proportional to the difference between $P(t_1)$ and the value $P(t_1 = 0) = \frac{1}{2}$ at the RK-point, i.e. $\tilde{P} \propto (P - \frac{1}{2})$. If the fermionic dimer is considered to be on the edge of the lane, a lane with n bosonic dimers yields an energy cost of $V(n - 1)$. The probability for a lane with n bosons is given by $(1 - \tilde{P}) (\tilde{P})^n$, where $1 - \tilde{P}$ is the necessary "break"

condition for a lane. Everything together, we expect to find the following energy cost ΔE_V as a function of \tilde{P} ,

$$\Delta E_V(\tilde{P}) = V\tilde{P} \left\{ (1 - \tilde{P}) \sum_{n=0}^{L-3} n \left(\tilde{P}\right)^n + (L - 2) \left(\tilde{P}\right)^{L-2} \right\}. \quad (5.21)$$

Here, the second term in the brackets of Eq.(5.21) corresponds to the case of the lane winding around the whole lattice, where because of the periodic boundary conditions there is no break probability $1 - \tilde{P}$. Note that the sum over the probabilities of all possible lengths of the lane,

$$(1 - \tilde{P}) \sum_{n=0}^{L-2} \left(\tilde{P}\right)^n + \left(\tilde{P}\right)^{L-1} = 1, \quad (5.22)$$

is normalized to unity as required.

We now make use of the general formula $\sum_{n=0}^N nx^n = \frac{x}{(1-x)^2} [1 - (N+1)x^N + Nx^{N+1}]$ for $0 \leq x < 1$ in Eq.(5.21) to obtain

$$\Delta E_V(\tilde{P}) = V \left\{ (L - 2) \left(\tilde{P}\right)^{L-1} + \frac{1}{1 - \tilde{P}} \left[\left(\tilde{P}\right)^2 - (L - 2) \left(\tilde{P}\right)^{L-1} + (L - 3) \left(\tilde{P}\right)^L \right] \right\}. \quad (5.23)$$

Now we have to relate the probability \tilde{P} , which determines ΔE_V , to the probability P . The easiest approach is to use a linear relation

$$P = a\tilde{P} + b. \quad (5.24)$$

The constants a and b can now be determined by making use of the boundary conditions for $t_1 \rightarrow 0$ and $t_1 \rightarrow \infty$. For P , these conditions were already mentioned above. For \tilde{P} , we must have $\tilde{P}(t_1 \rightarrow 0) = 0$ as there will be no finite sized lane at all, with every possible background configuration weighted equally. On the other hand, $\tilde{P}(t_1 \rightarrow \infty) = 1$, as the lane will span over the entire lattice length. This leads to

$$P = \frac{\tilde{P} + 1}{2}. \quad (5.25)$$

We then obtain a condition for the minimum of the energy function Eq.(5.20) by differentiation

$$\begin{aligned} \frac{\partial E}{\partial P} = & -2t_1 + 2V \left\{ (L - 1)(L - 2) \left(\tilde{P}\right)^{L-2} + \right. \\ & + \frac{1}{1 - \tilde{P}} \left[2\tilde{P} - (L - 1)(L - 2) \left(\tilde{P}\right)^{L-2} + L(L - 3) \left(\tilde{P}\right)^{L-1} \right] + \\ & \left. + \frac{1}{(1 - \tilde{P})^2} \left[\left(\tilde{P}\right)^2 - (L - 2) \left(\tilde{P}\right)^{L-1} + (L - 3) \left(\tilde{P}\right)^L \right] \right\} \stackrel{!}{=} 0, \end{aligned} \quad (5.26)$$

which corresponds to a polynomial equation in \tilde{P} of order L . For given L and t_1 , this equation can be solved numerically for $0 \leq \tilde{P} \leq 1$. For t_1 exceeding a certain value $t_1 > t_1^c$,

the solution to Eq.(5.26) shifts to $\tilde{P} > 1$ which is unphysical. In this case, we simply set $\tilde{P} = 1$, which corresponds to the lane spanning over the whole lattice length. Inserting the resulting $\tilde{P}(t_1)$ (or $P(t_1)$) into Eq.(5.20) yields the energy at $\mathbf{p} = 0$ for a given value of t_1 in our approximation and is compared to the outcomes of the ED in Fig.(24) and (25).

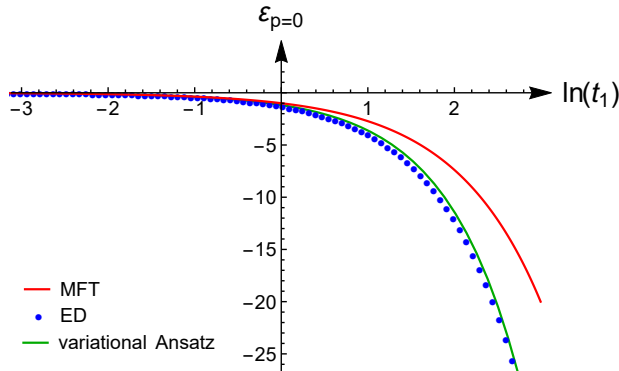


Figure 24: Comparison of ground state energies at $\mathbf{p} = 0$ and $V = J = 1$ between variational Ansatz, the MFT of Eq.(2.30) and ED results. Blue points: ED, Green: variational Ansatz, Red: MFT with the parameter $P = 1/2$ to which the variational Ansatz reduces for $t_1 \rightarrow 0$.

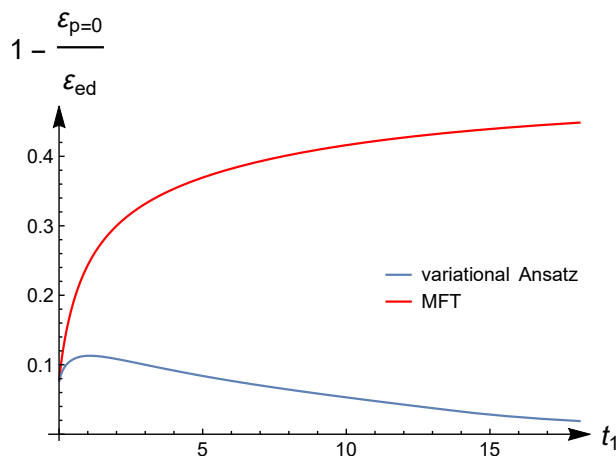


Figure 25: Relative error of variational Ansatz (blue) and MFT (red) from Eq.(2.30) with respect to ED results as a function of t_1 for $V = J = 1$. We see that the variational method yields a good approximation throughout the range of t_1 .

To close this section, we remark that due to the appearance of finite size effects for momenta away from $\mathbf{p} = 0$, our Ansatz can only be tested against ED in a very limited scope. In particular, whether or not the Ansatz for ΔE_V from Eq.(5.21) (or possibly a similar one) provides a reliable estimate of the energy cost in a system with modified correlations around a fermionic dimer away from $t_1 = 0$ should ideally be tested in bigger system sizes, such that arbitrary momenta may be accessed without the occurrence of finite

size effects. As these finite size effects, like the attachment of momentum to the bosonic background, are not included in the above variational approach, it is effectively restricted to the Γ -point of the BZ.

6 Outlook

In the preceding work we have explored a variety of analytical approaches to investigate the model introduced in [1]. We have employed diagrammatic techniques, therefore setting precedent in applying coherent states functional methods to quantum dimer models. This approach could be carried out successfully due to the fractionalized Fermi liquid structure of the system, which we were further able to examine by means of constructing exact ground state wave functions on the RK line of the model. The resulting form of the positive definite Hamiltonian and the present hard core constraint suggest that the model might feature a supersymmetric formulation or extension. In this context, a given supersymmetric system can be expressed in terms of a so called supersymmetric operator \hat{Q} via $\hat{H} = \{\hat{Q}^\dagger, \hat{Q}\}$ such that \hat{Q} is nilpotent, i.e. $\{\hat{Q}, \hat{Q}\} = 0$. If, for a given system, such an operator \hat{Q} can be constructed, the ground states of the corresponding model are in one to one correspondence with the homology of \hat{Q} that is defined as $H_Q = \ker(\hat{Q}) \setminus \text{Im}(\hat{Q})$ via the kernel and the image of \hat{Q} [47]. Supersymmetric models have been shown to realize simple quantum dimer models, see e.g.[48] and were also considered as possible formulation of a more involved fermionic dimer system, see [33]. For the model we considered in this thesis, we have explored the possibility of supersymmetric formulations and extensions as well. We found operators \hat{Q} that can indeed reproduce the plaquette interactions of the model, but that also induce other interaction terms as by-products. In particular, terms that violate the constraint do in general occur. We further found some supersymmetric mixed species dimer models where the corresponding supersymmetric singlet ground states can be constructed easily in some fermion number sectors, yet with mostly valence bond solid like order. The question whether supersymmetric models with RVB liquid like ground states, and in particular whether a supersymmetric formulation for our system at the RK line can be constructed, remains open to further investigation.

Another prospective direction of investigation may be the establishment of a connection between our mixed dimer model and the use of height fields in order to find continuum field theories of dimer models. The author of [49] constructed a height field $h(x)$ to find a continuum description of the original (bosonic) RK model at the critical RK point. The details of this construction can be found in [49], here we point out the important aspect that any hard core dimer configuration can be mapped bijectively to a field configuration $h(x_i)$, with the positions x_i of the square plaquette centers. The classical dimer problem can then be described by the following action for the coarse-grained continuum height $h(x)$ via

$$S = \int d^2x \frac{K}{2} |\nabla h(x)|^2 - \lambda \cos(2\pi h(x)), \quad (6.1)$$

where the stiffness constant K has to be chosen such that the original long-range dimer correlations are recovered and where the cos-term enforces the constraint to an integer valued field $h(x)$. This sine-Gordon theory features a Kosterlitz-Thouless phase transition, and at the value $K = \pi/16$ for the square lattice it is in the 'rough' phase where the cos-term becomes RG irrelevant [50]. This leaves one with a free field theory for the classical dimer problem. By setting up dynamics via a Langevin equation for the height field and employing the implied Fokker-Planck equation for the corresponding probability

distribution $P[h]$, it can be shown, see [49, 39], that the quantum dimer model can be described by the following action in $2 + 1$ dimensions,

$$S = \int d^2x d\tau \left[\frac{1}{2}(\partial_\tau h)^2 + \frac{K^2}{2}(\nabla^2 h)^2 \right]. \quad (6.2)$$

This is the so called quantum Lifschitz model with dynamic critical exponent $z = 2$ and dimensionless field h . This model features a quadratic gapless mode that corresponds exactly to the mode that Rokhsar and Kivelson found within a single-mode approximation, see [50]. The action of Eq.(6.2) can be generalized to describe the system near the RK point,

$$S = \int d^2x d\tau \left[\frac{1}{2}(\partial_\tau h)^2 + \frac{A}{2}(\nabla h)^2 + \frac{K^2}{2}(\nabla^2 h)^2 \right], \quad (6.3)$$

where the parameter $A = 1 - \frac{V}{J}$ controls the phase transition [50, 39]. For $A \neq 0$, the $(\nabla^2 h)^2$ term is RG irrelevant compared to the $(\nabla h)^2$ term and we obtain a $z = 1$ theory which favours either a columnar ($A > 0$) or staggered ($A < 0$) configuration.

A question of possible interest is now whether it is feasible to find a continuum description analogous to Eq.(6.3) for the quantum dimer model with a second, fermionic species of dimers in the system, possibly under the assumption of a small density of fermions, i.e. at low doping. In particular, it could be interesting to verify whether modified dimer correlations and quasiparticle dispersions in the presence of a small number of fermions with t_1 - and t_2 -interactions can be captured by such a continuum model. The realization of this theory might involve two corresponding fields $h(x)$ and a two-component fermion field $\vec{\phi}(x) = (\phi_1(x), \phi_2(x))^T$. The first field $h(x)$ can be imagined to describe the dimer covering of the lattice regardless of the species, hence $h(x)$ is just the height field from before. The field $h(x)$ then maps to a certain dimer configuration where the positions of the fermions are not yet specified. This specification would then be accounted for by the fermion field $\vec{\phi}(x)$, where the two components correspond to the orientation index. The fermion density is reflected directly via the relation

$$N_f = \int d^2x \sum_{i=1,2} \phi_i^\dagger(x) \phi_i(x). \quad (6.4)$$

This construction is similar to the reformulation of the dimer model from Eq.(2.23) as a lattice gauge theory that was carried out in [46]. Yet here, we intend to take a continuum limit that reduces to the action of Eq.(6.3) for $N_f \rightarrow 0$. Just like the construction of the quantum Lifschitz model for the bosonic case, this procedure will presumably not be possible in a rigorous way starting from the microscopic model. A task for future work on the quantum dimer model may therefore be to find a suitable action $S[h, \vec{\phi}]$ that contains terms that represent a coupling between the height field $h(x)$ and the fermion field $\vec{\phi}(x)$. The advantage of such a description would be to have a field theory that can capture not only the interactions between the fermions and the RVB background, as was the case in our diagrammatic approach, but also the internal interactions of the background, all within one framework.

In summary, our work on the quantum dimer model has not only led to new insights, but also to new questions and interesting prospects, a further investigation of which in the future would be desirable.

References

- [1] M. Punk, A. Allais, and S. Sachdev, “Quantum dimer model for the pseudogap metal,” *Proceedings of the National Academy of Sciences*, vol. 112, no. 31, pp. 9552–9557, 2015.
- [2] J. W. Loram, K. A. Mirza, J. R. Cooper, and W. Y. Liang, “Electronic specific heat of $\text{YBa}_2\text{Cu}_3\text{O}_{6+x}$ from 1.8 to 300 K,” *Phys. Rev. Lett.*, vol. 71, pp. 1740–1743, Sep 1993.
- [3] J. Loram, J. Luo, J. Cooper, W. Liang, and J. Tallon, “Evidence on the pseudogap and condensate from the electronic specific heat,” *Journal of Physics and Chemistry of Solids*, vol. 62, no. 1, pp. 59–64, 2001.
- [4] C. C. Homes, T. Timusk, R. Liang, D. A. Bonn, and W. N. Hardy, “Optical conductivity of c axis oriented $\text{YBa}_2\text{Cu}_3\text{O}_{6.70}$: Evidence for a pseudogap,” *Phys. Rev. Lett.*, vol. 71, pp. 1645–1648, Sep 1993.
- [5] S. Uchida, “Spin gap effects on the c-axis and in-plane charge dynamics of high- T_c cuprates,” *Physica C: Superconductivity*, vol. 282, pp. 12–18, 1997.
- [6] C. Renner, B. Revaz, J.-Y. Genoud, K. Kadowaki, and O. Fischer, “Pseudogap Precursor of the Superconducting Gap in Under- and Overdoped $\text{Bi}_2\text{Sr}_2\text{CaCu}_2\text{O}_{8+\delta}$,” *Phys. Rev. Lett.*, vol. 80, pp. 149–152, Jan 1998.
- [7] H. Alloul, T. Ohno, and P. Mendels, “ ^{89}Y NMR evidence for a fermi-liquid behaviour in $\text{YBa}_2\text{Cu}_3\text{O}_{6+x}$,” *Phys. Rev. Lett.*, vol. 63, pp. 1700–1703, Oct 1989.
- [8] N. J. Curro, T. Imai, C. P. Slichter, and B. Dabrowski, “High-temperature $^{63}\text{Cu}(2)$ nuclear quadrupole and magnetic resonance measurements of $\text{YBa}_2\text{Cu}_4\text{O}_8$,” *Phys. Rev. B*, vol. 56, pp. 877–885, Jul 1997.
- [9] A. Damascelli, Z. Hussain, and Z.-X. Shen, “Angle-resolved photoemission studies of the cuprate superconductors,” *Rev. Mod. Phys.*, vol. 75, pp. 473–541, Apr 2003.
- [10] K. M. Shen, F. Ronning, D. Lu, F. Baumberger, N. Ingle, W. Lee, W. Meevasana, Y. Kohsaka, M. Azuma, M. Takano, *et al.*, “Nodal quasiparticles and antinodal charge ordering in $\text{Ca}_{2-x}\text{Na}_x\text{CuO}_2\text{Cl}_2$,” *Science*, vol. 307, no. 5711, pp. 901–904, 2005.
- [11] M. Hashimoto, I. M. Vishik, R.-H. He, T. P. Devereaux, and Z.-X. Shen, “Energy gaps in high-transition-temperature cuprate superconductors,” *Nature Physics*, vol. 10, no. 7, pp. 483–495, 2014.
- [12] Z.-X. Shen, D. S. Dessau, B. O. Wells, D. M. King, W. E. Spicer, A. J. Arko, D. Marshall, L. W. Lombardo, A. Kapitulnik, P. Dickinson, S. Doniach, J. DiCarlo, T. Loeser, and C. H. Park, “Anomalously large gap anisotropy in the a-b plane of $\text{Bi}_2\text{Sr}_2\text{CaCu}_2\text{O}_{8+\delta}$,” *Phys. Rev. Lett.*, vol. 70, pp. 1553–1556, Mar 1993.

-
- [13] H. Ding, M. R. Norman, J. C. Campuzano, M. Randeria, A. F. Bellman, T. Yokoya, T. Takahashi, T. Mochiku, and K. Kadowaki, “Angle-resolved photoemission spectroscopy study of the superconducting gap anisotropy in $\text{Bi}_2\text{Sr}_2\text{CaCu}_2\text{O}_{8+x}$,” *Phys. Rev. B*, vol. 54, pp. R9678–R9681, Oct 1996.
- [14] W. Lee, I. Vishik, K. Tanaka, D. Lu, T. Sasagawa, N. Nagaosa, T. Devereaux, Z. Hussain, and Z.-X. Shen, “Abrupt onset of a second energy gap at the superconducting transition of underdoped $\text{Bi}2212$,” *Nature*, vol. 450, no. 7166, pp. 81–84, 2007.
- [15] I. Vishik, M. Hashimoto, R.-H. He, W.-S. Lee, F. Schmitt, D. Lu, R. Moore, C. Zhang, W. Meevasana, T. Sasagawa, *et al.*, “Phase competition in trisected superconducting dome,” *Proceedings of the National Academy of Sciences*, vol. 109, no. 45, pp. 18332–18337, 2012.
- [16] I. Vishik, W. Lee, R. He, M. Hashimoto, Z. Hussain, T. Devereaux, and Z. Shen, “ARPES studies of cuprate Fermiology: superconductivity, pseudogap and quasiparticle dynamics,” *New Journal of Physics*, vol. 12, no. 10, p. 105008, 2010.
- [17] S. I. Mirzaei, D. Stricker, J. N. Hancock, C. Berthod, A. Georges, E. Van Heumen, M. K. Chan, X. Zhao, Y. Li, M. Greven, *et al.*, “Spectroscopic evidence for Fermi liquid-like energy and temperature dependence of the relaxation rate in the pseudogap phase of the cuprates,” *Proceedings of the National Academy of Sciences*, vol. 110, no. 15, pp. 5774–5778, 2013.
- [18] M. K. Chan, M. J. Veit, C. J. Dorow, Y. Ge, Y. Li, W. Tabis, Y. Tang, X. Zhao, N. Barišić, and M. Greven, “In-Plane Magnetoresistance Obeys Kohler’s Rule in the Pseudogap Phase of Cuprate Superconductors,” *Phys. Rev. Lett.*, vol. 113, p. 177005, Oct 2014.
- [19] Y. Ando, Y. Kurita, S. Komiya, S. Ono, and K. Segawa, “Evolution of the Hall Coefficient and the Peculiar Electronic Structure of the Cuprate Superconductors,” *Phys. Rev. Lett.*, vol. 92, p. 197001, May 2004.
- [20] P. W. Anderson, “The resonating valence bond state in La_2CuO_4 and superconductivity,” *Science*, vol. 235, no. 4793, pp. 1196–1198, 1987.
- [21] P. A. Lee, N. Nagaosa, and X.-G. Wen, “Doping a Mott insulator: Physics of high-temperature superconductivity,” *Reviews of modern physics*, vol. 78, no. 1, p. 17, 2006.
- [22] T. Senthil, S. Sachdev, and M. Vojta, “Fractionalized Fermi Liquids,” *Phys. Rev. Lett.*, vol. 90, p. 216403, May 2003.
- [23] J. Feldmeier, S. Huber, and M. Punk, “Exact solution of a two-species quantum dimer model for pseudogap metals,” *arXiv preprint arXiv:1712.01854*, 2017.
- [24] S. Sachdev, “Spin-Peierls ground states of the quantum dimer model: A finite-size study,” *Phys. Rev. B*, vol. 40, pp. 5204–5207, Sep 1989.

-
- [25] P. W. Leung, K. C. Chiu, and K. J. Runge, “Columnar dimer and plaquette resonating-valence-bond orders in the quantum dimer model,” *Phys. Rev. B*, vol. 54, pp. 12938–12945, Nov 1996.
- [26] R. Moessner and S. L. Sondhi, “Resonating Valence Bond Phase in the Triangular Lattice Quantum Dimer Model,” *Phys. Rev. Lett.*, vol. 86, pp. 1881–1884, Feb 2001.
- [27] P. Fendley, R. Moessner, and S. L. Sondhi, “Classical dimers on the triangular lattice,” *Phys. Rev. B*, vol. 66, p. 214513, Dec 2002.
- [28] O. F. Syljuåsen, “Plaquette phase of the square-lattice quantum dimer model: Quantum Monte Carlo calculations,” *Phys. Rev. B*, vol. 73, p. 245105, Jun 2006.
- [29] E. Fradkin and S. Kivelson, “Short range resonating valence bond theories and superconductivity,” *Modern Physics Letters B*, vol. 4, no. 03, pp. 225–232, 1990.
- [30] R. Moessner, S. L. Sondhi, and E. Fradkin, “Short-ranged resonating valence bond physics, quantum dimer models, and Ising gauge theories,” *Phys. Rev. B*, vol. 65, p. 024504, Dec 2001.
- [31] A. Y. Kitaev, “Fault-tolerant quantum computation by anyons,” *Annals of Physics*, vol. 303, no. 1, pp. 2–30, 2003.
- [32] N. Shannon, G. Misguich, and K. Penc, “Cyclic exchange, isolated states, and spinon deconfinement in an XXZ Heisenberg model on the checkerboard lattice,” *Phys. Rev. B*, vol. 69, p. 220403, Jun 2004.
- [33] F. Pollmann, J. J. Betouras, K. Shtengel, and P. Fulde, “Fermionic quantum dimer and fully-packed loop models on the square lattice,” *Phys. Rev. B*, vol. 83, p. 155117, Apr 2011.
- [34] S. Huber, J. Feldmeier, and M. Punk, “Electron spectral functions in a quantum dimer model for topological metals,” *arXiv preprint arXiv:1710.00012*, 2017.
- [35] D. S. Rokhsar and S. A. Kivelson, “Superconductivity and the quantum hard-core dimer gas,” *Physical review letters*, vol. 61, no. 20, p. 2376, 1988.
- [36] P. W. Anderson, “Resonating valence bonds: A new kind of insulator?,” *Materials Research Bulletin*, vol. 8, no. 2, pp. 153–160, 1973.
- [37] B. Sutherland, “Systems with resonating-valence-bond ground states: Correlations and excitations,” *Physical Review B*, vol. 37, no. 7, p. 3786, 1988.
- [38] M. E. Fisher and J. Stephenson, “Statistical mechanics of dimers on a plane lattice. II. Dimer correlations and monomers,” *Physical Review*, vol. 132, no. 4, p. 1411, 1963.
- [39] C. Lacroix, P. Mendels, and F. Mila, *Introduction to Frustrated Magnetism: Materials, Experiments, Theory*. Springer, 2013.

-
- [40] S. Samuel, “The use of anticommuting variable integrals in statistical mechanics. I. The computation of partition functions,” *Journal of Mathematical Physics*, vol. 21, no. 12, pp. 2806–2814, 1980.
- [41] R. Youngblood, J. Axe, and B. McCoy, “Correlations in ice-rule ferroelectrics,” *Physical Review B*, vol. 21, no. 11, p. 5212, 1980.
- [42] G. Goldstein, C. Chamon, and C. Castelnovo, “d-wave superconductivity in boson+fermion dimer models,” *Physical Review B*, vol. 95, no. 17, p. 174511, 2017.
- [43] M. Ferrero, P. S. Cornaglia, L. De Leo, O. Parcollet, G. Kotliar, and A. Georges, “Pseudogap opening and formation of Fermi arcs as an orbital-selective Mott transition in momentum space,” *Phys. Rev. B*, vol. 80, p. 064501, Aug 2009.
- [44] J. Reuther and P. Wölfle, “ J_1 - J_2 frustrated two-dimensional Heisenberg model: Random phase approximation and functional renormalization group,” *Physical Review B*, vol. 81, no. 14, p. 144410, 2010.
- [45] S. Sachdev and D. Chowdhury, “The novel metallic states of the cuprates: Topological Fermi liquids and strange metals,” *Progress of Theoretical and Experimental Physics*, vol. 2016, no. 12, p. 12C102, 2016.
- [46] A. A. Patel, D. Chowdhury, A. Allais, and S. Sachdev, “Confinement transition to density wave order in metallic doped spin liquids,” *Phys. Rev. B*, vol. 93, p. 165139, Apr 2016.
- [47] L. Huijse, K. Schoutens, *et al.*, “Supersymmetry, lattice fermions, independence complexes and cohomology theory,” *Advances in Theoretical and Mathematical Physics*, vol. 14, no. 2, pp. 643–694, 2010.
- [48] P. Fendley, K. Schoutens, and J. de Boer, “Lattice Models with $\mathcal{N} = 2$ Supersymmetry,” *Phys. Rev. Lett.*, vol. 90, p. 120402, Mar 2003.
- [49] C. L. Henley, “Relaxation time for a dimer covering with height representation,” *Journal of statistical physics*, vol. 89, no. 3, pp. 483–507, 1997.
- [50] E. Fradkin, *Field theories of condensed matter physics*. Cambridge University Press, 2013.

Statement of Authorship

I hereby declare that this thesis is the result of my own work. All references and contributions of others have been cited and acknowledged accordingly.

Munich, February 1, 2018

Johannes Feldmeier